Development and Application of pH-sensitive Fluorescent Probes to Study Synaptic Activity in the Brain

Matthew R. Dunn

Submitted in partial fulfillment of the

requirements for the degree of

Doctor of Philosophy

in the Graduate School of Arts and Sciences

COLUMBIA UNIVERSITY

2015

Abstract

Development and Application of pH-sensitive Fluorescent Probes to Study Synaptic Activity in the Brain

Matthew R. Dunn

This thesis describes efforts at the interface of chemistry and neuroscience to design and characterize fluorescent probes capable of tracing neurotransmitters from individual release sites in brain tissue. As part of the Fluorescent False Neurotransmitters (FFNs) program, small organic fluorophores have been developed that undergo uptake into specific presynaptic release sites and synaptic vesicles by utilizing the native protein machinery, which can then be released during neuronal firing. The most advanced generation of FFNs are pH-sensitive, and display an increase in fluorescence when released from the acidic vesicular lumen into the extracellular space, called a "FFN Flash." In Chapter 2, the utility of the dopamine-selective and pH-sensitive functionality of FFN102 to study the mechanisms that regulate changes in pre-synaptic plasticity, a critical component of neurotransmission was explored. This included using the FFN flash to quantitatively trace dopamine release, changes in the release probability of individual release sites, and changes in vesicular loading that can affect quantal size.

The second goal of this thesis research, as detailed in Chapters 3 and 4, sought to expand the substrate scope of the FFN program to neurotransmitter systems other than dopamine. Described in Chapter 3, is the identification of a fluorescent phenylpyridinium, APP+, with excellent labeling for dopamine, norepinephrine, and serotonin neurons, however, the properties of the probe were found to be ill-suited for measuring neurotransmitter release. As a result, it was

concluded that this class of compounds was not suitable for generating viable FFN leads. In contrast, Chapter 4 highlights the design, synthesis, and screening towards generating the novel noradrenergic-specific FFN, FFN270. This probe was further tested for application in acute murine brain slices where it labeled noradrenergic neurons, and was demonstrated to release upon stimulation. This chapter also describes the application of this compound in a series of *in vivo* experiments, where the ability to measure norepinephrine release from individual release sites was demonstrated in a living animal for the first time. This work opens the possibility for many exciting future FFN experiments studying the presynaptic regulation of neurotransmission *in vivo*.

Table of Contents

Acknowledgements

None of this work would have been possible without the guidance and opportunities provided by my advisor, Professor Dalibor Sames. I am sincerely thankful for your help over the past five years, and the chance to work on such an exciting and interdisciplinary project. I must also acknowledge Professor David Sulzer, who graciously accepted me into his laboratory as well. Thank you for all of your advice and your willingness to help with any neuroscience questions. Both of you have been excellent mentors and helped me develop as a scientist and critical thinker. I would also like to thank my undergraduate mentors, Professor Adam Cassano and Professor Steven Dunaway from the Biochemistry department at Drew University. Thank you both for my first research experiences and for making science fun.

I would also like to thank the great group of peers I have enjoyed having by my side throughout this process. The members of the Sames and Sulzer laboratories have provided invaluable insight and friendship over the years. I would like to especially thank Dr. Adam Henke and Dr. Rich Karpowicz, for their mentorship, friendship and direct help in the work of this thesis. Thank you to Dr. Linda Suen and soon to be Dr. Andrew Kruegel for your friendship from Day 1 of the graduate program. Thank you to Yekaterina Kovalyova for your friendship and for helping make the last few years the most fun.

Lastly, but most importantly, I am thankful for my wonderful family. It has been a real pleasure having so many great people so close. A special thanks to my brother for all the competition over the years and instilling a drive to always be better. To my parents, you two have always been my most important role models, and the balance of your personalities was the best guidance and inspiration I could ever ask for. Thank you.

Chapter 1: An Introduction to Neurotransmission

1.1 Preface

Studying the organizational complexity interconnecting the ~ 100 billion neurons[1] that comprise the human brain is proving to be one of the most difficult challenges faced by the scientists of this generation. Since the coining of the term in 1960's[2], "neuroscience" has rapidly expanded as a field over the past few decades. With the number of neuroscience publications in the past year (2014) almost doubling that of the previous year[3], every new discovery creates more questions to explore. Undaunted by this overwhelming complexity, however, neuroscientists continue to push forward. Just as every neuron has a specific function, this thesis describes my role in developing novel tools to augment this endeavor. Observation has always been the foundation of science, and through the creation of new ways to observe previously undetectable neurological phenomenon we can continue to add new pieces to the seemingly endless puzzle.

1.2 The Neuron

One of the best ways to start understanding how the brain functions as a whole is to look at one of its primary individual elements, the neuron (**Figure 1**). The neuron is a highly specialized cell capable of transferring information across potentially large distances. In general, signals are collected in the cellular branches extending off the cell body, called dendrites. Based on the information collected by the dendrites, an all-or-nothing signal is then initiated at the axon hillock and then propagated down the axon through a change in the electrical potential across the axonal membrane. Ultimately, the signal reaches structurally defined locations along the axon,

called synapses, which are capable of releasing neurotransmitters. These “pre-synaptic” release sites then chemically transfer the signal across the synaptic cleft through the use of neurotransmitters to the dendrites, cell bodies, or synapses of the next neurons in the circuit.

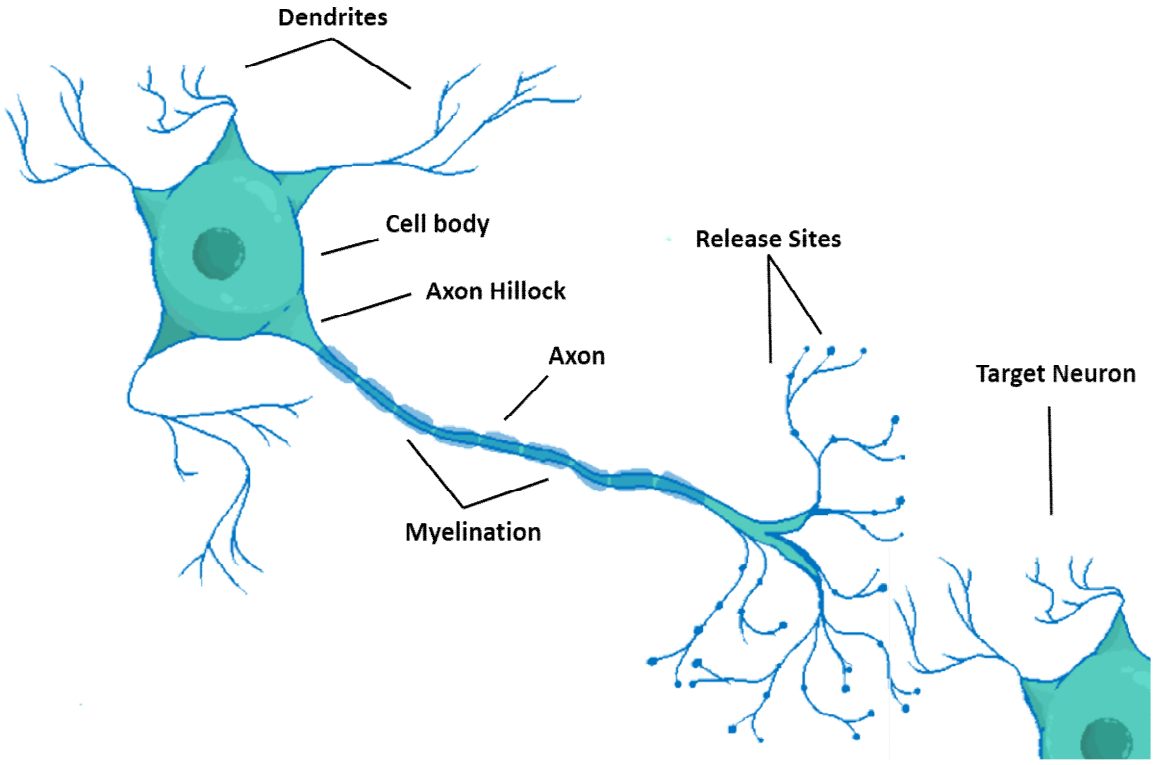

Figure 1. A general illustration of a neuron. A signal is received in the dendrites, which the receiving neuron then can continue or not. Its own signal is initiated in the axon hillock and travels down the axon, which can be myelinated, to the individual release sites, where the signal is then sent across the extracellular space to the target neuron.

While this general mechanism holds true for most neurons, there can be a great amount of diversity between each of the steps along this process. The illustration in **Figure 1** highlights release sites found after arborization of the axon, but in reality, neurotransmitters can also be released by dendrites and cell bodies depending on the neuronal cell type. There is also retrograde neurotransmission, in which signals are sent in reverse, from the postsynaptic side to communicate back to the presynaptic release site. Using just structural characteristics, it is possible to classify different types of neurons into specialized groups. For example, most

GABAergic inhibitory neurons are called “interneurons” because they have very short axons that only affect a local area, while other neurons are called “projection neurons” that have long myelinated axons and connect different brain regions to each other[4]. Some neurons, like in the olfactory bulb, process a whole collection of signal inputs and then send out an organized convergent signal onto only a few targets[5]. These neurons have very little axonal branching, which is contrary to other types of divergent neurons, such as the dopaminergic neurons that project to the striatum. Each individual dopaminergic neuron in this area of the brain has extensive arborization of its axons, which allows its signal to be sent to an estimated ~75,000 other neurons[6]. While **Figure 1** depicts a generic neuronal structure, simply examining the diversity of structures occurring with specialized neurons reveals an added layer of complexity to understanding neuronal function, which is just the tip of the iceberg.

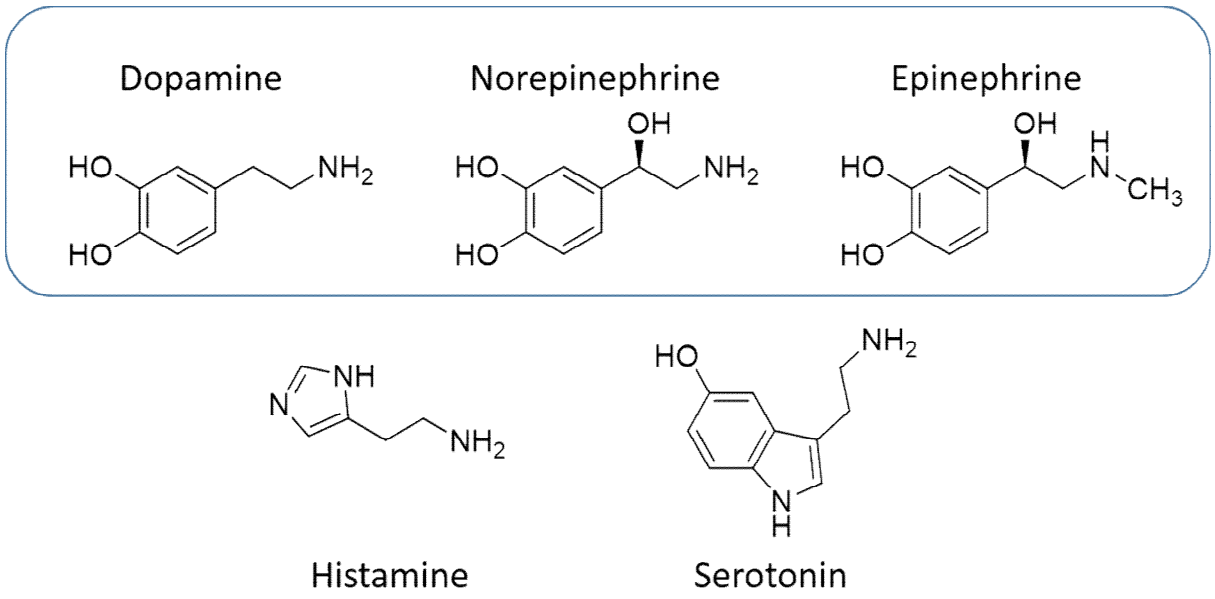

Figure 2. The members of the monoamine neurotransmitter family. Those members that are part of the catecholamine sub-family are encircled (Dopamine (DA), Norepinephrine (NE), and epinephrine).

1.3 Monoamines

1.3.1 The Monoamine Family

Just as different neurons come in different shapes and sizes, the language in which they communicate with other neurons differs as well. The actual identity of the neurotransmitter that creates the chemical connectivity with their neighbors can range from small molecules to peptide chains of up to 30 amino acids. While each neurotransmitter is important in its own right, the majority of the Fluorescent False Neurotransmitter (FFN) program, and the bulk of this thesis, focuses on a particular class of neurotransmitters, the monoamines. This family of neurotransmitter is named for the common ethylamine side chain present in all its members: dopamine (DA), norepinephrine (NE), epinephrine, histamine, and serotonin (**Figure 2**). The catecholamines, DA, NE, and epinephrine are a further sub-class of this neurotransmitter family, which share a catechol moiety and biosynthetic pathway (**Figure 3**). I will describe the DA (Chapter 2) and NE (Chapter 3 and 4) neurotransmitter systems in more detail later in this thesis, but will provide a general overview of this neurotransmitter family here.

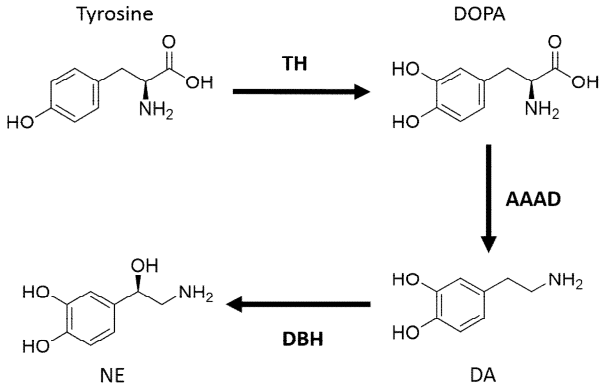

Figure 3. Shared biosynthetic pathway for dopamine (DA) and norepinephrine (NE). Ortho-hydroxylation of the amino acid, tyrosine, by tyrosine hydroxylase forms dihydroxyphenylalanine (DOPA). Decarboxylation of DOPA by aromatic L-amino acid decarboxylase (AAAD) forms DA, which can by oxidized by dopamine β-hydroxylase (DBH) to form NE.

1.3.2 Biosynthesis

The synthesis of catecholamines starts with the amino acid tyrosine. Tyrosine first undergoes an ortho-hydroxylation through the enzyme tyrosine hydroxylase (TH) to produce dihydroxyphenylalanine (DOPA). DOPA is then decarboxylated by aromatic L-amino acid decarboxylase (AAAD) to produce DA. In dopaminergic neurons this would be the final step of synthesis, but in noradrenergic neurons dopamine is further converted to NE through dopamine β-hydroxylase (DBH) (**Figure 3**)[7]. The amine on NE can be further methylated by phenylethanolamine-N-methyltransferase to form epinephrine, but the main focus of this thesis will be directed towards NE and DA.

1.3.3 Synaptic vesicles

After synthesis, the neuron then packages the neurotransmitter into synaptic vesicles where it is stored until the neuron is ready to send its chemical signal. In catecholamine neurons this process is controlled by the vesicular monoamine transporter (VMAT2)[8]. VMAT2 is a member of the solute carrier 18 (SLC18) family of proteins, specifically SLC18A2, and is found both in the brain and peripheral tissue[9]. In catecholamine neurons, VMAT2 pumps neurotransmitters into the synaptic or large dense core vesicles using a proton electrochemical gradient, generated by the vacuolar H^+-ATPase (vATPase), as an energy source[10]. vATPase hydrolyzes ATP to pump protons into the vesicle creating a concentration difference of approximately 1.5 pH units. For every individual neurotransmitter pumped into the vesicles, two protons are pumped out, in an antiport mechanism[11]. This electrochemical proton gradient is strong enough to generate a 10^4 increase in catecholamine concentration in the vesicle[10]. A summarized schematic of the vesicle life cycle, and the process of neurotransmission described later in 1.3.3, is found in **Figure 4**.

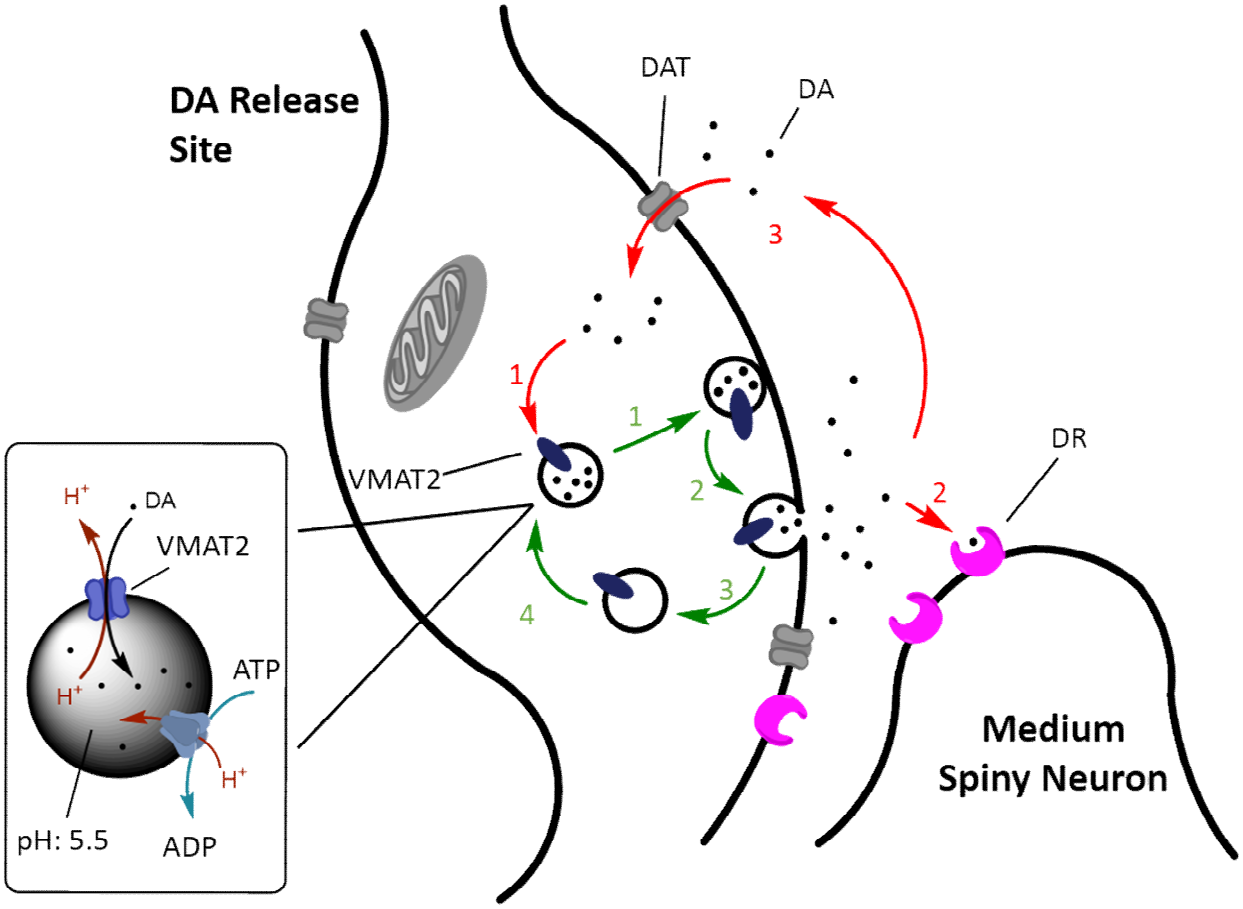

Figure 4. General summary of the processes involved in dopamine (DA) neurotransmission from a dopaminergic neuron in the striatum, although the process is very similar for NE. Highlighted in green is the life cycle for vesicles. 1) A vesicle loaded with DA docks at the membrane through the help of the SNARE complex. 2) After calcium influx, the vesicle fuses with the membrane and releases its contents. 3) The vesicle is then recycled, 4) where it is again loaded with DA. Highlighted in red is the life cycle of DA. 1) DA is first loaded into vesicles through the vesicular monoamine transporter 2 (VMAT2). This process is powered by the proton gradient generated by the vesicular-ATPase (inset). 2) After release, DA then fills the synaptic cleft and binds to dopamine receptors (DR) both pre-, post-, and extrasynaptically. 3) DA is then cleared from the synapse through reuptake by the dopamine transporter (DAT) or metabolism by monoamine oxidase (not shown).

After neurotransmitter loading, the vesicle then needs to be docked near the cellular membrane before it can be released. This task is performed by a complex of proteins that make up the soluble NSF-attachment protein receptor (SNARE) machinery. Synapotobrevin bound to the vesicular membrane complexes with other members of the complex attached to the cellular membrane, such as SNAP-25, Syntaxin, and Munc18[12]. Conformational changes of this complex then open a fusion pore that allows for the release of neurotransmitters. Once they perform

exocytosis, the vesicles then recycle through three possible mechanisms, “kiss and stay”, “kiss and run”, or full recycling[13]. Kiss and stay involves refilling with neurotransmitters without the vesicle ever undocking. Kiss and run also keeps the vesicle intact, but it undocks from the membrane and SNARE complex before refilling. Lastly, full recycling of the vesicle involves binding and reforming through an endosomal intermediate[13]. Once the vesicle has undergone one of these recycling pathways it is then ready for the next release signal.

1.3.4 Signaling

The vesicle fusion process is initiated by the opening of voltage-gated calcium channels due to changes in the membrane potential from the electrical signal traveling down the axon. Once calcium enters the release site, it binds to the synaptotagim calcium sensor on the vesicular membrane. This then leads to the activation of the SNARE complex and neurotransmitter release during vesicular fusion[14]. After the neurotransmitter is released into the synaptic cleft it can then bind to pre- or postsynaptic receptors completing the signaling process between neurons. The catecholamine binding targets are metabotropic G-protein-coupled receptors (GPCRs)[15]. These receptors have three main structural motifs, an extracellular neurotransmitter binding site, a seven transmembrane helices domain, and an intracellular G-protein binding domain[16]. When an agonist of these receptors occupies the binding pocket, the GPCR undergoes a conformational change that affects the G-protein binding domain intracellularly. This then changes the affinity of this domain for the heteromeric G-protein complex, which initiates an intracellular signaling cascade. Depending on the specific neurotransmitter-GPCR pair, this binding leads to a number of different intracellular pathways with different downstream targets.

Catecholamines are classified as modulatory neurotransmitters because their receptors can lead to either downstream activation or inhibition. I will briefly discuss DA receptors (DRs)

as an example here. More information on NE and adrenergic receptors can be found in Chapter 4 (4.1.2). There are two main groups of DRs, ones that activate adenylyl cyclase (D1-family) and those that inhibit adenylyl cyclase (D2-family). Members of the D1 family lead to the activation of the G_s-protein pathway, an increase of cAMP production, and activation of protein kinase A (PKA), and include the receptors D1 and D5. Members of the D2 family lead to the activation of the G_i- and G_o-protein pathways, a decrease in cAMP production, and deactivation of PKA, and include the receptors D2, D3, and D4[17]. There is evidence that DA can also influence the G_q-protein pathway, which can lead to increases in intracellular calcium[18], but this process is still not fully understood (The G_q pathway is described in more detail in 4.1.2 with adrenergic receptors). While the downstream consequences of activating these second messengers is highly variable depending on the particular example, it is important to note that DA, or NE, can either enhance or inhibit a particular connection. This modulating effect can also be strengthened or weakened through pre-synaptic changes in neurotransmitter release.

After a release event, the duration and extent of this signaling process is also tightly controlled by regulating the amount of available neurotransmitter in the synaptic cleft and surrounding area. Free extracellular neurotransmitter can either be cleared from the cleft through enzymatic degradation or primarily through the reuptake by a specific monoamine transporter (**Figure 4**). Each catecholamine has its own corresponding membrane transporter (MAT), dopamine transporter (DAT) for DA or norepinephrine transporter (NET) for NE, although there are cases of promiscuity between these transporters and their neurotransmitter substrates[19]. Depending on the environment around a specific release site, the neurotransmitter signal can be considered “wired” or “volume” transmission[20]. Wired transmission is the direct and discrete communication of one presynaptic synapse to a specific postsynaptic target. For this type of

neurotransmission, the most common type found in the brain, postsynaptic target receptors are found primarily right in the synaptic cleft, with the majority of neurotransmitter molecules never escaping from the synaptic junction due to MAT activity. The catecholamines, however, are also known to undergo volume transmission in most cases. This is where the extracellular neurotransmitter concentration is relatively long-lived and potentially affects the receptors on multiple target neurons in the area[20]. This is particularly true for monoamines, such as NE or DA, which have been shown in certain cases to exist extracellularly in the cortex for seconds, orders of magnitude longer than that typically observed in wired transmission[21]. The reasoning behind this type of transmission, and its biological significance in affecting neurotransmission, will be covered more in Chapter 2 (2.1.3). Once the neurotransmitter is cleared from the extracellular space and re-enters the neuron, it can then be repackaged into vesicles or metabolized by monoamine oxidase (MAO) or catechol-O-methyl transferase (COMT). This uptake process is tightly regulated and occurs after every vesicle fusion event.

1.4 Studying neurotransmission

1.4.1 The Connectome

The connectome is a comprehensive map that would describe all the neuronal wiring and connections in the brain[22]. Understanding this intricate network of billions of neurons is thought to be one of the most important goals along the path to understanding the brain. If the whole network is the ultimate puzzle, then its smallest piece would be a single synaptic connection. Recent advancements in mapping the functional connectivity of the brain have relied on imaging the activity of whole neurons and the connection between a particular neuron and its local neighbors through intracellular calcium indicators[23]. The activity of a specific individual neuron can be artificially induced using light activated membrane dyes[24], caged glutamate[25], or genetically encoded membrane channels[26]. While these techniques, and others like them, are

very powerful at obtaining general information about neuronal circuits, they still do not directly look at all the synapses that make up that connection, or the regulation of those synaptic connections that ultimately control firing patterns and circuit function[27].

One of the reasons studying neurotransmission at individual synaptic connections is so important is because these connections are not static. There are multiple biological changes that can occur in a synaptic connection that alter the way the individual neurons communicate with each other. Post-synaptic dendritic spines are highly dynamic and undergo pruning and formation as part of normal development[28] or behavioral learning[29]. Dysregulation of this process has been linked to mental disorders, such as autism[30]. Further, post-synaptic changes in receptor expression levels can drastically affect the downstream outcome of the same neurotransmitter signal.

On the pre-synaptic side of the connection, there are also regulatory mechanisms in place that can affect neuronal signaling. The neurotransmission of particular synapses can be fairly plastic over time, either increasing or decreasing their amount of neurotransmitter released. In hippocampal mossy fiber neurons, there is a drastic decrease in the failure rate of their firing after undergoing long trains of activation (>30min), an observation termed long-term potentiation (LTP)[31]. Additionally, these same mossy fiber neurons under different activation conditions can actually demonstrate long-term depression (LTD)[32], or even forms of short-term plasticity[33]. The ultimate effect of each of these changes is an alteration in how that particular neuron communicates with its targets. It is important to note that these changes in synaptic activity are part of normal neuronal function, and synaptic impairment or degeneration is common during the progression of many diseases or disorders[34]. Some examples that involve

catecholamine synapses in particular are addiction[35], depression[36], as well as, Parkinson's[37] and Alzheimer's[38] diseases.

Therefore, to truly understand how the circuits of the brain function, it is important to study exactly how neurotransmission at a particular synaptic connection can be regulated over time and under different physiological conditions or disease states. Due to the nature of this project, a particular focus will be placed on the pre-synaptic modulation that leads to changes in neurotransmission, with a particular emphasis on catecholamines.

1.4.2 Electrochemistry

Historically, one of the most common ways to directly measure neurotransmitter release is through cyclic voltammetry and amperometry. These techniques work by sending a small electric potential to the area of interest and oxidizing certain analytes with an appropriate redox potential. This technique works for catecholamines, since these neurotransmitters have redox potentials within the typical -0.4 to 1V scanning range[39]. Electrochemical techniques are highly sensitive to analyte concentrations with excellent temporal resolution (up to 1ms)[40], but lack sufficient spatial resolution. It is estimated that typical carbon-fiber electrodes measure neurotransmitter release from hundreds of release sites depending on the density of the projections (**Figure 5**)[41]. In particular to measuring catecholamine release, these techniques are also limited in their ability to distinguish between DA and NE signals, due to the similarities of their redox potentials. Advancements in the standard electrochemical techniques have designed multiple special electrode surface modifications that preferentially enhance DA detection[40], however, specificity for NE remains difficult[42,43]. Electrochemical recordings have also been paired with other biosensors, such as liquid chromatography, capillary electrophoresis, and mass spectrometry, using newly designed dual-functioning sensors[40]. These techniques have helped

with the collection of information from multiple analytes, but still do not address the problems with spatial resolution.

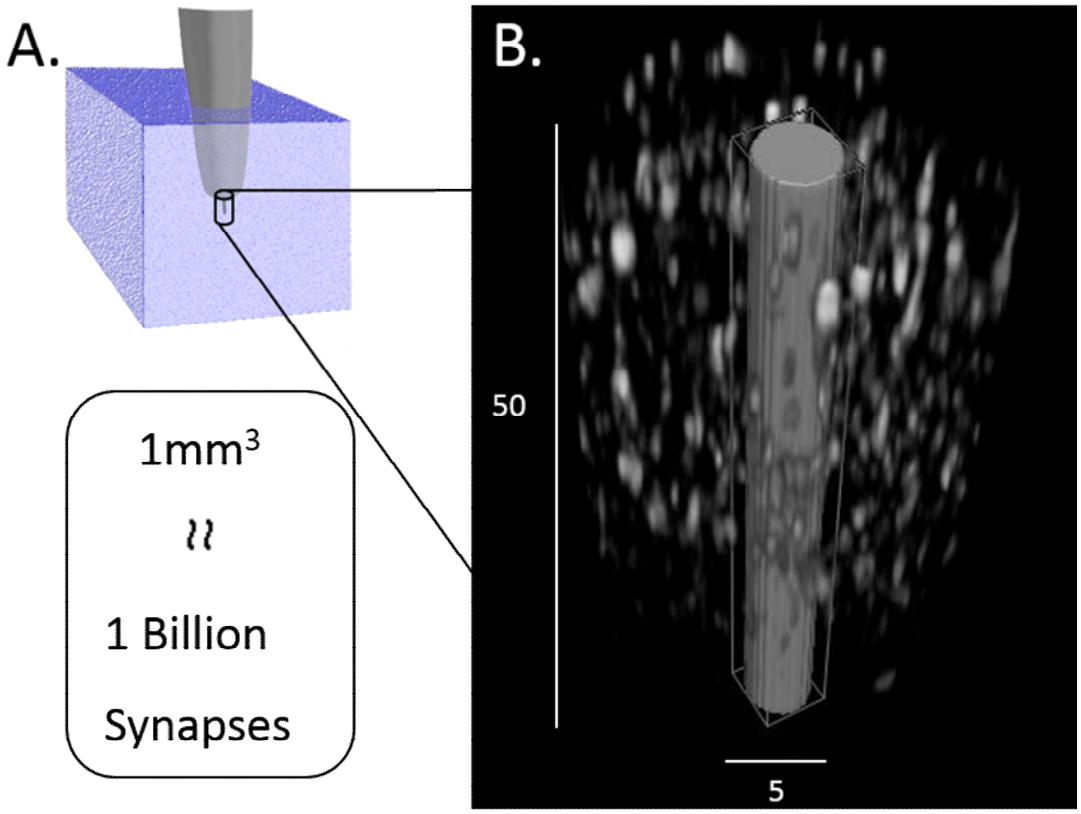

Figure 5. A) Representation of an electrode in a 1 mm^3 volume of brain tissue (grey matter), which is expected to contain ~1 billion synapses. B) Zoomed in area surrounding the representative tip of the electrode. Surrounding the tip are all the dopaminergic release sites (labeled with the DA label, FFN102, described in 1.4.4) in the expected volume measured with current electrochemical methods (estimated to be ~100's of release sites for DA in the striatum)[44]. Scale bars are in µm.

1.4.3 Previous Optical Techniques

While electrochemistry has provided a wealth of knowledge about bulk neurotransmitter release patterns and regulatory mechanisms, to further the understanding of how the individual members of that bulk population operate, the field turned to optical imaging. Advancements in imaging techniques now allow for the collection of information from areas as small as the single synapse with excellent temporal resolution. As a result, there has been a wealth of imaging

techniques developed to study neurotransmitter exocytosis, each with their own benefits and limitations. Almost each step along the neuron activation pathway can now be mapped optically; (1) voltage dyes measuring the electrical potential change traveling down the axon, (2) calcium indicators measuring the influx of calcium after the electrical potential opens their channels, (3) membrane bound dyes measuring vesicular membranes fusing to the outer cellular membrane, (4) intravesicular pH sensors measuring vesicular content being exposed to the extracellular space, and (5) receptor-based sensors measuring neurotransmitter binding.

(1) Voltage dyes:

Neurons are tightly held at a resting electrochemical potential that changes up to 100mV upon the opening of voltage gated sodium channels and subsequent potassium and calcium channels. This voltage change across the relatively narrow plasma membrane results in a huge electric field of 10^7-10^8V/m [45]. As a result, several imaging tools have been developed that harness this change in electric field to create an optical signal change. One example of how these sensors work is through redistribution, which requires a dye that maintains an equilibrium between two environments (for example, Rhodamine-6G: extracellular vs intracellular)[46]. When the membrane potential changes, this concentration equilibrium can shift drastically resulting in more uptake or release of the dye. While redistribution in general is slow, non-specific, and has poor signal to noise, advancements in this field have developed many other ways to harness this change in electric field, such as membrane reorientation[47], electrochromic dyes[48], FRET-based[49,50], genetically encoded protein sensors[51], and even other methods. However, I describe only one common example here, due to the fact that even as this field progresses further and overcomes some of its earlier limitations, measuring voltage is still an upstream reporter of neurotransmission, and does not always lead to neurotransmitter release. Actual release at a

synapse is a dynamic probabilistic event that can change depending on conditions[52], and even release sites along the same axon can have different release probabilities[53]. As a result, there may be functionally different strengths of neurotransmission occurring, but distinguishing this with a voltage sensor would be impossible.

(2) Calcium indicators:

Following the previously described large change in membrane potential, there is a subsequent opening of voltage gated calcium channels, which increases the intracellular Ca^{2+} concentration in active neurons. In tandem, there are also intracellular stores of Ca^{2+} that can participate in generating a transient Ca^{2+} concentration spike[54,55]. Increased Ca^{2+} concentration near the active zone of the synapse causes activation of vesicular membrane bound proteins, such as synapototagmin-1, which leads to initiation of the SNARE complex[56]. As such, measuring these transient Ca^{2+} concentration spikes has been a widely used tool to study neuron activity. This can be done with calcium sensitive organic fluorophores, as well as genetically encoded calcium indicators (GECIs).

Synthetic calcium indicators combine a fluorophore with a calcium coordinating motif. One example, fura-2, combines a stilbene fluorophore with an octacoordinate, tetracarboxylate calcium coordinating motif[57]. Binding of calcium to fura-2 results in a ratiometric and measurable wavelength shift that can be used to measure intracellular Ca^{2+} concentrations. In practice, these dyes can be loaded into neurons using a membrane permeable AM-ester form, which is then cleaved by cytosolic esterases and then locked inside. The requirement of this loading method has proven to be a major drawback in the application of this technology, as it is time consuming and non-specific (i.e. labels all cells).

Calcium sensors have gained neuron-type-specific labeling through genetic control with the introduction of genetically encoded calcium indicators (GECIs). Sensors in this class commonly combine the Ca^{2+} binding domain of calmodulin (CaM) and circularly permuted GFP (cpGFP). cpGFP, in its native state, is not fluorescent, but can be turned on by the conformational change that occurs when Ca^{2+} binds to the linked CaM domain[58]. While GECIs have improved targeted selectivity, they have historically had poorer Ca^{2+} sensitivity or kinetics than the synthetic calcium sensors. Recent advancements in this class of sensors has led to the availability of GECIs, such as GCaMP6f, which can now compete with synthetic calcium sensors while maintaining selective neuron control[59]. However, like the voltage dyes previously described, intracellular Ca^{2+} concentration levels are still an upstream reporter for actual neurotransmission, and not all Ca^{2+} transients cause the same response. The relationship between Ca^{2+} and neurotransmitter release is dependent on the availability of readily releasable vesicles, the actual Ca^{2+} concentration at the active zone, and the molecular coupling between Ca^{2+} and the vesicular fusion machinery[52]. The mechanisms that regulate these parameters will be discussed in more detail in Chapter 2, but it is clear that while release probability and calcium transients are related, this factor is not uniform for all synapses, and can be dynamic over time. As a result, a tool for measuring actual neurotransmitter release will be more useful when studying neurotransmission than calcium sensors.

(3) Vesicular membrane dyes:

In an attempt to more directly measure the kinetics and understand vesicular fusion, a series of endocytic membrane dyes have been used. These dyes are structurally designed to have a high affinity for the cellular phospholipid bilayer membrane. The most successful example of this is FM1-43, a styryl pyridinium molecule that has a hydrophobic tail and charged head group,

similar to a phospholipid[60,61]. After this dye is bath applied and inserted into all membranes, the neurons are stimulated, causing vesicle recycling. As a result, some of the dye is incorporated into the vesicular membranes inside the neuron through endocytosis. The remaining dye on the extracellular membranes is then washed away with a β-cyclodextrin derivative, ADVASEP-7. This is possible due to the higher affinity binding between FM1-43 and ADVASEP-7 over the membrane[61,62]. After these loading steps, synaptic vesicle fusion kinetics can be correlated with an observed loss of FM1-43 fluorescence when it washes away after it is re-exposed to the extracellular ADVASEP-7.

While this optical technique is even closer to measuring direct neurotransmission, it is limited by many drawbacks. First, the dye can only be loaded into vesicles after long neuronal stimulation protocols, which have been shown to cause drastic changes in synaptic behavior[63]. Additionally, this means that FM1-43 will also only label the synaptic vesicles in currently active release sites, making it difficult to study functionally plastic release sites[64]. This is a potentially important parameter when studying dopamine neurotransmission, and will be further discussed in Chapter 2 (2.1). Another problem with FM1-43 loading is the requirement of the presence of ADVASEP-7, which further makes the use of FM1-43 *in vivo* impractical. Second, the change in fluorescence associated with a single vesicular recycling event is very small relative to the total fluorescence in all the vesicles in the whole synapse. As a result, the dye is typically used to observe kinetics over a large number of action potentials, and is poorly suited to study single synaptic events[65,66]. Lastly, the measurement of vesicular recycling is only correlative to actual neurotransmission. While this technique can be paired with electrochemistry[67], inherently, it does not measure actual neurotransmitter release.

(4) SynaptopHluorins:

Similar to the endocytic dyes, synaptopHluorin (SpH) also measures vesicular behavior. SpH is a genetically encoded protein that contains a pH-sensitive GFP variant linked to the vesicular membrane bound protein, synaptobrevin[68]. The pH-sensitive GFP used has a ratiometric fluorescence excitation spectrum, which changes in acidic environments, such as the loaded vesicle (pH ~ 5.5), and more basic environments, such as the extracellular environment (pH ~ 7.4)[69]. This technique improves upon the endocytic dyes in both specificity and sensitivity. As a genetically encoded protein, the sensor can be expressed in only the particular neurons of interest, and it can be modified to use other vesicular membrane proteins as an anchor, such as VGlut[70]. SpH also shows high sensitivity of vesicular fusion events due to the large change in fluorescence resulting from the transient pH change it measures, which allows for the study of presynaptic activity from single action potential measuments[71–73].

While this technique has been very successful in cell culture, its application for intact mammalian systems remains limited by high background[74]. Therefore, the use of SpH in mice *in vivo* (and even *ex vivo* brain slices) has been limited, and only capable of measuring spatially large activations of groups of neurons, such as in the olfactory bulb[75]. Moreover, similar to the endocytic dyes, this technique still is not a direct measurement of neurotransmission. SpH can only measure if the lumen of a synaptic vesicle equilibrated with the extracellular space, and is not capable of describing how much neurotransmitter was loaded or released.

(5) Receptor-based neurotransmitter sensors:

There are two main types of receptor based sensors that have been developed to monitor neurotransmitter concentrations. First, there are receptor binding domains that have been linked to fluorescent proteins that increase in fluorescence after an allosteric modulation. This allosteric modulation has been engineered to be induced by the neurotransmitter-bound conformational

change of the receptor domain. In this category are the glutamate optical sensor (EOS) and the intensity-based glutamate-sensing fluorescent reporter (iGluSnFR). EOS combines the ligand binding domain of the glutamate receptor 2 subunit with the fluorescent dye, Oregon green[76]. A drawback of this system has been number of steps involved in preparing the experimental system. First, a genetically encoded linker is needed to be expressed on the cell surface, which can serve as an anchor of the EOS complex and immobilizes it on the target membrane surface. The number of steps was reduced with the iGluSnFR construct, which can be directly genetically encoded, transcribed, and membrane-expressed in the neurons of interest. iGluSnFR uses a circularly permutated GFP as its fluorescent reporter, and the *E. coli* glutamate-binding protein (gltI)[77]. Because this sensor can be expressed right at the synapse, pre- or post-synaptically, it can directly measure neurotransmitter release from a single synapse. However, the fact that this sensor must be genetically encoded, limits its potential use in species not readily amenable to genetic manipulations, including humans. Additionally, as of now, this system has only been demonstrated to work for the glutamate neurotransmitter, and is not yet developed for catecholamine studies.

The second type of sensors in this group are cell-based neurotransmitter fluorescent engineered reporters (CNiFERs), which utilize a signal transduction pathway to cause a whole cell fluorescent readout[78]. For this technique, whole cells must be implanted in the area of interest and then they only report on neurotransmitter changes that happen to escape the synaptic junction. Just recently, DA and NE CNiFERs were constructed and their use was demonstrated *in vivo*[79]. These particular catecholamine CNiFERs work by using either the D2 GPCR for DA, or α_{1A} for NE, and linking their downstream G-protein cascade with an increase in intracellular calcium levels. The intracellular calcium levels then result in fluorescent readout by the FRET-

based calcium sensor, TN-XXL[80]. This technique is quite useful since it directly measures neurotransmitter release, has a high signal to noise ratio, and is very specific. In this regard, this particular sensor is actually very similar to electrochemistry, but with the addition of better selectivity. However, like electrochemistry, it is measuring the neurotransmitter released from many release sites and is not capable of observing release from individuals of that population.

1.4.4 Fluorescent False Neurotransmitters

After reflecting on all of the available tools to study catecholamine release, it was clear that none were ideal. There is currently no reporter capable of measuring direct catecholamine release from a single event at a signal release site. However, with the development of fluorescent false neurotransmitters (FFNs), we think that we are approaching this goal. While not directly measuring catecholamine concentrations, the idea behind FFNs was to create small fluorescent molecules that, as closely as possible, mimic native catecholamines during release. By designing FFNs to have common structural recognition elements of the catecholamines, such as the ethylamine sidechain, in combination with a fluorescent core, it was possible to generate fluorescent compounds that were also substrates of transporters involved in catecholamine neurotransmission (**Figure 6**). While for early generation FFNs (FFN511) this simply meant activity at VMAT2[81], newer generation FFNs (FFN102) were also selected for their activity at the appropriate membrane transporter (DAT or NET)[82]. Therefore, instead of passively diffusing into neurons and then getting trapped in vesicles through VMAT, newer generation FFNs were designed to be more polar and only cross the membrane through transporter activity. This resulted in FFNs, such as FFN102, that are dual VMAT2 and MAT substrates with higher selectivity and better signal to background ratios than earlier generation FFNs[82]. Our laboratory is continuing to advance this technology through characterization of new functionality and

applicability, as well as expanding the neurotransmitter systems with which they can be used. These advancements will be the main focus of this thesis in the following chapters, but I will include here a brief description of how FFNs work and some of the previously published work in this area.

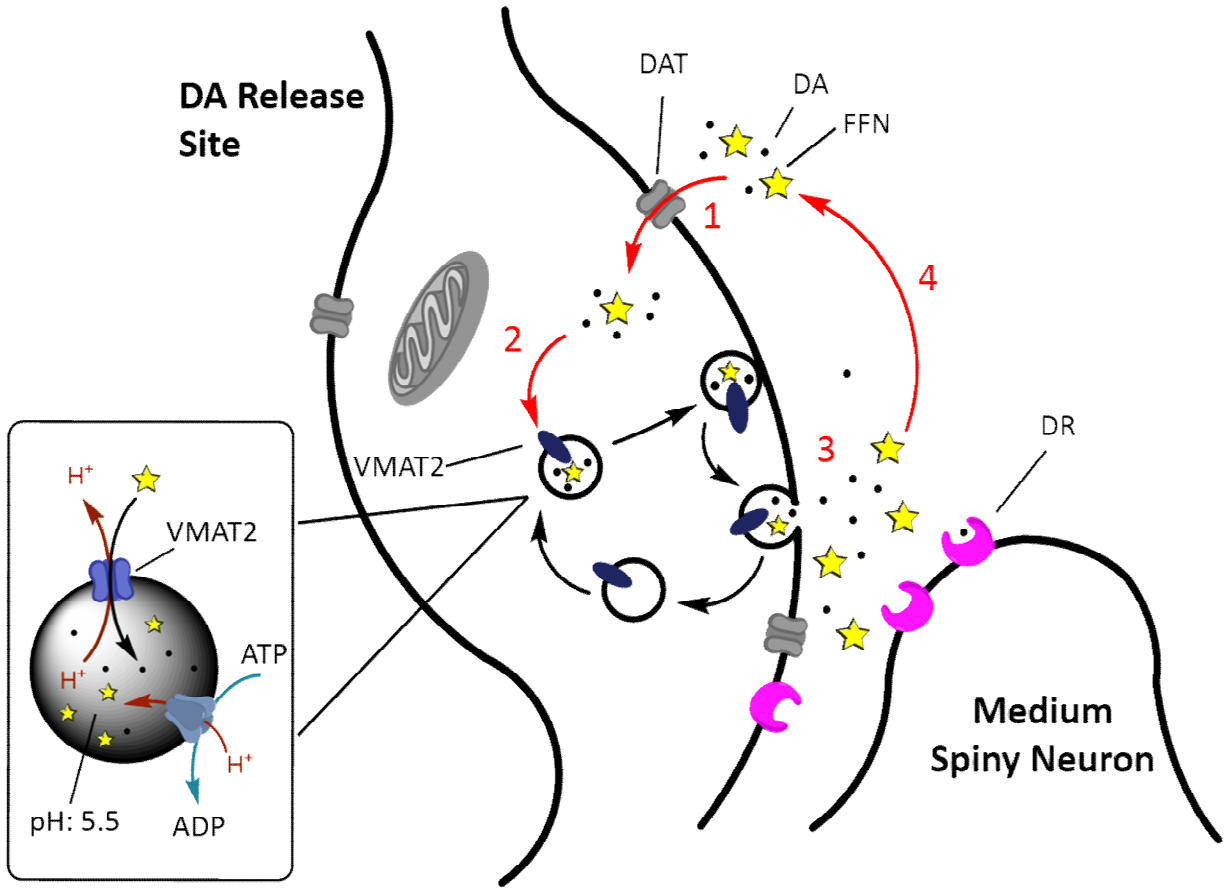

Figure 6. Modified schematic of the neurotransmitter life cycle to include FFNs (yellow stars). 1) The applied FFN is actively loaded into release sites through DAT activity. FFN in the cytoplasm is then loaded in vesicles through VMAT2 activity (inset). As described in more detail in Chapter 2, loading into the acidic vesicles can lead to a change in fluorescence for pH-sensitive FFNs. 3) After vesicle fusion, the FFN is released into the extracellular space, where the pH returns to ~7.4. 4) Through DAT uptake, the FFN is then reloaded into release sites or washed away.

Since FFNs are actively accumulated through transporter activity, they can be loaded into cells or synaptic release sites by simple bath application. Unlike some of the previously described genetically encoded sensors, which require time consuming viral injections or selective

breeding, or endocytic dyes, which require harsh loading conditions, the FFN loading concept is relatively quick and widely applicable to multiple experimental systems. One system that has been of particular importance for studying our early generation dopaminergic FFNs has been the dorsal striatum of *ex vivo* acute mouse brain slices. This is an area rich in dopaminergic projections primarily from the substantia nigra (SN) that can be visualized with FFNs[83]. When loaded into release sites, the FFN appears as small points (~1μm) of increased fluorescence intensity, which we call "puncta". Due to the inherent benefits of fluorescence imaging, we are able to observe changes in these puncta with a spatial resolution applicable to a single release site, and temporal resolution on the millisecond timescale. By measuring these same fluorescent changes in the presence of compounds that cause neuromodulation or animal models of different disease states, it is possible to understand the role of these conditions in changing neurotransmitter uptake, vesicular loading, and release with single synapse resolution. The use of FFNs to study each of these parameters, which all affect neurotransmission, is discussed throughout Chapter 2.

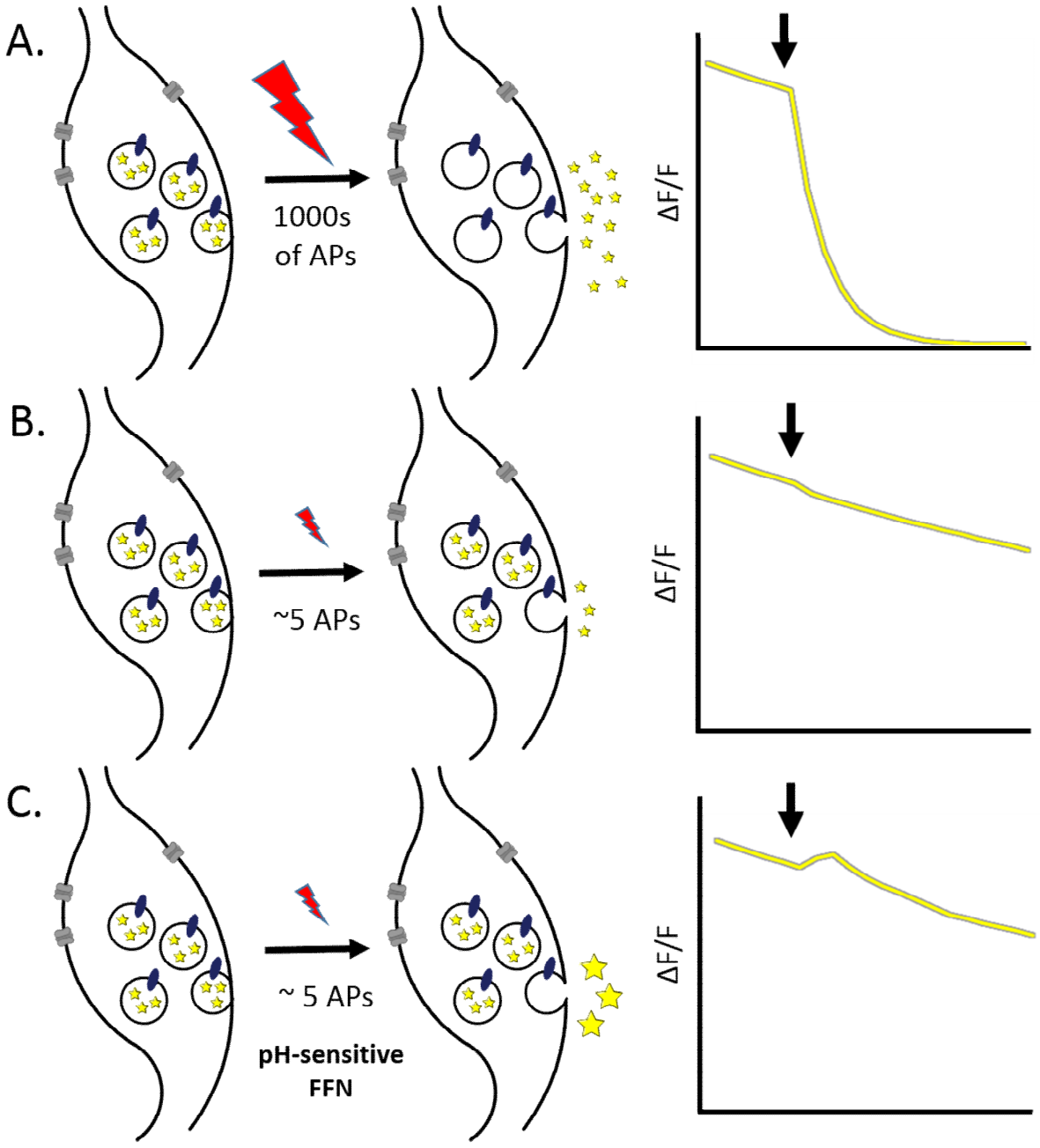

Figure 7. Measuring neurotransmitter release with FFNs. A) General mechanism for measuring tonic neurotransmitter release with FFNs. Loaded FFN can be detectably released when a significant portion of the vesicular stores eventually fuse with the plasma membrane after 1000s of electrical pulses (EPs), stimulation begins at arrow. This results in a significant decrease in the total fluorescence at the release site. B) Short bursts of EPs, which mimic DA phasic firing patterns, lead to only slight FFN release, and a small change in fluorescence (ΔF/F) compared to the total fluorescence left within the release site. Compared to the fluorescence rundown pre-stimulation present in all conditions (due to FFN102 washing away or leaking out), this change is difficult to measure. C) Using a pH-sensitive FFN that increases in fluorescence when released, a "FFN flash" can be created that results in a significant ΔF/F from only a few EPs.

For measuring neurotransmitter release, we have designed new FFNs capable of exhibiting changes in fluorescence that are sensitive enough for studying both phasic and tonic firing regimes (**Figure 7**). Tonic firing patterns are the relatively slow (2-10Hz for dopaminergic neurons[84]) and consistent pace-making activity that is prevalent in some neurons, and particularly important in the dopaminergic[85] and noradrenergic[86] systems. Experimentally, the tonic firing behavior can be studied using long electrical trains at a slow frequency (1-10Hz, 100s - 1000s of pulses). For these experiments, we look for a decrease in the fluorescence intensity of puncta over time, as the probe is consistently released from the puncta during a long train of activation (**Figure 7A**). Useful FFN probes for this purpose are excellent VMAT2 substrates and not pH-sensitive, so there is no conflicting increase in fluorescence signal. These probes are used in experiments aimed at studying differences in the extended behavior of individual release sites, such as reserve pool activation[87]. For studying phasic activity, however, the decrease in fluorescent signal caused by only a few action potentials using this type of FFN would not be sufficient when compared to the overwhelming fluorescent signal that remained in the puncta (**Figure 7B**). To overcome this challenge, and increase the signal to background fluorescence following phasic release, we further developed FFNs with enhanced functionality.

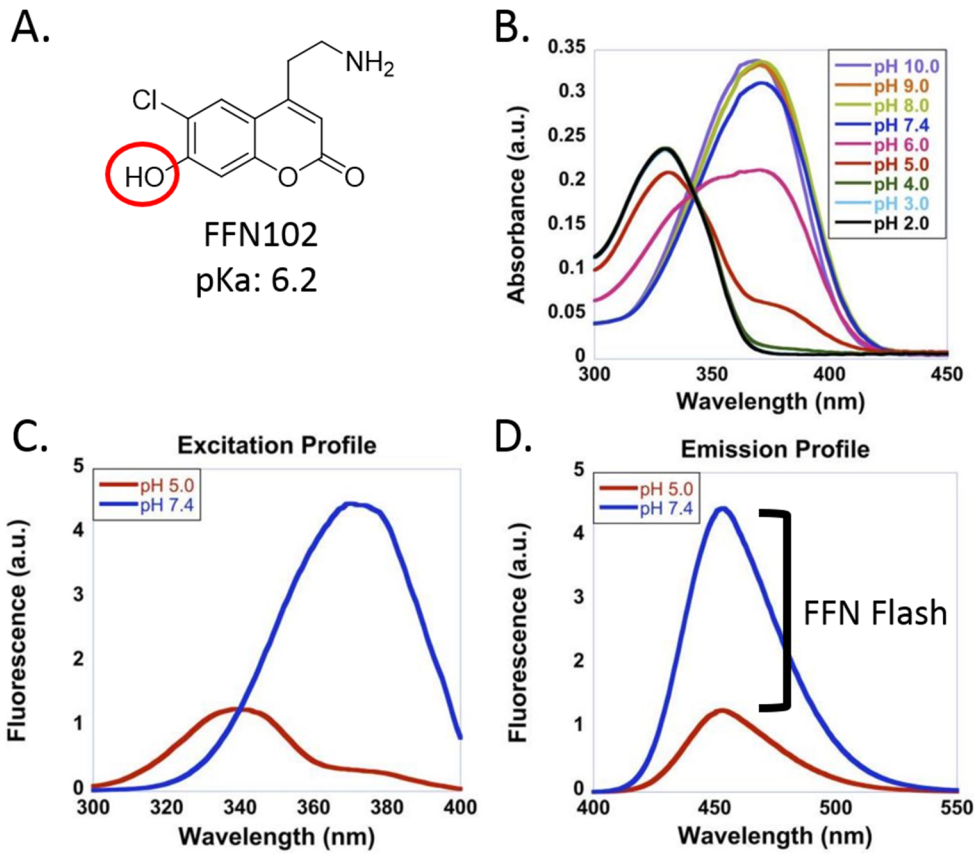

Figure 8. A) Structure of FFN102, the first DA-selective and pH-sensitive FFN. Highlighted in red, the 7-hydroxy group has a pKa (6.2) between the pH of the vesicles (~5.5) and extracellular space (~7.4). B) The protonated and deprotonated 7-hydroxyl have different spectrophysical properties, and therefore the absorbance of FFN102 is pH-sensitive. Based on the excitation (C) and emission (D) fluorescence profiles of FFN102, there is an observable increase in fluorescence when FFN is released from the vesicles, which we call the "FFN flash."

Phasic firing is a transient burst of activity that increases extracellular neurotransmitter concentrations to a higher level than basal tonic firing, but only for a very short time (2-10 spikes at ~20Hz for dopaminergic neurons[88]). Phasic firing of DA is important for its role in modulating post-synaptic targets, and changes in phasic firing patterns have been shown to influence behavioral conditioning[89]. Due to the relatively few vesicular fusion events that occur within a single burst window, newer generation FFNs were designed to harness the pH difference that exists between loaded vesicles and the extracellular space in order to generate a more significant change in fluorescence per vesicle fusion (**Figure 7C**)[82,90]. These FFNs utilize a fluorescent

coumarin structural core with a 7-hydroxy motif that is tuned to a pK_a between the vesicular lumen (~5.5) and the extracellular space (~7.4, **Figure 8**). There is a significant change in the fluorescence excitation spectrum between the protonated (vesicular) form and the non-protonated (extracellular) form (**Figure 8C**). As a result, when a vesicle loaded with this type of FFN fuses with the membrane and releases its content, there will be an increase in fluorescence emission, or "FFN flash" (**Figure 8D**). Being pH-sensitive, these FFNs also have the ability to report on the changes in vesicular loading that occur intracellularly, which can lead to modulations of quantal size. In Chapter 2, I will discuss the use of pH-sensitive FFNs in both of these functional applications in more detail.

1.5 Outlook

The success of a new tool in neuroscience is measured by its ability to fill a void between what neuroscientists want to know and how they can know it. Such research tools can prove something that was previously only speculated through correlation. While I described a few of the most common and well integrated methods of studying neurotransmission, the tools of the future are continually being developed. I believe that FFNs have the potential to be the next significant tool to make a valuable impact on how neuroscientists think about, and study, catecholamine neurotransmission. In this effort, this thesis will describe some examples of how chemical synthesis and FFN characterization has led to a novel FFN for the NE neurotransmitter systems, as well as how DA- and NE-FFNs can be effectively applied to build-upon, or complement, the short-comings of previous imaging technologies to study the regulation of neurotransmission in new ways.

1.6 Summary of Thesis Chapters

Chapter 2: Chapter 2 will explore the use of the pH-sensitive functionality of FFN102 to study the mechanisms that regulate changes in pre-synaptic plasticity, a component of neurotransmission. This includes using the FFN flash to quantitatively trace DA release, changes in the release probability of individual release sites, and changes in vesicular loading that can affect quantal size. While, we have successfully demonstrated use of the FFN102 to measure DA release and changes in vesicular loading, continued work is needed to measure the release probability from single release sites.

Chapter 3: Chapter 3 will summarize efforts to expand the scope of the FFN program to study neurotransmitter systems other than DA using fluorescent phenylpyridiniums. We identified a fluorescent phenylpyridinium, APP+, with excellent labeling properties for DA, NE, and serotonin. However, the properties of the probe were found to be ill-suited for measuring neurotransmitter release, and as a result, we concluded this class of compounds were not viable FFN leads.

Chapter 4: Chapter 4 will highlight the thought process, synthesis, and screening required to generate a novel NE-FFN lead, followed by its characterization and application in acute murine brain slices where it loads noradrenergic cell bodies and synapses, and enables stimulated NE release studies. This chapter also describes the application of this compound in a series of *in vivo* experiments, following the optimization of this experimental system for successful use with FFNs. This work opens the possibility for many exciting future FFN experiments studying the regulation of presynaptic neurotransmission *in vivo*, some of which are discussed in “Future directions”.

1.7 References

1. Azevedo, F. A. C. *et al.* Equal numbers of neuronal and nonneuronal cells make the human brain an isometrically scaled-up primate brain. *J. Comp. Neurol.* **513,** 532–41 (2009).

2. Cecala, A. L. Creating Modern Neuroscience: The Revolutionary 1950s. *Journal of Undergraduate Neuroscience Education* **11,** R1

3. PubMed. *Natl. Cent. Biotechnol. Inf.* (2015).

4. Caputi, A., Melzer, S., Michael, M. & Monyer, H. The long and short of GABAergic neurons. *Curr. Opin. Neurobiol.* **23,** 179–86 (2013).

5. Gao, Q., Yuan, B. & Chess, A. Convergent projections of Drosophila olfactory neurons to specific glomeruli in the antennal lobe. *Nat. Neurosci.* **3,** 780–5 (2000).

6. Matsuda, W. *et al.* Single nigrostriatal dopaminergic neurons form widely spread and highly dense axonal arborizations in the neostriatum. *J. Neurosci.* **29,** 444–53 (2009).

7. Costa, E. & Meek, J. L. Biosynthesis of Catecholamines and Serotonin in the CNS. *Annu. Rev. Pharmacol.* **25,** 329–340 (1973).

8. Erickson, J. D. & Eiden, L. E. Functional Identification and Molecular Cloning of a Human Brain Vesicle Monoamine Transporter. *J. Neurochem.* **61,** 2314–2317 (1993).

9. Eiden, L. E., Schäfer, M. K.-H., Weihe, E. & Schütz, B. The vesicular amine transporter family (SLC18): amine/proton antiporters required for vesicular accumulation and regulated exocytotic secretion of monoamines and acetylcholine. *Pflugers Arch.* **447,** 636–40 (2004).

10. Schuldiner, S., Shirvan, A. & Linial, M. Vesicular neurotransmitter transporters: from bacteria to humans. *Physiol. Rev.* **75,** 369–92 (1995).

11. Lawal, H. O. & Krantz, D. E. SLC18: Vesicular neurotransmitter transporters for monoamines and acetylcholine. *Mol. Aspects Med.* **34,** 360–72 (2013).

12. Südhof, T. C. & Rizo, J. Synaptic vesicle exocytosis. *Cold Spring Harb. Perspect. Biol.* **3,** a005637– (2011).

13. Sudhof, T. C. The synaptic vesicle cycle. *Annu. Rev. Neurosci.* **27,** 509–47 (2004).

14. Chapman, E. R. How does synaptotagmin trigger neurotransmitter release? *Annu. Rev. Biochem.* **77,** 615–41 (2008).

15. Beaulieu, J.-M. & Gainetdinov, R. R. The physiology, signaling, and pharmacology of dopamine receptors. *Pharmacol. Rev.* **63,** 182–217 (2011).

16. Strader, C. D., Fong, T. M., Tota, M. R., Underwood, D. & Dixon, R. A. F. Structure and Function of G Protein-Coupled Receptors. *Annu. Rev. Biochem.* **63,** 101–132 (1994).

17. Beaulieu, J.-M. & Gainetdinov, R. R. The physiology, signaling, and pharmacology of dopamine receptors. *Pharmacol. Rev.* **63,** 182–217 (2011).

18. So, C. H. *et al.* Calcium signaling by dopamine D5 receptor and D5-D2 receptor hetero-oligomers occurs by a mechanism distinct from that for dopamine D1-D2 receptor hetero-oligomers. *Mol. Pharmacol.* **75,** 843–54 (2009).

19. Carboni, E., Tanda, G. L., Frau, R. & Di Chiara, G. Blockade of the noradrenaline carrier increases extracellular dopamine concentrations in the prefrontal cortex: evidence that dopamine is taken up in vivo by noradrenergic terminals. *J. Neurochem.* **55,** 1067–70 (1990).

20. Agnati, L. F., Guidolin, D., Guescini, M., Genedani, S. & Fuxe, K. Understanding wiring and volume transmission. *Brain Res. Rev.* **64,** 137–59 (2010).

21. Mundorf, M. L., Joseph, J. D., Austin, C. M., Caron, M. G. & Wightman, R. M. Catecholamine release and uptake in the mouse prefrontal cortex. *J. Neurochem.* **79,** 130–142 (2008).

22. Sporns, O., Tononi, G. & Kötter, R. The human connectome: A structural description of the human brain. *PLoS Comput. Biol.* **1,** e42 (2005).

23. Nikolenko, V., Poskanzer, K. E. & Yuste, R. Two-photon photostimulation and imaging of neural circuits. *Nat. Methods* **4,** 943–50 (2007).

24. Farber, I. C. & Grinvald, A. Identification of presynaptic neurons by laser photostimulation. *Science* **222,** 1025–7 (1983).

25. Callaway, E. M. & Katz, L. C. Photostimulation using caged glutamate reveals functional circuitry in living brain slices. *Proc. Natl. Acad. Sci. U. S. A.* **90,** 7661–5 (1993).

26. Nagel, G. *et al.* Channelrhodopsin-2, a directly light-gated cation-selective membrane channel. *Proc. Natl. Acad. Sci. U. S. A.* **100,** 13940–5 (2003).

27. Seung, H. S. Neuroscience: Towards functional connectomics. *Nature* **471,** 170–2 (2011).

28. Huttenlocher, P. R. Synaptic density in human frontal cortex - developmental changes and effects of aging. *Brain Res.* **163,** 195–205 (1979).

29. Knott, G. W., Quairiaux, C., Genoud, C. & Welker, E. Formation of dendritic spines with GABAergic synapses induced by whisker stimulation in adult mice. *Neuron* **34,** 265–73 (2002).

30. Tang, G. *et al.* Loss of mTOR-Dependent Macroautophagy Causes Autistic-like Synaptic Pruning Deficits. *Neuron* **83,** 1131–43 (2014).

31. Nicoll, R. A. & Roche, K. W. Long-term potentiation: peeling the onion. *Neuropharmacology* **74,** 18–22 (2013).

32. Kobayashi, K., Manabe, T. & Takahashi, T. Presynaptic Long-Term Depression at the Hippocampal Mossy Fiber--CA3 Synapse. *Science (80-.).* **273,** 648–650 (1996).

33. Nicoll, R. A. & Schmitz, D. Synaptic plasticity at hippocampal mossy fibre synapses. *Nat. Rev. Neurosci.* **6,** 863–76 (2005).

34. Marttinen, M., Kurkinen, K. M., Soininen, H., Haapasalo, A. & Hiltunen, M. Synaptic dysfunction and septin protein family members in neurodegenerative diseases. *Mol. Neurodegener.* **10,** 16 (2015).

35. Koob, G. F. Dopamine, addiction and reward. *Semin. Neurosci.* **4,** 139–148 (1992).

36. Ressler, K. J. & Nemeroff, C. B. Role of norepinephrine in the pathophysiology and treatment of mood disorders. *Biol. Psychiatry* **46,** 1219–1233 (1999).

37. Picconi, B., Piccoli, G. & Calabresi, P. Synaptic dysfunction in Parkinson's disease. *Adv. Exp. Med. Biol.* **970,** 553–72 (2012).

38. Marcello, E., Epis, R., Saraceno, C. & Di Luca, M. Synaptic dysfunction in Alzheimer's disease. *Adv. Exp. Med. Biol.* **970,** 573–601 (2012).

39. Robinson, D. L. & Wightman, R. M. Rapid Dopamine Release in Freely Moving Rats. (2007). at <http://www.ncbi.nlm.nih.gov/books/NBK2575/>

40. Perry, M., Li, Q. & Kennedy, R. T. Review of recent advances in analytical techniques for the determination of neurotransmitters. *Anal. Chim. Acta* **653,** 1–22 (2009).

41. Sames, D., Dunn, M., Karpowicz, R. J. & Sulzer, D. Visualizing neurotransmitter secretion at individual synapses. *ACS Chem. Neurosci.* **4,** 648–51 (2013).

42. Bian, C., Zeng, Q., Xiong, H., Zhang, X. & Wang, S. Electrochemistry of norepinephrine on carbon-coated nickel magnetic nanoparticles modified electrode and analytical applications. *Bioelectrochemistry* **79,** 1–5 (2010).

43. Lu, L.-P., Wang, S.-Q. & Lin, X.-Q. Fabrication of layer-by-layer deposited multilayer films containing DNA and gold nanoparticle for norepinephrine biosensor. *Anal. Chim. Acta* **519,** 161–166 (2004).

44. Arbuthnott, G. W. & Wickens, J. Space, time and dopamine. *Trends Neurosci.* **30,** 62–9 (2007).

45. Peterka, D. S., Takahashi, H. & Yuste, R. Imaging voltage in neurons. *Neuron* **69,** 9–21 (2011).

46. Ehrenberg, B., Montana, V., Wei, M. D., Wuskell, J. P. & Loew, L. M. Membrane potential can be determined in individual cells from the nernstian distribution of cationic dyes. *Biophys. J.* **53,** 785–94 (1988).

47. Dragsten, P. R. & Webb, W. W. Mechanism of the membrane potential sensitivity of the fluorescent membrane probe merocyanine 540. *Biochemistry* **17,** 5228–40 (1978).

48. Fromherz, P. & Schenk, O. Voltage-sensitive fluorescence of amphiphilic hemicyanine dyes in a black lipid membrane of glycerol monooleate. *Biochim. Biophys. Acta - Biomembr.* **1191,** 299–308 (1994).

49. Akemann, W., Mutoh, H., Perron, A., Rossier, J. & Knöpfel, T. Imaging brain electric signals with genetically targeted voltage-sensitive fluorescent proteins. *Nat. Methods* **7,** 643–9 (2010).

50. Zou, P. *et al.* Bright and fast multicoloured voltage reporters via electrochromic FRET. *Nat. Commun.* **5,** 4625 (2014).

51. Siegel, M. S. & Isacoff, E. Y. A genetically encoded optical probe of membrane voltage. *Neuron* **19,** 735–41 (1997).

52. Branco, T. & Staras, K. The probability of neurotransmitter release: variability and feedback control at single synapses. *Nat. Rev. Neurosci.* **10,** 373–83 (2009).

53. Cooper, R. L., Harrington, C. C., Marin, L. & Atwood, H. L. Quantal release at visualized terminals of a crayfish motor axon: intraterminal and regional differences. *J. Comp. Neurol.* **375,** 583–600 (1996).

54. Augustine, G. J. How does calcium trigger neurotransmitter release? *Curr. Opin. Neurobiol.* **11,** 320–6 (2001).

55. Berridge, M. J. Neuronal Calcium Signaling. *Neuron* **21,** 13–26 (1998).

56. Südhof, T. C. A molecular machine for neurotransmitter release: synaptotagmin and beyond. *Nat. Med.* **19,** 1227–31 (2013).

57. Grynkiewicz, G., Poenie, M. & Tsien, R. A new generation of Ca2+ indicators with greatly improved fluorescence properties. *J. Biol. Chem.* **260,** 3440–3450 (1985).

58. Mank, M. & Griesbeck, O. Genetically encoded calcium indicators. *Chem. Rev.* **108,** 1550–64 (2008).

59. Chen, T.-W. *et al.* Ultrasensitive fluorescent proteins for imaging neuronal activity. *Nature* **499,** 295–300 (2013).

60. Betz, W. J. & Bewick, G. S. Optical analysis of synaptic vesicle recycling at the frog neuromuscular junction. *Science* **255,** 200–3 (1992).

61. Amaral, E., Guatimosim, S. & Guatimosim, C. Using the fluorescent styryl dye FM1-43 to visualize synaptic vesicles exocytosis and endocytosis in motor nerve terminals. *Methods Mol. Biol.* **689,** 137–48 (2011).

62. Kay, A. R. *et al.* Imaging Synaptic Activity in Intact Brain and Slices with FM1-43 in C. elegans, Lamprey, and Rat. *Neuron* **24,** 809–817 (1999).

63. Malenka, R. C. & Bear, M. F. LTP and LTD: an embarrassment of riches. *Neuron* **44,** 5–21 (2004).

64. Moulder, K. L. *et al.* Plastic Elimination of Functional Glutamate Release Sites by Depolarization. *Neuron* **42,** 423–435 (2004).

65. Ahmed, M. S. & Siegelbaum, S. A. Recruitment of N-Type Ca(2+) channels during LTP enhances low release efficacy of hippocampal CA1 perforant path synapses. *Neuron* **63,** 372–85 (2009).

66. Zakharenko, S. S., Zablow, L. & Siegelbaum, S. A. Visualization of changes in presynaptic function during long-term synaptic plasticity. *Nat. Neurosci.* **4,** 711–7 (2001).

67. Chen, G., Harata, N. C. & Tsien, R. W. Paired-pulse depression of unitary quantal amplitude at single hippocampal synapses. *Proc. Natl. Acad. Sci. U. S. A.* **101,** 1063–8 (2004).

68. Miesenböck, G., De Angelis, D. A. & Rothman, J. E. Visualizing secretion and synaptic transmission with pH-sensitive green fluorescent proteins. *Nature* **394,** 192–5 (1998).

69. Burrone, J., Li, Z. & Murthy, V. N. Studying vesicle cycling in presynaptic terminals using the genetically encoded probe synaptopHluorin. *Nat. Protoc.* **1,** 2970–8 (2006).

70. Voglmaier, S. M. *et al.* Distinct Endocytic Pathways Control the Rate and Extent of Synaptic Vesicle Protein Recycling. *Neuron* **51,** 71–84 (2006).

71. Granseth, B., Odermatt, B., Royle, S. J. & Lagnado, L. Clathrin-mediated endocytosis is the dominant mechanism of vesicle retrieval at hippocampal synapses. *Neuron* **51,** 773–86 (2006).

72. Sankaranarayanan, S., De Angelis, D., Rothman, J. E. & Ryan, T. A. The use of pHluorins for optical measurements of presynaptic activity. *Biophys. J.* **79,** 2199–208 (2000).

73. Balaji, J. & Ryan, T. A. Single-vesicle imaging reveals that synaptic vesicle exocytosis and endocytosis are coupled by a single stochastic mode. *Proc. Natl. Acad. Sci. U. S. A.* **104,** 20576–81 (2007).

74. Dreosti, E., Odermatt, B., Dorostkar, M. M. & Lagnado, L. A genetically encoded reporter of synaptic activity in vivo. *Nat. Methods* **6,** 883–9 (2009).

75. Bozza, T., McGann, J. P., Mombaerts, P. & Wachowiak, M. In Vivo Imaging of Neuronal Activity by Targeted Expression of a Genetically Encoded Probe in the Mouse. *Neuron* **42,** 9–21 (2004).

76. Namiki, S., Sakamoto, H., Iinuma, S., Iino, M. & Hirose, K. Optical glutamate sensor for spatiotemporal analysis of synaptic transmission. *Eur. J. Neurosci.* **25,** 2249–59 (2007).

77. Marvin, J. S. *et al.* An optimized fluorescent probe for visualizing glutamate neurotransmission. *Nat. Methods* **10,** 162–70 (2013).

78. Nguyen, Q.-T. *et al.* An in vivo biosensor for neurotransmitter release and in situ receptor activity. *Nat. Neurosci.* **13,** 127–32 (2010).

79. Muller, A., Joseph, V., Slesinger, P. A. & Kleinfeld, D. Cell-based reporters reveal in vivo dynamics of dopamine and norepinephrine release in murine cortex. *Nat. Methods* **11,** 1245–52 (2014).

80. Nguyen, Q.-T. *et al.* An in vivo biosensor for neurotransmitter release and in situ receptor activity. *Nat. Neurosci.* **13,** 127–32 (2010).

81. Gubernator, N. G. *et al.* Fluorescent false neurotransmitters visualize dopamine release from individual presynaptic terminals. *Science* **324,** 1441–4 (2009).

82. Rodriguez, P. C. *et al.* Fluorescent dopamine tracer resolves individual dopaminergic synapses and their activity in the brain. *Proc. Natl. Acad. Sci. U. S. A.* **110,** 870–5 (2013).

83. Björklund, A. & Dunnett, S. B. Dopamine neuron systems in the brain: an update. *Trends Neurosci.* **30,** 194–202 (2007).

84. Grace, A. A., Floresco, S. B., Goto, Y. & Lodge, D. J. Regulation of firing of dopaminergic neurons and control of goal-directed behaviors. *Trends Neurosci.* **30,** 220–7 (2007).

85. Grace, A. A. Phasic versus tonic dopamine release and the modulation of dopamine system responsivity: A hypothesis for the etiology of schizophrenia. *Neuroscience* **41,** 1–24 (1991).

86. Benarroch, E. E. The locus ceruleus norepinephrine system: functional organization and potential clinical significance. *Neurology* **73,** 1699–704 (2009).

87. Rizzoli, S. O. & Betz, W. J. Synaptic vesicle pools. *Nat. Rev. Neurosci.* **6,** 57–69 (2005).

88. Hyland, B. ., Reynolds, J. N. ., Hay, J., Perk, C. . & Miller, R. Firing modes of midbrain dopamine cells in the freely moving rat. *Neuroscience* **114,** 475–492 (2002).

89. Tsai, H.-C. *et al.* Phasic firing in dopaminergic neurons is sufficient for behavioral conditioning. *Science* **324,** 1080–4 (2009).

90. Lee, M., Gubernator, N. G., Sulzer, D. & Sames, D. Development of pH-responsive fluorescent false neurotransmitters. *J. Am. Chem. Soc.* **132,** 8828–30 (2010).

Chapter 2: FFN102: Functional Applications of the Dopamine-selective and pH-sensitive FFN

2.1 Introduction

2.1.1 Preface

A fluorescent false neurotransmitter (FFN) is designed to trace neurotransmitter release with a small fluorescent molecule that, using the native protein machinery, is loaded into neurons, packaged into synaptic vesicles, and then released. This concept for the FFN program was established well before I began my thesis research, and the work of my predecessors has contributed significantly to the development of this program. In the introduction to this chapter, I will briefly summarize the status of the FFN program at the time I started working on the project (2.1.2), and then describe how the progress made to that point led to the ambitious objectives we set for the next phase of the FFN program – exploring the utility of the first pH-sensitive FFN in a series of experiments designed to examine the mechanisms that regulate presynaptic neurotransmission release (2.1.3). I would like to thank all the members of the FFN team, from the laboratories of both Dr. Sames and Dr. Sulzer, as well as our collaborators over the years, for providing the intellectual groundwork on which my work was built.

2.1.2 Identification of the First pH-sensitive and DA-selective FFN, FFN102

My story begins with the identification and initial characterization of FFN102, the first prospective FFN that had been selected as a dual substrate for the dopamine (DA) plasma membrane transporter (DAT) and the vesicular monoamine transporter (VMAT2), based on a series of screening experiments performed in transfected HEK cells[1]. When tested *ex vivo* in the

striatum (an area rich with dopaminergic release sites) of acute murine brain slices, this probe demonstrated major improvements in DA-selectivity versus previous generation probes. As a DAT substrate, FFN102 was actively transported across the plasma membrane of DAT-expressing cells, in contrast to earlier generation FFNs that were substrates for only VMAT2, and as such, needed to be lipophilic enough to cross the plasma membrane, through non-specific passive diffusion[2]. The lower lipophilicity of FFN102 (LogD: -1.45, compared to FFN511 LogD: 1.0) resulted in much lower non-specific staining and higher colocalization with dopaminergic structures[1].

Additionally, as a 7-hydroxycoumarin, the fluorescence of FFN102 is pH-sensitive. The differences in electronic excitation of the protonated versus deprotonated states of the 7-hydroxycoumarin led to exploitable pH-dependent photophysical properties of FFN102. Designed with an electron withdrawing chlorine on the 6-position, the pKa of the 7-hydroxyl group on FFN102 is 6.2, between the vesicular (~5.5) and extracellular (~7.4) pHs[3]. The fluorescence excitation spectra of FFN102 is ratiometric with peaks at 340 nanometers for the protonated form and 370 nanometers for the deprotonated form (Chapter 1, **Figure 8**). When deprotonated, the electrons of the 7-hydroxyl group are more readily donated into the ring, decreasing the energy required to reach the excited state, which undergoes rapid acid-base equilibration and has a modified pKa around 1-2[4]. Therefore, the shared excited form only leads to a single fluorescence emission wavelength at 453 nanometers that has a pH-dependent magnitude (Chapter 1, **Figure 8**). Thus, the transition of FFN102 from the acidic environment of the vesicular lumen into the more neutral pH environment of the extracellular space should result in a significant increase in fluorescence. With its dual membrane transporter selectivity and new pH-sensitive functionality, FFN102 appeared to be a prime candidate to take the FFN program in

a new direction: exploring the utility of FFNs in studying the mechanisms involved in regulating neurotransmission in native systems.

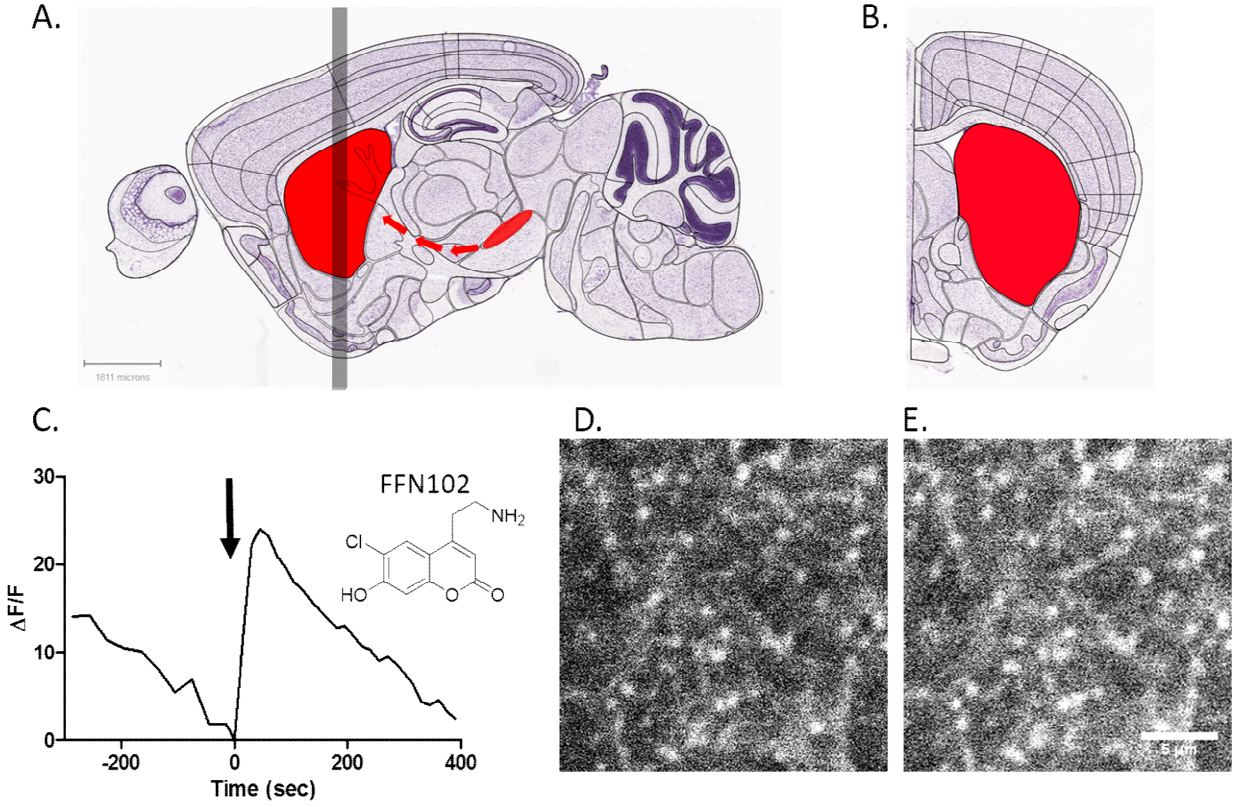

Figure 1. A representative example of the acute murine brain slice from the dorsal striatum and the changes in fluorescence that occur following electrical stimulation of loaded FFN102-treated acute murine brain slices[1] (Allen Brain Atlas). A) Sagittal mouse brain slice highlighting the dopaminergic cell bodies in the substantia nigra and where the acute slice was collected in the dorsal striatum that contains the dopaminergic release sites. B) The collected coronal slice. C) Plot that depicts the change in total fluorescence of the entire field of view over time, relative to initial fluorescence. At t=0 (marked by an arrow), 10Hz local electrical stimulation started and then continued for the remainder of the trace. The observed rundown in fluorescence prior to stimulation results from some FFN102 washing away or leaking out of the puncta. Panels B and C are images of a representative field the FFN102 fluorescence observed (D) right before initiation of the electrical stimulation, and E) at the time of maximum fluorescence increase: 50sec after electrical stimulation. This peak in fluorescence represents the fluorescent "flash" that occurs when FFN102 transitions from the acidic environment of the vesicle to the extracellular space.

In the 2013 paper initially characterizing FFN102, its new functionality was briefly explored in acute murine brain slices[1]. Specifically, the dorsal striatum of acute murine brain slices was loaded with FFN102 and the resultant fluorescence was measured before and during extended electrical stimulation (1-10Hz for 1000s of pulses – a firing pattern comparable to tonic

neuronal firing). Prior to the initiation of the electrical stimulation, a punctate pattern of fluorescence was observed within the dopaminergic projections of this brain region, as confirmed by pharmacological DAT inhibition, colocalization with established dopaminergic markers, and DAT-knockout experiments[1]. Following the local electrical stimulation, known to trigger vesicular DA release into the extracellular space, a significant increase in fluorescence (approximately 20 percent) was observed throughout the whole frame[1]. This change in diffuse fluorescence was consistent with a portion of the FFN102 within vesicles (visual punctate fluorescence) being released into the less acidic environment of the extracellular space. As seen in **Figure 1**, the timeline for the increase in fluorescence (the fluorescent "flash") started instantly after stimulation and then peaked approximately 1 minute following 10 hertz electrical stimulation, before gradually decreasing. Note that the slow decrease in fluorescence observed pre-stimulation ("rundown" fluorescence) was thought primarily to result from nonspecific staining of the FFN probe washing away, or some degree of leaking from the puncta.

The fluorescence remaining in the FFN-loaded dopaminergic release sites following electrical stimulation was also measured. After subtracting the increases of the FFN flash in the background, similar (although slower) destaining kinetics of the release sites were observed with FFN102 as compared with FFNs that were not pH-sensitive[5]. Therefore, it was concluded that the electrical stimulation triggered the release of FFN102 from acidic vesicles in the dopaminergic projections, which led to increases in diffuse fluorescence in the extracellular space and the eventual depletion of all FFN102 from a sub-set (10-20%) of dopaminergic release sites[1]. These initial experiments validated the concept that a pH-sensitive FFN was capable of generating a detectable fluorescent flash in a functional model of neurotransmission.

2.1.3 Rationale for Applying Functional FFNs to Study Presynaptic Neurotransmission Regulation

Essentially, at the start of my thesis research, we had learned that the pH-sensitive FFN102 could generate observable changes in fluorescence in electrically stimulated acute brain slices *ex vivo*, but not much more. To put into perspective the subsequent research to be described later in this chapter, I will first describe the rationale for using FFN102 in the functional experiments we performed. Additionally, while the specific experiments described in this chapter relate to dopamine (DA) specific neurotransmission, due to the specificity of FFN102, the rational for using FFNs for these type of presynaptic regulation experiments can be applied to other functional, pH-sensitive FFNs, both current and those in development. This aligns well with the overall objective behind the FFN program, which is developing, and using, novel fluorescent research tools to support the study presynaptic neurotransmission regulation in a wide range of neurotransmission pathways, with a sensitivity and specificity not before possible.

Initially, we sought to further characterize the FFN release phenomenon in murine brain slices following tonic stimulation, in which we observed full destaining of only a small percentage (10-20%) of fluorescent puncta in the dopaminergic projections loaded with FFN102, or FFN200 (a pH-insensitive DA-FFN), after the local electric stimuli[1]. The remaining "silent puncta" (80-90%), which did not release all of their fluorescent tracer, did not show statistically significant decreases in fluorescence over the long trains of electrical stimulation (1-10Hz for 1000s of pulses) compared to the "rundown" in fluorescence observed in non-stimulated puncta. We sought to determine whether it was possible to use the FFN102 pH-sensitive "flash" to further characterize this heterogeneity in puncta release, and explore whether heterogeneity of puncta was also present during physiologically relevant phasic burst firing patterns. In such an

experimental design, highlighted in **Figure 7C** of Chapter 1, we would measure the increase in fluorescence after only a few electrical pulses (EPs) delivered at a higher frequency (>20Hz), a frequency similar to the patterns commonly observed during DA phasic release[6,7].

Phasic firing patterns are a particularly important means for regulating DA presynaptic neurotransmission, because they provide a mechanism of modulating the target neurons of the dopaminergic signal. During tonic activity, the DA release sites deliver a signal more similar to "wired transmission" (discussed in more detail in Chapter 1), as the DAT activity near the synapse is capable of fully recycling extracellular DA before the following pulse[8]. During phasic firing, however, released DA saturates the available DAT and there is an increased degree of DA spill-over that can reach multiple postsynaptic targets[9,10]. Depending on frequency of the firing events, the spread of the released DA can be controlled. The importance of this type of "volume transmission" generated by phasic firing patterns is supported by evidence that shows DA receptor and transporter expression located extrasynaptically[11,12]. In living animals, DA burst firing is related to the response of sensory[13] and conditioned[14] stimuli. Therefore, animal behavior changes are directly related to dopaminergic firing patterns presynaptically, which not only affect the strength, but also the targets of a particular regulatory signal. It is our hope that pH-sensitive FFNs would be able to trace these changes in extracellular dopamine following a phasic burst firing event.

Another potential application of functional FFNs would be to study the release probability from individual release sites – a second means of presynaptic neurotransmission regulation. Neurotransmitter-filled vesicle fusion is a stochastic event that occurs after EPs arrive at the release site with a certain probability. That release probability can change over time: either increasing (potentiation) or decreasing (depression) depending on a still growing list of identified

conditions. Additionally, the release probability of synapses, even along the same axon[15], are generally heterogenous[16–18]. Potential explanations for this heterogeneity include the variabilities in the postsynaptic target[19], the size and replenishment rate of the vesicular pool[20], or differential presynaptic protein expression levels that can lead to synaptic plasticity[21,22]. Current optical tools for estimating this probability at individual release sites primarily include the use of a pH-sensitive GFP (e.g. VGLUT-pHluorin[23]) or vesicular dye (e.g. FM1-43[24,25]). The use of vesicle-labeling dyes is limited in its application due to poor change in fluorescence relative to total fluorescence (ΔF/F). As such, the use of dyes, like FM1-43, for measuring release probability has been limited to estimations based on the release caused from a train of many EPs[25]. On the other hand, vesicular-linked pHluorins can have substantial ΔF/Fs, and have been used to image single vesicular fusion events in cell culture, enabling the direct determination of the probability of vesicular fusion[23]. However, application of pHluorins in more intact experimental systems, such as acute murine brain slice or *in vivo*, remains problematic.

It is also possible with a pH-sensitive FFN to trace changes in VMAT2 activity and therefore measure the amount of neurotransmitter loaded and released per vesicle (quantal size). This is another important presynaptic mechanism for regulating plasticity[26], and is a regulatory mechanism that cannot be studied using pHluorins and vesicular dyes. Unlike either of the two previous optical techniques, FFNs are substrates of VMAT2 and therefore have the potential to trace concentration changes in loaded vesicles at individual release sites, as well as the amount of final content that gets released. In addition to changes in release probability, neurons have been shown to regulate the amount of neurotransmitter released and strength of a particular synaptic connection through quantal size[27]. While some synaptic connections lead to neurotransmitter-receptor saturation, there is growing evidence that other connections do not naturally have

saturated receptors and increases in quantal size can directly lead to changes in the strength or duration of postsynaptic signaling[28]. This is potentially even more important for dopaminergic release sites that can participate in volume transmission, as described above. This "synaptic scaling" is thought to work in combination with firing rate changes to allow for the multiplicative control of presynaptic regulation[29,30], and to be an important controlling mechanism that changes during chronic perturbations of normal conditions[27,29,31].

The mechanisms behind how quantal release is controlled, however, are still poorly understood. It is possible to regulate release after fusion, through controlling the duration of the vesicle fusion pore during a "kiss and run" event, and thereby preventing full neurotransmitter release[32]. This type of neurotransmission regulation has been shown to be especially prevalent with DA release[33,34]. Other regulatory methods are thought to occur before fusion and involve changes in the dynamics of neurotransmitter concentrations between the plasma and vesicular membranes. These mechanisms, with particular emphasis on the DA system, will be explored in more detail in section 2.2.7.

In summary, following the initial characterization of FFN102, a pH-sensitive fluorescent probe with dual DAT/VMAT2 activity, we designed a series of experiments to explore the utility of FFN102 in studying three potential mechanisms of dopaminergic presynaptic regulation: burst firing patterns, release probability, and quantal size at individual dopaminergic release sites. The following Results and Discussion will describe some of the interdependent steps taken along the way to accomplish these goals, and highlight some of the hurdles that still need to be overcome.

2.2 Functional Experiments Examining DA Release - Results and Discussion

2.2.1 Applying FFN102 to Study the Paradoxical Depression Effects of Cocaine and Methylphenidate on DA Release

The next step to validating the potential functional application of FFN102, and the beginning of my thesis work, was to further characterize the increase in fluorescence observed following an extended tonic stimulation. Our goal was to determine whether this FFN fluorescent flash was quantitatively related to DA release, by comparing changes in the flash to changes observed with established methodologies to assess DA release. Specifically, in a collaborative effort with Dr. Nicola Mercuri (University of Rome), we had the opportunity to explore whether the FFN102 flash directly correlated with DA release following the pharmacological modulation of dopaminergic neurotransmission in acute brain slices as measured by electrochemistry, microdialysis and FFNs in tandem[35].

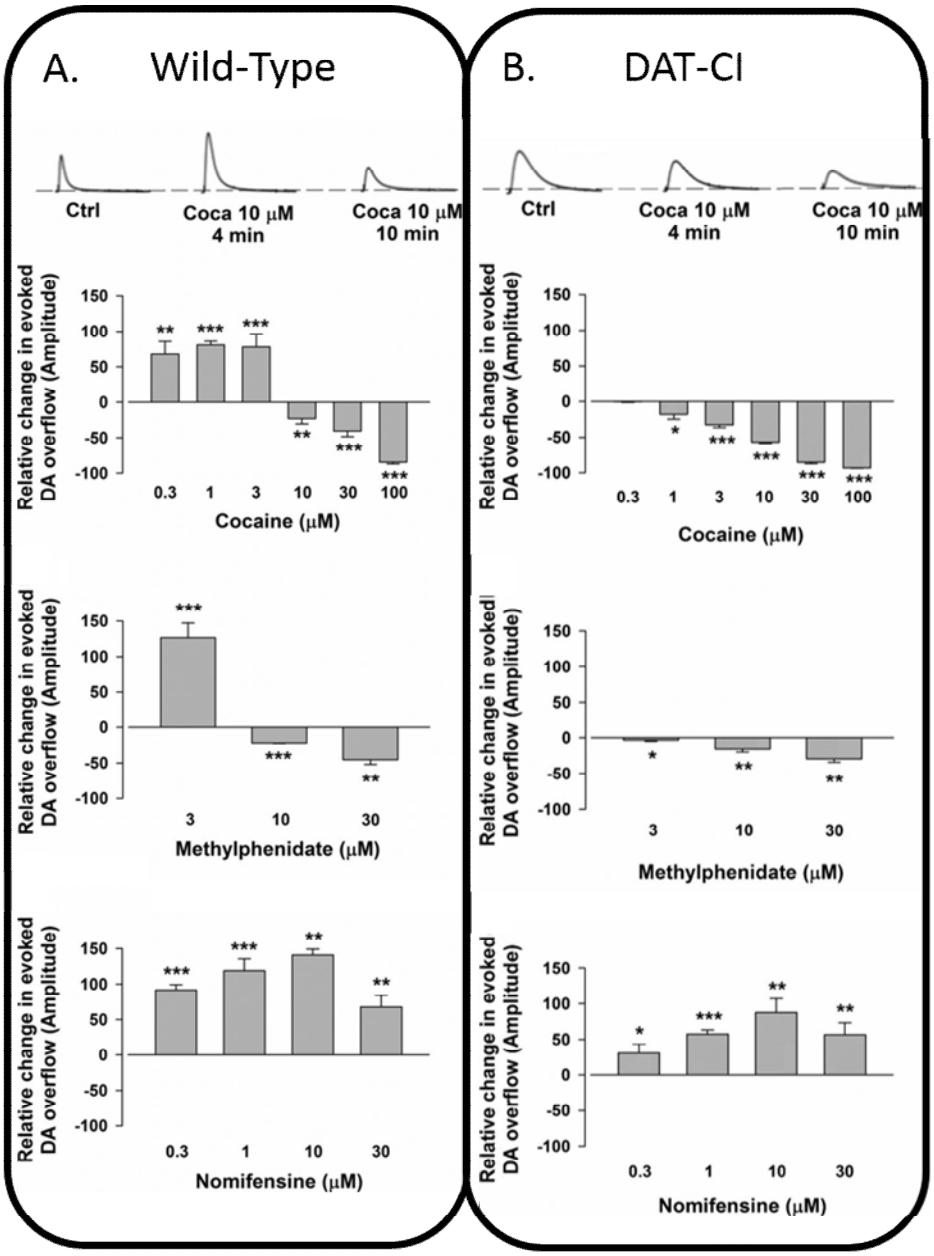

Figure 2. Constant potential amperometry (CPA) recordings of DA release under varying concentrations with 3 different DAT-inhibitors, cocaine, methylphenidate, and nomifensine. This set of experiments was conducted in wild-type mice (Panel A) and mice with a mutation in DAT (Panel B) that caused it to be insensitive to inhibition from cocaine (DAT-CI). The top panels depict the time delay for depression of DA release as measured by CPA following 10μM cocaine administration. The next two figures show the effect of increasing concentrations of cocaine or methylphenidate on DA release. Lower concentrations of cocaine and methylphenidate in WT mice led to an increase in DA by blocking DA reuptake, but at higher concentrations they led to a decrease through an unknown mechanism. In DAT-CI mice, all concentrations led a decrease in DA release, as these compounds can no longer inhibit DA reuptake in the modified DAT. Treatment with the DA inhibitor nomifensine (final figures) led to an increase in DA at all concentrations, which suggests that this effect is not common to all DAT-inhibitors.

Importantly, this experimental design also allowed us to use FFN102 to explore the paradoxical depression effects that cocaine and methylphenidate have on DA release when applied at high concentrations (≥10μM) in the striatum of acute murine brain slices. Both of these neuropharmacological agents are relatively potent inhibitors of DAT (K_i's: cocaine ~200nM, methylphenidate ~50nM), which typically lead to increased extracellular DA concentrations through inhibition of DA reuptake[36]. However, at high concentrations of both of these agents, our collaborators observed an unexpected depression in DA release. This depression was observed using both constant potential amperometry (CPA) (**Figure 2**) and microdialysis (see publication[35]). The lack of DAT-mediation of this effect was demonstrated when this depressive effect was still observed in mice expressing a cocaine-insensitive DAT mutant (**Figure 2**, panel B), and not when using an alternative DAT inhibitor (nomifensine) (**Figure 2**, lower panels). Additionally, our collaborators did not observe any modification of the field excitatory postsynaptic potentials in the striatum, suggesting that this effect was not due to the anesthetic-like effect of cocaine[37]. This was supported by the fact that methylphenidate, which is not known to have anesthetic effects, also led to depression of DA release.

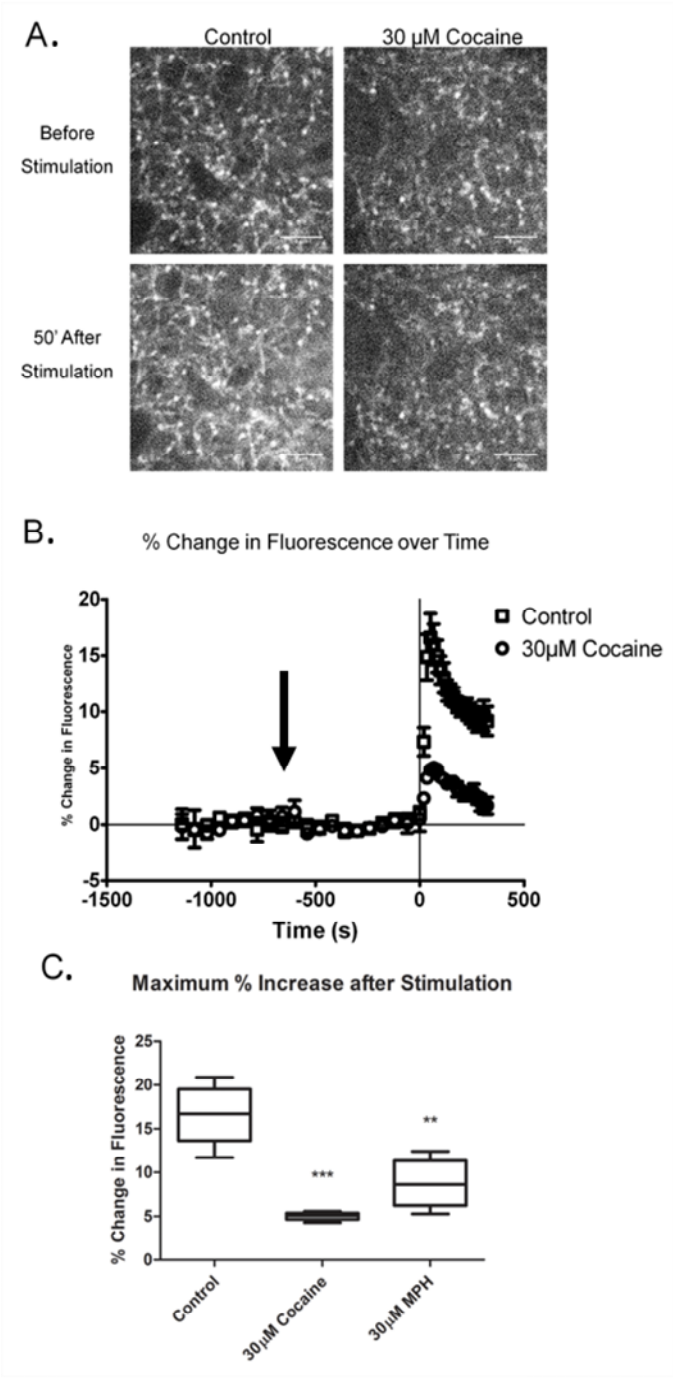

Figure 3. A) Representative images of FFN102-labeled dopaminergic projections in the dorsal striatum of acute murine brain slices before and after local electrical stimulation in untreated, or 30µM cocaine-treated conditions. We observed significantly less fluorescence increase following electrical stimulation in the presence of cocaine. B) Time course of change in normalized FFN102 fluorescence during a washing period, a cocaine treatment period (starting at arrow), and electrical stimulation period (10Hz local stimulation, starting at t=0). No change in rate of fluorescence decay was observed prior to electrical stimulation, with or without cocaine treatment. Following electrical stimulation, the maximum magnitude of the FFN flash occurred at 50sec. C) Significant reductions in the FFN flash were observed in both the 30µM cocaine (70%) and 30µM methylphenidate (MPH, 48%) treated conditions.

In an effort to further understand the mechanism causing depressed DA release, FFN102 was used in high-cocaine experimental conditions, and the effects on the tracer inside the neuron before stimulation, and on the FFN flash caused after stimulation were observed. For these experiments, FFN102 (10μM) was loaded into dopaminergic projections of the striatum of acute murine brain slices over 30 minutes. FFN102 was then imaged for 10 minutes during a washing period, followed by another 10 minutes in the presence or absence of 30 micromolar cocaine (or methylphenidate). Finally, the acute slice was locally stimulated by a bipolar electrode for 5 minutes at 10 hertz (**Figure 3**). In this experiment, we observed that there was no significant change in the decay of FFN102 fluorescence during washing, with or without cocaine (−1.17 ± 0.54 w/o cocaine, −0.98 ± 0.11 w cocaine change/minute; mean ± S.E.; 2-3 slices per animal, 5 different animals/condition; non-significant, one-way ANOVA) (**Figure 3B**). However, we did observe a significant decrease in the maximal ΔF/F after electric stimulation. Treatment with cocaine resulted in a 70 percent reduction of the FFN flash ($p < 0.0001$, one-way ANOVA), while methylphenidate resulted in a 48 percent reduction ($p < 0.0001$, one-way ANOVA) compared to untreated conditions (**Figure 3C**). Therefore, it is probable that the DA loaded into release sites remained unaffected by the cocaine treatment, since otherwise there would have been an expected change in the decay rate of FFN102 fluorescence pre-stimulation due to leaking of FFN102 from the vesicles or due to the vesicular pH gradient being decreased. More likely, the reduction in FFN102 flash (correlating with the reduction in DA release) was due to a reduction in the number of vesicles fusing with the plasma membrane following electrical stimulation.

This experiment was exciting for the FFN program for two reasons. First, relative changes in the FFN flash mirrored the increases of extracellular dopamine concentrations

measured with established methodology. This suggested that the magnitude of the flash has a direct relationship with the amount of vesicular DA being released. Second, this is the first example of using a pH-sensitive FFN to provide insights into the mechanism behind an unknown biological phenomenon. There is currently no other technique applicable to acute murine brain slices that would have been able to generate the same data, and demonstrate that DA release was reduced, but the vesicular loading of individual dopaminergic release sites remained unchanged under these conditions.

2.2.2 Applying FFN102 to Study DA Release under Phasic Firing Conditions

Satisfied that the FFN flash had a direct correlation with DA release, we next explored using FFN102 to trace DA release under phasic firing conditions. For dopamine, *in vivo* phasic firing patterns are usually bursts of 2-10 spikes that occur around a frequency of 20 hertz[6]. To mimic this pattern in acute slice, we chose to electrically stimulate at 25 hertz with 5 EPs. Previous observations of FFN102's flash under tonic firing conditions (10Hz) showed that peak fluorescence was not reached until 40-50 seconds after stimulation, or 400-500 EPs. Considering that the maximal ΔF/F achieved during that time frame was only approximately 20 percent, there was concern that a hundred-fold reduction in the number of EPs might result in an insignificant ΔF/F signal to noise ratio. Nevertheless, acute murine brain slices were loaded with FFN102 using the same method described above (2.2.1), but electrically stimulated under the new phasic conditions.

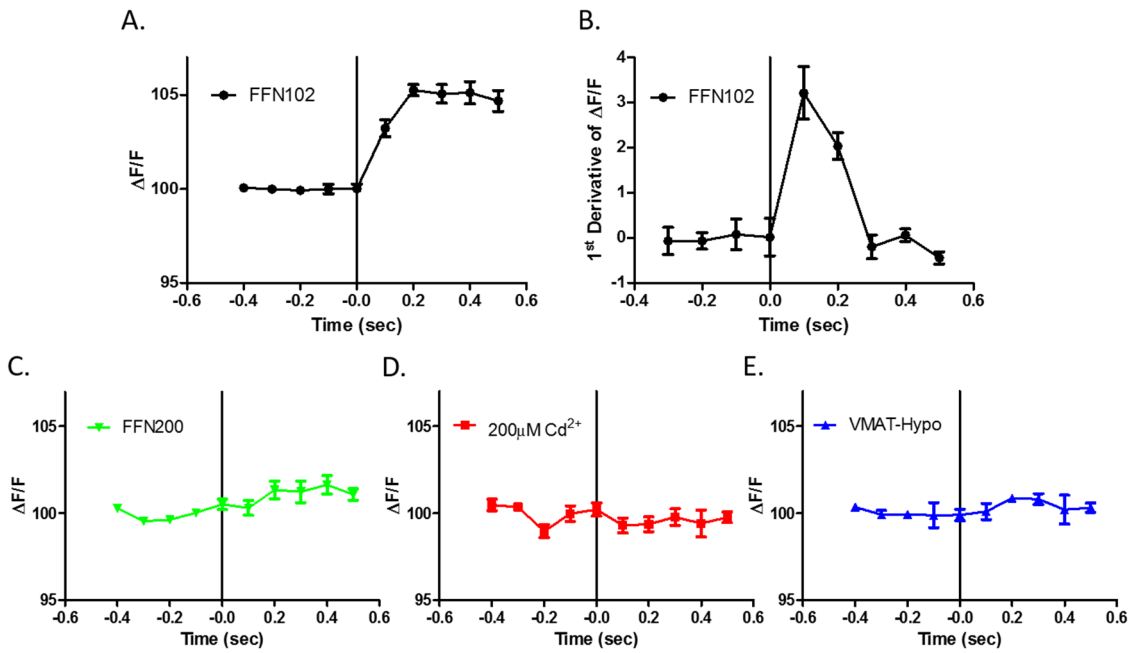

Figure 4. Change in DA-FFN fluorescence after application of 5 electrical pulses (5EPs) at 20Hz under varying conditions. A) Normal conditions with FFN102 (pH-sensitive), resulting in a 5.3% maximum increase. B) The first derivative of the fluorescence change of FFN102 release highlighting the increased release of the first time point (first 2 EPs) compared to the following ones. C) Normal conditions with FFN200 (not pH-sensitive), resulting in a 1.3% maximum increase. D) FFN102 flash during inhibition of calcium channels with cadmium ions (200μM Cd^{2+}), resulting in no significant increase. E) FFN102 flash in mice that express 5% VMAT2 (VMAT-hypomorphs), resulting in a 0.9% maximum increase.

For these experiments, the imaging rate was dramatically increased from an image collected every 10's of seconds to one every 100 milliseconds (10Hz). This was achieved by scanning a smaller area (5x5μm) with a shorter pixel dwell time, but with the same pixel resolution as before. The increased imaging rate allowed for the collection of more detailed temporal information about the kinetics of the FFN flash. Under these imaging and stimulation conditions, we observed a significant increase (5.3±0.2) in fluorescence attributed to the FFN flash, as measured by an average ΔF/F measured over the whole 5x5 micron frame (**Figure 4A**) (2-3 slices per animal, 3 animals). Excitingly, the ΔF/F from only 5 EPs was already a third of the maximum ΔF/F achieved from 500 EPs. Also interestingly, compared to extracellular DA levels after release, this fluorescence increase was relatively long-lasting, and persisted for

seconds before returning to basal levels. This was most likely due to the fact that even after reuptake of the probe by DAT into the cell, FFN102 continued to add to the increase in total fluorescence until the fluorophore was reloaded into acidic vesicles. Additionally, protonated FFN102 from other areas of the striatum could have been diffusing into the field of view from other release sites. This is consistent with the relatively slow loading time of FFN102 by DAT compared to DA.

In an effort to further characterize the fluorescence increase observed following phasic burst firing, we next repeated these experiments under a series of varied conditions: using a DA-FFN that is not pH-sensitive (FFN200); inhibiting calcium channels with cadmium ions; or using a mouse line with low expression of VMAT2 (**Figure 4**)[38,39]. First, using FFN200 under the same experimental conditions led to a ΔF/F increase of only 1.3±0.5 percent (**Figure 4C**) (2-3 slices per animal, 3 animals). We believe this increase was due to the "inner filter effect," which occurs when fluorescent dyes are highly concentrated, where the dye is not equally excited throughout the sample, or the emission is partially quenched internally[40]. Therefore, at the high concentrations found in loaded vesicles, the fluorescence signal was no longer directly related to fluorophore concentration. We believe that the 1.3 percent increase is representative of the degree to which the inner filer effect was decreasing the overall FFN fluorescence within the release sites, an effect that was observable without a pH-sensitive FFN. It is likely that the inner filter effect was also responsible for a small portion of the ΔF/F observed with FFN102, but the majority of the fluorescent signal was resulting from the pH-sensitive functionality.

Next, we completely blocked vesicular release by inhibiting calcium channel function using 200 micromolar cadmium ion conditions ($CdCl_2$). This resulted in a complete elimination of the FFN flash (**Figure 4D**). This suggests that none of the increase in ΔF/F was due to an

artifact of the electrical stimulation protocol, and that fluorescent changes were only occurring in combination with vesicular fusion.

Lastly, we repeated the burst firing stimulation in a mouse line that expresses VMAT2 at 5 percent the normal level in wild-type mice (VMAT2-hypomorphs)[39]. Note that in the VMAT2-hypomorphs, measured DA release was unexpectedly high compared to what might have been expected based on only 5 percent VMAT2 expression. The DA release in this mouse line was approximate 30% of that compared to wild-type littermate mice. In quantifying the FFN102 flash, we measured a similar reduction DA release as measured by the ΔF/F observed in this mouse line (0.9±0.2, mean ± SEM, 2-3 slices per animal, 3 animals) (**Figure 4E**. This represents an 83 percent reduction compared to the ΔF/F observed in wild-type littermate mice. This indicated that the FFN102 flash was dependent on FFN102 being loaded into vesicles through VMAT2. Additionally, the degree of correlation between VMAT2-dependent vesicular DA loading and observed DA release was comparable to VMAT2-dependent vesicular FFN102 loading and the resulting magnitude of the FFN flash. By experimenting with different conditions during the burst firing experiments, we concluded that the FFN flash from FFN102 was dependent primarily on increases in fluorescence due to changes in pH when FFN-loaded vesicles fused with the plasma membrane, and was not an artifact of electrical stimulation. Additionally, vesicular loading was dependent on VMAT2 active transport.

2.2.3 Applying FFN102 to Observe Single Action Potentials

Even when imaging at 10 hertz, we observed that the first frame imaged after the initiation of the stimulation already had a significant fluorescent increase. In fact, over 50 percent of the total ΔF/F generated over the 5 EPs occurred within the first frame (100ms, **Figure 4B**), after only 2 EPs. This is consistent with the timeframe of DA release patterns in acute murine

brain slices. Dopaminergic projections in the striatum of acute coronal slices are severed from the cell bodies in the substantia nigra, and are therefore inactive, with no endogenous tonic firing in this experimental system. Therefore, using cyclic voltammetry (CV) to measure DA release, stimulation from one EP results in a massive release of dopamine, while subsequent EPs release very little[41]. If the dopaminergic projections were allowed to rest for over a minute, the massive first pulse release phenomenon is restored. It is likely that this same phenomenon could be observed with the FFN102 flash if it were quantitatively tracing DA release. Therefore, our next objective was to explore whether it was possible to image the FFN102 flash after just one EP using even faster imaging conditions.

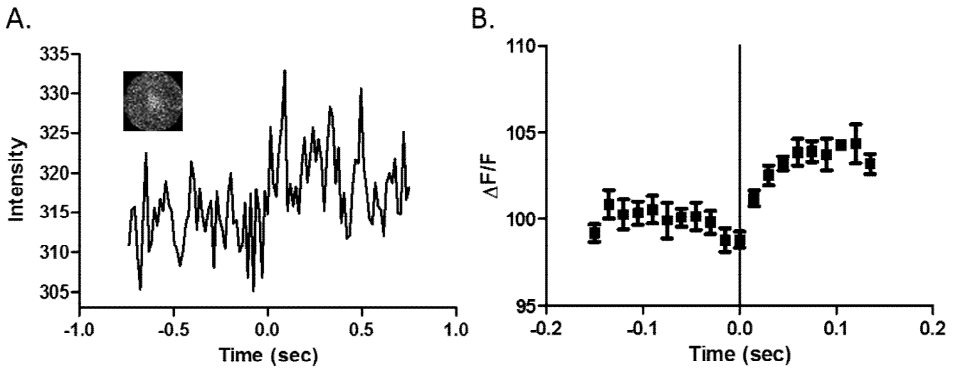

Figure 5. Timeframe of FFN flash in murine acute brain slices following stimulation with a single electrical pulses (EP). A) Representative individual trace of the fluorescence change in an ~2μm^2 field of view centered on one FFN102-labeled release site (inset) after electrical stimulation from 1 EP (t=0). B) Average of all traces resulted in a significant increase (4.0%) that peaked after 60ms.

The next set of experiments were conducted using the same FFN loading conditions as described previously (2.2.1), but imaged using a spiral scanning image collection method of an even smaller area (2x2μm) centered around a single puncta. Instead of imaging in a square pattern similar to a printer, a spiral scan more efficiently images a circular field of view through spirals of decreasing size. These temporal improvements allowed us to further increase our imaging rate to 67 hertz (15ms per frame). An electrical stimulus of just one EP was then applied

locally and the change in fluorescence of the whole frame was measured. From these experiments we observed a significant flash with a ΔF/F of 4.0±0.7 percent from one EP (**Figure 5**), only 25 percent smaller than the magnitude observed with 5 EPs. This magnitude of ΔF/F is consistent with our observations of DA release in the acute brain slice, however, the peak ΔF/F was not reached until time point 4, or 60 milliseconds following the stimulation. This suggests that a large portion of the flash measured could have been generated by FFN102 release occurring outside of the field of view and then diffusing into the area being measured. Nevertheless, while the average fluorescent flash appeared delayed, there was evidence that for certain puncta the increase in fluorescence was almost immediate. The relationship between the imaged puncta and the time delay will be explored in more detail in 2.2.5.

2.2.4 Applying FFN102 to the Measurement of DA-release Paired Pulse Ratios

Excited by the relatively large ΔF/F of the flash achievable from one EP, we wanted to further use this parameter to explore the paired pulse phenomenon observed with DA release in the striatum. While an initial electrical pulse results in a large release of dopamine, a second "chase" pulse can be applied, the response magnitude of which increases logarithmically with the increase in the interval time[41]. After 60 seconds, the subsequent pulse results in an equivalent amount of DA release. To measure if the paired pulse effect was also observable with the FFN flash, acute murine slices were collected from individual animals and distributed evenly for electrochemical and optical measurements. I would like to thank Dr. Danny Korostyshevsky, a laboratory technician in Dr. Sulzer's laboratory for his help with performing the CV recordings.

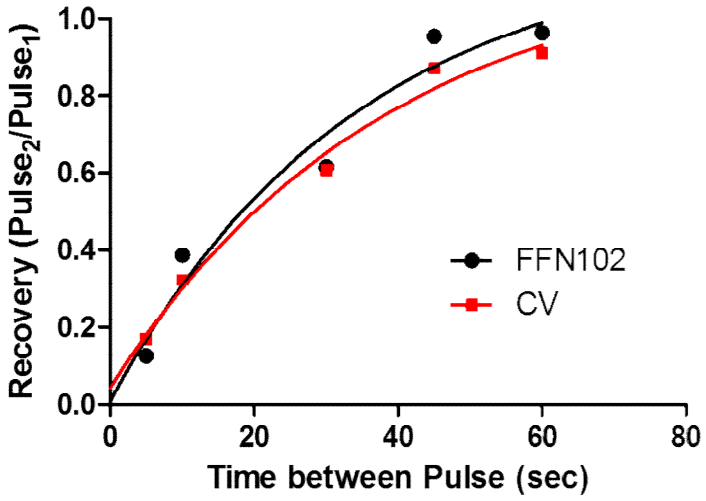

Figure 6. Ratio of the DA release between the first electrical pulse and the subsequent paired pulse depending on the time interval between them. Resulting paired pulse rate of DA-release recovery as measured by the FFN102 flash or cyclic voltammetry (CV). The $T_{1/2}$'s for each are similar – FFN flash: 34s, CV: 38s.

Coronal acute murine brain slices of the striatum were cut in half and equally separated for optical measurements with two-photon microscopy or electrochemical recordings with CV, which were then run in tandem. Simultaneous imaging and recording within the same slice would have been ideal, but was problematic due to the effects of the laser interfering with the recording electrode of CV. For measurements, each half was treated equally, which included using the same solutions, loading FFN102 in parallel (10µM for 30min), and initiating the stimulation at the same time for both halves. Five pairs of pulses with varying delay intervals were delivered to each slice, and then the order was reversed and the process repeated in the next slice. The resulting paired pulse ratios of DA release as measured by CV or optical fluorescence, were then plotted depending on the interval lengths between the pulses (**Figure 6**). We observed an almost identical trend in measured DA release between the two methods, and very similar kinetics for the time required to restore DA release ($T_{1/2}$'s – CV: 38s, FFN Flash: 34s). This

further supports the conclusion that the FFN flash relates directly to DA release and can be used as an optical measure of this parameter.

Importantly, it was noted that in the optical measurements of DA release the maximum ΔF/F of the FFN102 flash throughout the set of pulses within the same slice decreased steadily over time. While the paired pulse ratio of the last set of EPs still matched well with the CV data, the relative magnitude of the ΔF/F compared to the first set of EPs was greatly diminished. Unlike DA which undergoes rapid reuptake through DAT, FFN102 is less efficiently recycled, potentially due to the weaker binding affinity ($K_{m\text{-}apparent}$: ~4.2μM), and slower uptake kinetics (as inferred from loading kinetics)[1]. Combined with the lack of internal biosynthetic protein machinery that can regenerate lost stores of FFN102, unlike DA, the overall amounts of vesicular FFN102 must steadily decrease after each pulse more rapidly than that observed with DA in acute brain slice. In fact, in the CV data from these experiments, it was observed that after the first couple of pulses the amount of DA released actually increased slightly, before slowly starting to decrease. We believe that this may have been due to a small competitive effect of FFN102 during loading, which replaced some of the vesicular DA. With each subsequent stimulation this effect would be diminished, as FFN102 concentrations in the slice would decrease more rapidly than DA. A similar effect was explored in the original FFN102 paper[1], where DA reuptake kinetics were measured with CV in the continuous presence of FFN102[1], but our recent data suggests that even a previous FFN102 incubation, followed by a washing period, still has an effect on DA release. Additionally, these observations help shaped the design of future FFN102 experiments. In an effort to reach a more stable FFN102 vesicular concentration over time, experiments described below (2.2.5) also included a low concentration

(1μM) of FFN102 in the artificial cerebral spinal fluid (ASCF) perfusing over the brain slice to replenish the FFN lost after each release event.

After successfully measuring comparable paired-pulse ratios, combined with previous observations, we concluded that the pH-sensitive FFN flash can be used to measure DA release analogously to electrochemical techniques, such as CV. With this type of "optical CV" it may be possible to measure DA release from very localized areas; however, efforts to identify "puncta-specific" changes in fluorescence have so far been unsuccessful. Nevertheless, even being able to measure general DA release from a small area (few microns) is potentially important when considering the location-specific variability of different areas of the striatum. This is supported by evidence that demonstrated *in vivo* heterogeneity of DA release found in relatively small areas (~100μm) of the striatum that had different spontaneous release patterns and responses to DAT-inhibition[42]. Another example of this type of heterogeneity is found in the ventral striatum, where local "hotspots" of opioid receptor expression[43] have been identified, which can be found on, and directly modulate, dopaminergic projections in that area[44].

To substantially improve on electrochemical techniques, however, we would need to fully realize the benefits possible with optical imaging techniques and measure neurotransmitter release from individual release sites. At current imaging rates, we have been unable to identify changes in fluorescence at a particular puncta that do not match the average change found across the field of view. This is why the previous quantification of these experiments has generally included the ΔF/F from the whole frame. Our lack of prior success with measuring changes at individual release site was likely due in part to the excitation volume of the microscope and the speed at which FFN102 is diffusing. First, due to the limitations of two-photon excitation, the z-plane spatial resolution of the microscope (~2μm), as measured with microbeads of uniform size,

is much larger than the average dopaminergic release site (~0.3μm)[45]. While the x-y resolution (~0.35μm) is capable of resolving an individual release site, there will always be a fluorescence contribution from the background signal included from the z-plane. Therefore, if the ΔF/F of the background is larger than any local fluorescence changes that might occur, the individual contribution will be diluted by the global background change. This leads into the second issue, the rate at which FFN102 diffuses throughout the field has been too fast to allow identification of the source location of signal generation. This is problematic if the ultimate goal is to be able to identify when an individual release site fires.

2.2.5 Applying FFN102 to the Measurement of Single Pulse Release Kinetics

Unable to change the spatial resolution properties of the microscope, we sought to tackle the problem of identifying individual firing events by changing the way we examine the flash from one EP. First, we needed to better understand our experimental system and to focus on how to best maximize the change in ΔF/F from an individual release site. At this point it had been confirmed with two different DA-FFNs (FFN102 and FFN200) that the majority of labeled dopaminergic release sites (80-90%) were "silent," and did not release a significant portion of their loaded FFN when stimulated with long trains of electrical pulses similar to tonic firing conditions (1000s of EPs)[1,5]. Similar observations have been observed with the membrane dye, FM1-43, which only loads recycling vesicular pools. Stimulation of dopaminergic projections in the presence of this dye, leads to FM1-43 loading of only 10 percent of dopaminergic release sites[5]. Using a mouse line expressing the genetic calcium sensor GCaMP3 under control of the DAT promoter (DAT-GCaMP3), it was confirmed that the majority of these silent dopaminergic release sites were actively being stimulated (~70%) and undergoing calcium transients, but did not result in significant release of FFNs or loading by FM1-43[5]. While presynaptically silent

puncta have been reported in the glutamatergic[46–48] and GABAergic[49,50] systems previously, and there are potential theories that vesicle priming might be the underling mechanism[51,52], this has not yet been explored in dopaminergic neurons.

We also knew from electrochemical and FFN flash experiments in acute brain slices, that the first EP results in a massive amount of DA release, while depending on the interval, the subsequent EPs release relatively little. Combined with our understanding of silent puncta, we hypothesized that during phasic bursts of EPs (or the first EP after a period of rest) a large portion of dopaminergic terminals must be participating in DA release, while after continuous stimulation of long trains of EPs, members of this population turn off. This would leave only a small portion of dopaminergic release sites that have the mechanisms in place to continually recycle their vesicular pool and release all of the loaded FFN. Based on this assumption, we hypothesized that if we delivered a relatively slow tonic sequence of EPs to dopaminergic projections that the majority of puncta might have a high release probability during the first couple pulses and then only a few (10-20%) maintain a high release probability for the remainder of the pulses or activate their reserve pool of FFN loaded vesicles[53]. This portion of release sites would be the same ones identified to fully destain after even longer sequences of EPs (100s-1000s). Additionally, the problems associated with significant background fluorescence contribution from a single EP, as discussed previously, would be greatly reduced when performing the imaging following a series of pulses. As seen with the paired-pulse experiments in 2.2.4, the global FFN flash from the EPs following the first EP by a few seconds was almost unmeasurable.

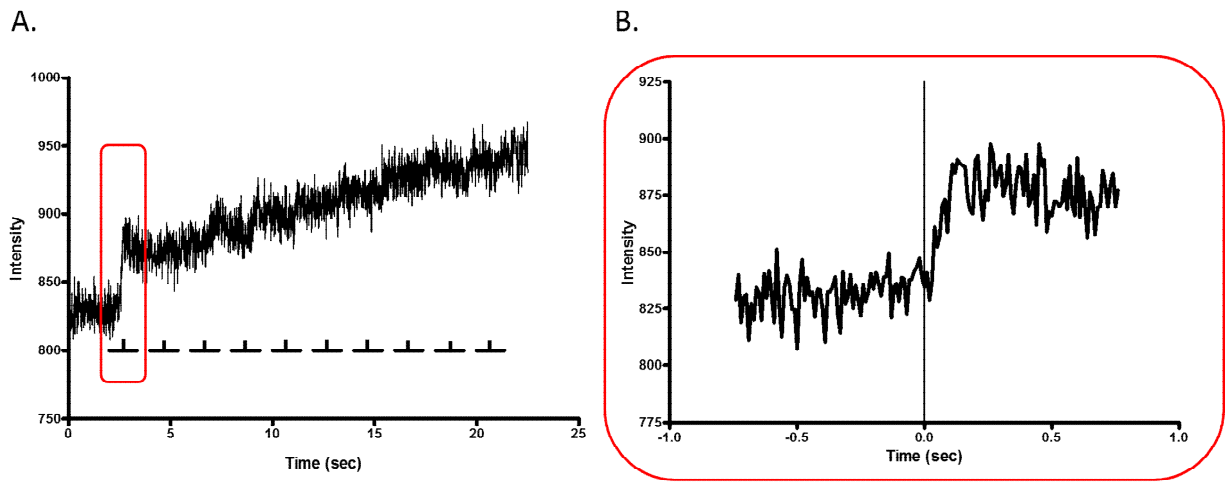

Figure 7. Time course of FFN102 fluorescent changes from a single time course at an individual release site in acute murine brain slices following single EPs separated by 2s (10 total). A) Representative individual trace from the fluorescence change in the field of view centered on one FFN102-labeled release site following 10 individual EPs (each horizontal bar indicates the duration of the individual trace analyzed in B, and the tick in the middle indicates the time when a single EP was delivered). B) Each individual EP from the 10 EP set was analyzed further individually to determine if and when a significant increase occurred. Panel B includes a representative individual EP trace extracted from the full trace in panel A as indicated by the red box.

To test our hypothesis, which can account for all of our FFN flash observations and our understanding of how dopaminergic release sites in acute brain slices behave, we designed imaging and stimulation conditions to attempt to measure release of FFN102 from individual release sites during a series of slow tonic EPs. Again, we used a spiral scanning imaging protocol with slightly modified parameters from section 2.2.3 to collect 2 micron^2 images of one FFN102-labeled release site at a rate of 100 hertz. For the stimulation protocol, we delivered 1 electrical pulse locally every 2 seconds, for 10 total pulses over 20 seconds (**Figure 7A**). At our imaging rate, this would allow for enough images to generate a pre- and post-EP fluorescence time course for each pulse of the set individually (**Figure 7B**). As discussed in 2.2.4, for these experiments, FFN102 at a low concentration (1μM) was included in the perfusion ACSF and present throughout the experiment to replenish FFN102 vesicular stores. To further allow for FFN102 reloading, after each set of stimulations, we included a 5 minute wait period before the total process was repeated multiple times at multiple release sites from each acute slice. As a negative

control, these experiments were also repeated without electrical stimulation. Using this experimental design we collected a large amount of FFN flash data from the area around individual release sites following 1 EP, which resulted in the massive release of DA, followed by 9 subsequent EPs that resulted in minimal DA release, as confirmed by CV.

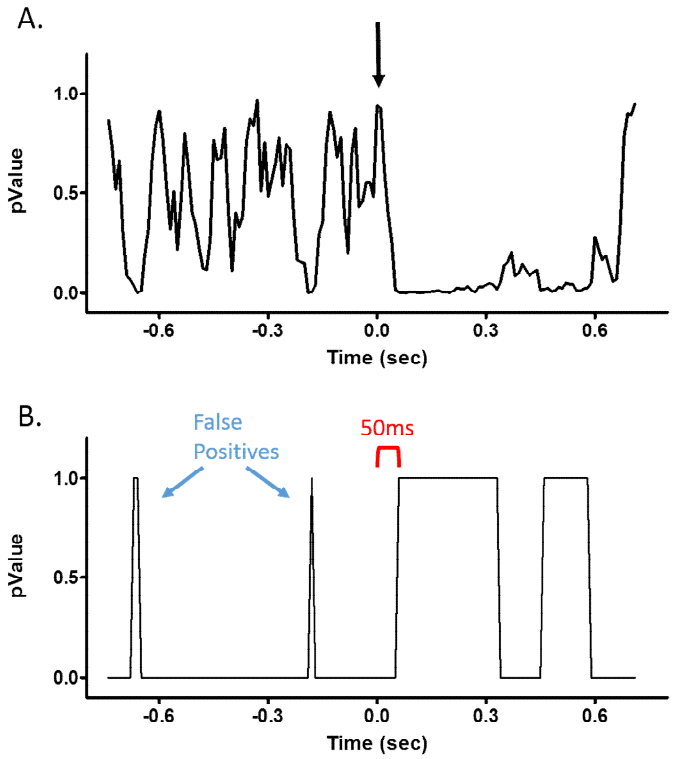

Figure 8. MATLAB analysis of the normalized changes in FFN102 fluorescence from the trace of a single EP at an individual release site in acute murine brain slice. A) Representative plot of p-values generated from a moving cluster of time points (5) over the course of an individual trace before and after 1 EP (arrow, t=0) from a t-test. B) Setting a p-value threshold of $p<0.05$, the periods when significant increase occurred were collected. In this example, a significant increase was observed 50ms after the initiation of the EP. Also highlighted are examples of false positive periods that were selected during pre-stimulation due to the noise of the data collection.

To analyze these data we developed a MATLAB script that separated the 10 EPs from a single set into 10 equally spaced traces centered on each of the electrical pulses (exemplified in **Figure 7B**). The fluorescence baseline signal pre-pulse for each individual trace was used to generate a line of best-fit, which was then used to normalize the post-pulse fluorescence for each. From this baseline-corrected trace, we next looked at a moving group of 5 time points and, using

a t-test, determined the probability that this particular cluster of points was statistically greater than the baseline. The p-values generated from the moving set of groups from each trace were then collected and plotted (exemplified in **Figure 8A**). Using a significance threshold, set as any p-value less than 0.05, the time periods with a statistically significant fluorescence increase were determined. This data was slightly smoothed to remove any time periods that only lasted two time points or less (**Figure 8B**). This process was repeated for each of the 10 EPs from a single set, and then from each set between all acute slices and animals. In total, we were able to analyze over a thousand fluorescent traces before and after individual EPs.

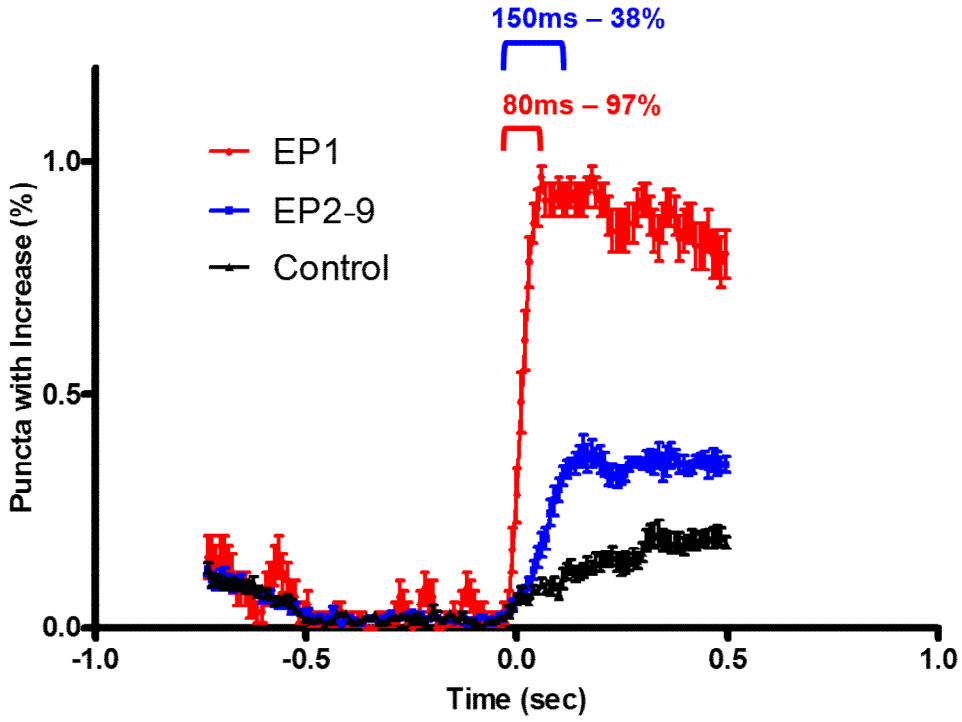

Figure 9. Analysis of combined MATLAB data for changes in FFN102 fluorescence observed following the initial EP (EP1), subsequent EPs (EP2-10), or no stimulus. This plot details what percentage of electrical pulses (EPs) generated a significant fluorescence increase over time (EP occurred at t=0). After the first EP in the set (EP1) a significant fluorescence increase was observed in 96.7% of the fields of view after 80ms. The average probability of observing significant increases in fluorescence of the following EPs (EP2-9), was much lower and slightly delayed (38.1% after 150ms) than after EP1, but still significantly higher than the control (EP10 was not included here due to the significantly lower flash described in **Figure 10**).

While collecting these data was a time consuming process, understanding the data collected proved to be the challenging part. The initial goals were to determine if we could observe significant increases in fluorescence from the weak DA-releasing signal that occurred after individual EPs (EP2-10) that followed the initial EP stimulus (EP1), and to understand the temporal relationship as to when significance was reached relative to when the EPs occurred. As expected, EP1 from each set virtually always resulted in a significant fluorescent increase, but surprisingly, we were also able to observe significant fluorescent increases in the FFN flash after subsequent individual EPs as well. We also observed that the percentage of EPs resulting in significant increases appeared to depend on the time interval after stimulation. Grouping only EP1s together from all sets collected, a significant increase was observed in 96.7 ± 2.3 percent of measured frames after 80 milliseconds (**Figure 9**) (mean ± SEM for 60 EP1s from 2-3 slices per animal, 6 animals). After this time point, the percentage of frames with a significant increase slowly started to decrease, presumably as FFN102 started to wash away or get recycled into acidic compartments. Importantly, using the diffusion coefficient for dopamine in acute brain slice ($2.7*10^{-6}$ cm^2/s), after 80 milliseconds the FFN could have traveled up to 6.5 microns, an area much larger than the field of view[54]. If the signal increase was generated from FFN102 being released from the individual release site in view, we would expect an increase after just the first time point (10ms). Therefore, we suspect that the delayed increases must have been due to diffusion of FFN102 released from other release sites, out of the field of view or a delayed circuit event from other neurons.

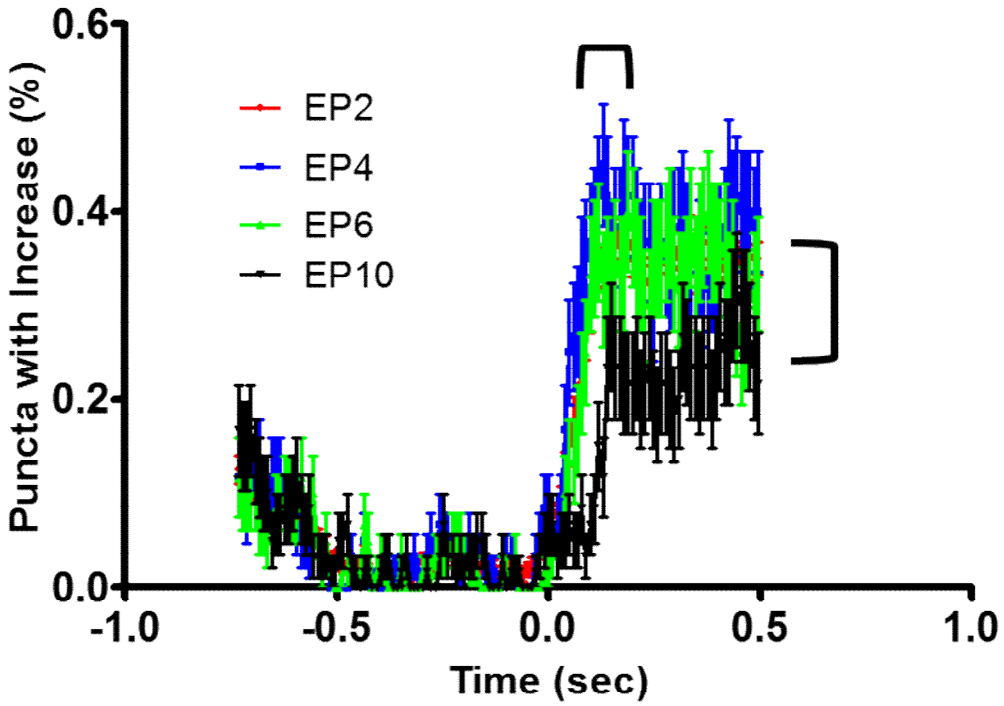

Figure 10. The data from representative individual EPs from the group of subsequent EPs (2-10) plotted as described in **Figure 9**. There was no statistical difference in any of the remaining EPs, except for EP10, which had a slower rise time and lower overall magnitude, highlighted by brackets.

A similar general delayed effect was observed with the subsequent EPs as well. EPs 2-9 all exhibited similar behavior with no significant differences when averaged together. EP10 did have a maximum release that was measurably slower and of lower overall magnitude than the others, and this difference is highlighted in **Figure 10**, which includes representative examples from individual EPs from the 2-10 group. When EPs 2-9 were grouped together, the maximum percent chance to observe significant release is 38.1±2.3 percent, occurring at 150 milliseconds post-stimulation (**Figure 9**). This is almost twice the amount of time observed after EP1, and could correspond to diffusion from release sites up to 9.2 microns away. We believe this timing factor is potentially important, and this parameter is further analyzed later in this section.

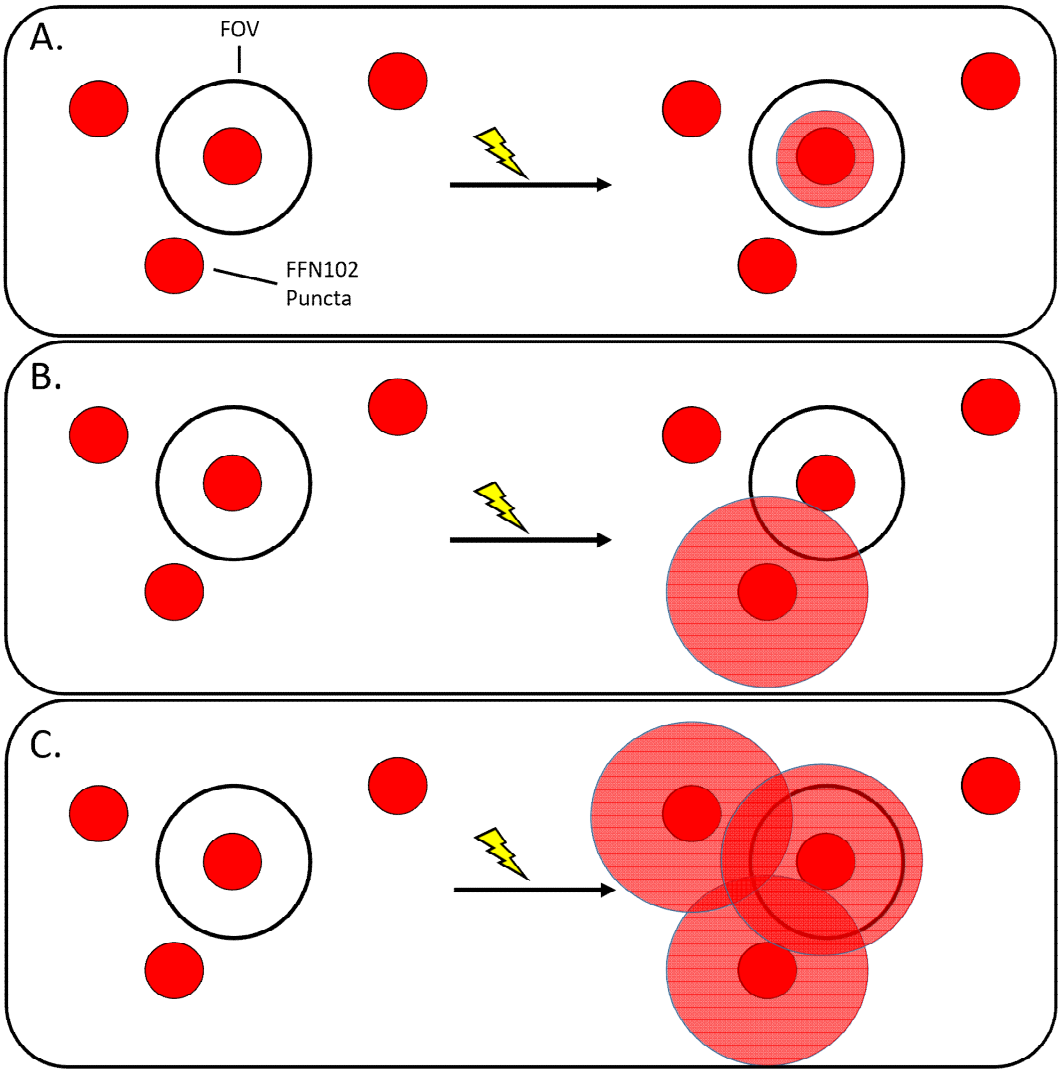

Figure 11. Some possible explanations based on diffusion for the variability observed in the temporal delay between when electrical stimulation occurred and when a significant fluorescence increase was observed. A) If the fluorescence change from an individual release is significant on its own, then the release from the puncta in the field of view (FOV) should cause an instantaneous increase in fluorescence (1-2 time points post-stimulation). B) If the imaged puncta did not fire, but a neighbor did, there would be a delayed increase based on the distance between the releasing puncta and the FOV. C) If the FFN released from one puncta was not sufficient to measure above the noise, then a significant increase would only be achieved when the additional fluorescence from neighboring release sites diffused into the FOV. This increase would also be delayed, as determined by the distances from the FOV, and density of neighboring release sites.

If we consider the current threshold of significance in the MATLAB analysis as involving some amount of new deprotonated FFN102 within the frame, relative to the fluorescence of the individual release site in the field of view, then there are multiple possibilities they may explain how that amount of FFN was reached based on diffusion (**Figure 11**). First, the

release site in the frame could release enough protonated FFN from its vesicular stores to generate a sufficient change in fluorescence relative to its remaining FFN fluorescence (ΔF/F) with a duration long enough to pass the threshold. We expect that for this type of event, statistical significance should be reached almost instantly after stimulation (**Figure 11A**). Encouragingly, for some EPs we were able to detect significant increases in fluorescence after just one or two time points. Second, we can continue to assume that the flash from one release site can generate a significant enough ΔF/F to be detected, however, this release site is now located out of the field of view. Therefore, depending on the distance from the imaging area, the significant signal caused by this release site would be delayed (**Figure 11B**). Lastly, it is possible that the amount of FFN102 released from a single site is not sufficient on its own to be detected by this method, especially if it is a distant neighbor to the release site being imaged. In this case, the number and location of nearby release sites relative to the imaging site would be the most important factor in determining whether significance is reached (**Figure 11C**). The more numerous the neighbors, the higher the probability that significance would be reached if a subpopulation of them were firing, as well as, the closer the neighbors, the shorter the time interval between stimulation and significance increases.

It is likely that there are examples of each within the current collection of data, but strict classification at this time is premature. To further determine the importance of the individual release sites within the imaging frame, these experiments need to be repeated with some FOVs focusing on only background (an area with no release site) or an area of fluorescence expected not to release (blood vessels). This would help us understand the role of the release site in producing the flash, versus the contribution of diffusion, and if the release from the puncta in the FOV is measurably significant on its own. These experiments have started, but are not yet ready

to allow us to draw conclusions. As described later, in future directions (4.2.2), there are also other ideas to help delineate signal from the release site in the field of view from signal generated from the neighboring area. For example, implementing microscope scanning upgrades that improve the imaging rate, or performing our imaging experiments in areas with less dense projections that may decreases the background signal. However, to complete this section, I will continue by analyzing the traces from individual EPs where increases in fluorescent signaling significance were reached within the first couple images following stimulation, because these fluorescent increases were most likely to result from release occurring at the release site within the field of view.

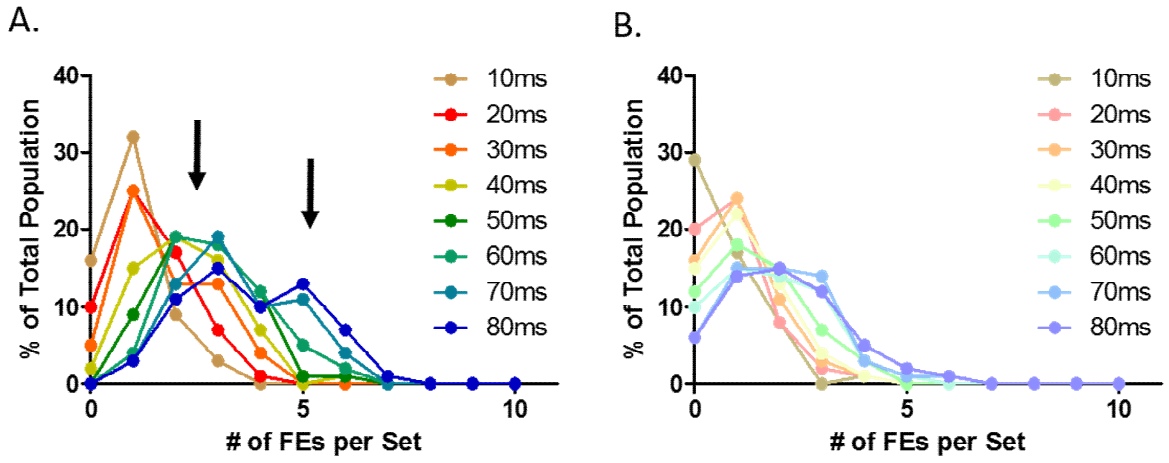

Figure 12. The probability of observing significant FFN102 fluorescent increases, "firing event" (FEs) when comparing different temporal cutoffs for when that increase must have occurred by. After setting the temporal cutoffs as a number of imaging frames (every 10ms, between 1 and 8 frames), each imaging set (10 EPs) was plotted based on how many FEs were detected out of the possible 10. A significant increase in FEs was observed for all temporal windows (even at 10ms) when comparing stimulated (A) and unstimulated conditions (B), with the average number of FEs detected increasing with the amount of time included post-stimulation. We also observed an apparent bi-modality in the number of FEs detected in the stimulated conditions (highlighted by arrows) that became more pronounced the longer the temporal windows.

While there is more work to complete, analyzing the current data set has already led to some potentially interesting findings. By setting a series of increasing temporal windows after an EP stimulation to asses when a significant increase in fluorescence was detected (FFN102 firing

event, or “FE”), indicating that DA release occurred, we were able to compare the timing of each FE detected, at each of the individual release sites, in each of the temporal windows. Specifically, for each of the 10 EPs within an imaging set, we assessed whether or not a significant fluorescent increase (or detectable FE) occurred within a designated time frame, and then the total number of FEs that occurred within each imaging set centered on an individual release site. The probabilities of detecting a certain number of FEs (out of 10) that occurred within each imaging set were then plotted for each of the temporal windows assessed (**Figure 12**). When assessing the 10ms temporal window (1 imaging frame after stimulation, corresponding to a potential FFN102 diffusion of 2.3 microns), we observed only a slight increase in the number of FEs after stimulation compared to the false positive rate observed in the non-stimulated control. However, as the duration of temporal window in the analyses increased, the increase in the number of FEs observed between the stimulated and non-stimulated conditions became more apparent (**Figure 12**).

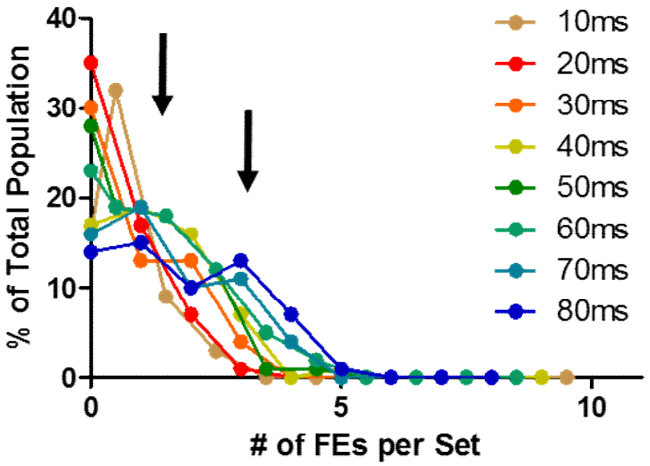

Figure 13. Normalization of the number of firing events (FEs) detected at individual release sites within specific temporal windows following EP stimulation. Using the data from **Figure 12**, the average number of false positive FEs detected in the control conditions (unstimulated) were subtracted from the stimulated condition and replotted. After subtraction, we observed a significant percentage of imaging sets that did not have any measurable fluorescence increases (FEs) within these temporal windows. However, we also observed a significant percentage of release sites with an increase in FEs, and which retained the bi-modality observed previously (highlighted by arrows). Depending on the duration temporal window, a large portion of the imaging sets demonstrated 1 FE or 3 FEs. If the average density and firing probabilities of dopaminergic projections were all the same, then it is likely this increase in FEs and bi-modality is not due solely to diffusion

After the false-positives, which had a good fit to a Poisson distribution (p-value <0.05 for all temporal intervals), in the non-stimulated condition (**Figure 12B**) were subtracted from the data derived from stimulated conditions, a significant increase in FEs were still observed from the first time temporal window onward (10ms, 20ms, 30ms, etc.) (**Figure 13**). When the temporal window exceeded 30 milliseconds, we observe a deviation in FEs from a Poisson distribution that became more pronounced as later time points were included (p-value increases from ~0.1 to ~0.7). There was a peak in the percentage of imaging sets that demonstrated few significant increases in fluorescence above control (0-1), and an observed second peak in the percentage of imaging sets that had multiple (~3 FEs). Assuming that all of the sets had a random distribution of neighbors, with equally random release probabilities, and the detection of FEs was primarily the result of diffusion of FFN102 from neighboring release sites, then we

would expect a normal distribution of the FE percentage for stimulated sets, similar to the control sets, but shifted to the right. The sets with many close neighbors to the field of view would likely have a higher percentage of FEs than sets with more sparse neighbors, leading to a normal distribution that would be centered based on the average density of release sites. Because the distribution in **Figure 13** appears to be bi-modal, it is possible that the existence of this second "hump" of imaging sets, which have a high percentage of multiple FEs (~3), suggest that diffusion of FFN102 fluorescence is not the only factor contributing to the flash detected at single release sites after EP stimulation. This is supported by recent evidence that suggested that DA release in the striatum from a single EP has two temporally distinct release events. First, an immediate release from direct stimulation of the dopaminergic release site, and then a delayed release (~100ms) due to an acetylcholine mediated circuit component[55]. We will confirm if this is related to the delayed FFN flash with nicotinic receptor antagonists.

In summary, we are optimistic about the observations we have generated so far. We have determined that it is possible to observe significant increases in FFN102 fluorescence after electrical stimulation on the millisecond timescale, potentially from individual release sites. Additionally, significant increases in florescence could be detected for each EP, including EPs other than just EP1 that release much less DA than the first stimulus.

2.3 Measuring Intracellular Vesicular Changes with FFNs - Results and Discussion

2.3.1 The Regulatory pathways Involved in the Loading of DA Vesicles

In addition to generating a flash upon release, a pH-sensitive FFN also has the potential to measure changes that occur within the release site before vesicular fusion occurs. An example of this behavior was explored in the experiment involving high concentrations of cocaine described in section 2.2.1, but under this condition, no apparent changes in vesicular pH were

responsible for the depression in DA release. However, through a collaborative effort with Dr. Zachary Freyberg (Columbia University), dopaminergic intracellular trafficking and quantal size was again explored using FFN102 in the context of glutamatergic co-transmission in the dopaminergic projections of the striatum.

How changes in quantal size can affect postsynaptic targets (and vice versa) was discussed in 2.1.3, but the presynaptic mechanisms in place for regulating how much neurotransmitter is loaded into vesicles will be further elaborated here. Within release sites there is a delicate balance between the concentration of the neurotransmitter in the cytoplasm and vesicular lumen. The equilibrium of neurotransmitter concentrations between the extracellular space, cytosol, and vesicles is maintained by biosynthesis, biodegradation/metabolism, membrane transport, and vesicular transport mechanisms. Changes in any of these mechanisms can ultimately affect the amount of neurotransmitter that is loaded per vesicle, and subsequently released per fusion event. As substrates for transporters on both the cell surface and vesicular membranes, FFNs have the potential to track changes in the mechanisms controlling both of these transport processes. While changes in the rate of neurotransmitter biosynthesis can impact quantal size, they will not be discussed here due to the fact that FFN loading and fluorescence is not directly related to these pathways.

In the design of our experiments, we considered the fact that neurons within the brain are highly resource efficient when it comes to their neurotransmitters. The vast majority of released neurotransmitter is recycled back into neurons through reuptake by plasma membrane transporters (such as DAT for DA). For dopaminergic neurons, loss of DAT in knockout mice led to an overall 95 percent reduction in total DA levels, as DA biosynthesis simply cannot keep up with the amount of DA released[56,57]. The critical importance of DAT has also been observed

in our own laboratory. The dopamine projections of the striatum in acute brain slice experiments were able to continue to release dopamine after hours of stimulation, as opposed to only a few EPs in DAT-KO mice. DAT functions by transporting one molecule of DA into the cytoplasm through the inward co-transport of two sodium and one chloride ion, thereby using the sodium concentration gradient and membrane potential found at the plasma membrane to power DA transport[58]. Through controlling the intracellular stores of DA available for vesicular loading, changes in DAT activity can affect DA quantal size. As a substrate for DAT, FFN102 has the potential to measure these changes in DAT activity by measuring initial rates of loading or clearance following a stimulus. Combined with the fluorescence flash after exocytosis that traces changes in relative DA release, FFN102 has the potential to assess whether changes in DA release are related to varying DAT or VMAT2 activity at an individual release site.

The second neurotransmitter equilibrium that is important for determining quantal size resides at the synaptic vesicular membrane. For monoamines, VMAT2 is the transporter responsible for loading DA into the vesicle. VMAT2 uses an antiport mechanism that transports one protonated DA molecule in for two protons out. The proton electrochemical gradient that powers VMAT2 activity is generated by the vacuolar H^+-ATPase (vATPase). Through ATP hydrolysis, protons are actively pumped into the vesicle generating a pH and electrical gradient. In monoamine synaptic vesicles, chloride ion antiport channels are also expressed on the vesicular membrane, which transport two chloride ions in for one proton out[59]. This transport helps dissipate the electrical component of the proton gradient by equilibrating more charge (net 3) than protons (1), allowing for a larger build-up of the pH gradient[60]. This pH gradient is then the primary driving force of monoamine loading, and changes within the vesicle that affect this pH gradient can have a drastic effect on neurotransmitter loading[61]. Other than transporters, the

degree of loading is also influenced by the rate at which neurotransmitters leak out of the vesicle, and the rate of neuronal firing. If vesicle fusion is occurring too fast for full equilibration by VMAT2, the quantal release of those vesicles is potentially diminished. The following work in this section describes a potential novel role of VGLUT in regulating vesicular loading in some dopaminergic neurons. Contrary to VMAT2, VGLUT activity is primarily driven by the electrical potential at the vesicular membrane, and transporting in negatively charged glutamate could be acting in a function similar to the chloride channels[28].

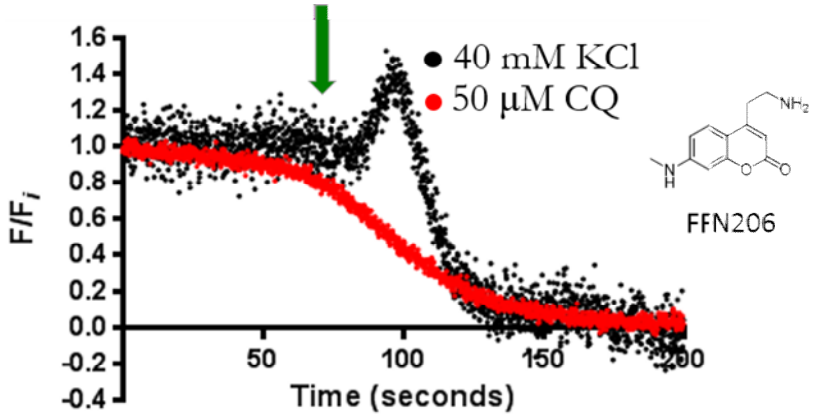

Figure 14. Uptake of FFN206 into dopaminergic projections of the fly brain after application of KCl as measured through change in fluorescence relative to initial fluorescence (F/F_i). With FFN206 in the perfusion, there was increased loading of FFN206 after application of 40mM KCl (highlighted by green arrow), but before exocytosis occurred. This increase in loading was not present with treatment of the lipophilic weak base, chloroquine (CQ, 50µM). Data obtained via two-photon microscopy of whole drosophila brains provided by Dr. Zachary Freyberg.

2.3.2 Exploring the Role of VGLUT in Vesicular Loading

The idea for these experiments was built upon an observation in fly brain experiments, with the identification of a strange phenomenon that occurred before exocytosis induced by high potassium concentrations. Here, I will include just the relevant observations from our collaborator's work that led to our own experimentation. First, using the pH-insensitive DA-FFN best suited for experiments in the fly, FFN206[62], they observed that in the presence of extracellular FFN, there was increased uptake of FFN206 into dopaminergic projections when

high potassium concentrations are added (**Figure 14**). This resulted in a 40% percent increase in fluorescence that occurred just prior to complete FFN release when exocytosis occurs. Using the genetically-encoded vesicular pH-sensor, dVMAT-pHluorin, they identified that during this period of increased uptake there was an acidification that occurred within the vesicles (**Figure 15B**). Through colocalization experiments, VGLUT was determined to be present in the dopaminergic neurons exhibiting this acidification phenomenon (**Figure 15A**). Suspecting that the negatively charged glutamate could be acting in a similar mechanism as chloride, to dissipate the electrical vesicular membrane potential and increase the pH gradient, these experiments were repeated using flies with VGLUT-RNAi. Reduction of VGLUT led to an approximately 50 percent decrease in the magnitude and duration of the acidification, indicating the potential importance of this transporter in this phenomenon (**Figure 15B**).

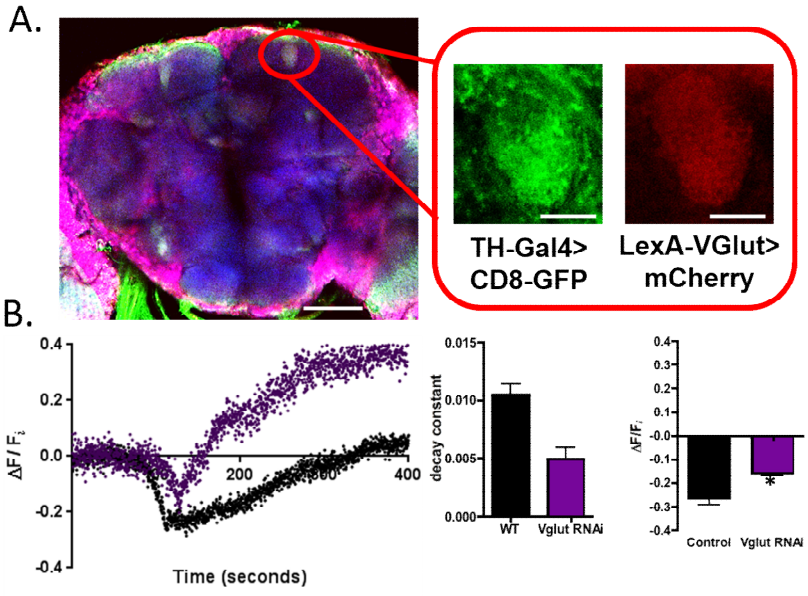

Figure 15. VGLUT involvement in the uptake of FFN206 in dopaminergic projection of the fly brain after treatment with KCl. A) Colocalization of the dopaminergic marker, tyrosine hydroxylase (TH-Gal4), with VGLUT (LexA-VGlut). Circled in red is a magnification of the area being studied, which has a high concentration of dopaminergic projections. B) The pH-sensitive dVMAT-pHluorin fluorescence decreased during the application of 40mM KCl, corresponding with an increase in acidity. The average duration and magnitude of the acidification were reduced by ~50%, when a VGLUT-RNAi sequence was introduced to dopaminergic neurons.

2.3.3 Using FFN102 to Study the Role of VGLUT in Vesicular Loading in Acute Murine Brain Slices

The next goal of the project was to evaluate the role of VGLUT in the loading of dopaminergic vesicles in mice. However, before building upon the observations derived from a fly experimental system, it was necessary to first determine if a similar acidification occurred in a mammalian system. Because the pHluorin system is not yet applicable for use in acute murine brain slices, the FFN program was utilized to repeat the fly VGLUT experiments in a mammalian system, using FFN102 as the intracellular/vesicular pH-sensor. These experiments were conducted by loading the dopaminergic projections in the striatum of acute murine brain slices with FFN102 (10μM for 30min) and then imaging them during washing, and throughout a KCl depolarization treatment (40mM). Typically, imaging of dopaminergic projections in the striatum is conducted in the dorsal lateral part, an area dense with dopaminergic innervation, but these experiments were conducted in the ventral medial area, an area with greater dopaminergic VGLUT expression[63]. Prior to the drastic increase of fluorescence caused by FFN102 release, we observed a shift in the rate of fluorescence decay that temporally aligned with the arrival of increased K^+ concentrations (**Figure 16**). The rate of fluorescence decay increased compared to the rate observed during washing, possibly indicative of increased transport of cytoplasmic FFN102 to vesicles, and/or a decreased pH inside the vesicles.

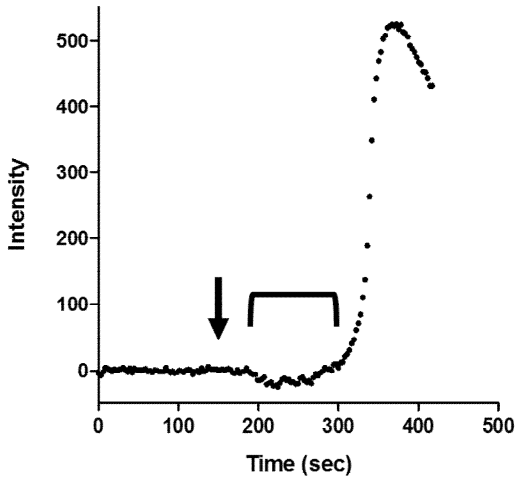

Figure 16. Changes to the fluorescence of FFN102-labeled dopaminergic projections in the ventral striatum of acute murine brain slice following a 40mM KCl treatment (started at arrow, ~150sec). After normalizing the exponential rate of decay from the trace pre-KCl treatment, there was an increase in the decay rate of FFN102 fluorescence, after-KCl treatment and before exocytosis (large increase in total fluorescence), as highlighted by the bracketed region.

Further exploration of this "dip" was made possible through the interlaced scanning of the same field of view with two lasers set as close to the excitation maxima of the protonated and deprotonated forms of FFN102. By simultaneously measuring the ratio of the two forms of the probe it was possible to determine if the observed dip was an artifact or indicative of a shift in the equilibrium of the two forms inside the release site. Using buffers of varying pH, the wavelengths of each laser were optimized to provide the greatest difference in fluorescent signal between the high and low pH conditions. Upon identifying optimal imaging conditions, the FFN102 high potassium experiment was repeated using interlaced scanning from two different lasers, and then the ratios between the fluorescence collected from each laser plotted over time (**Figure 17**). Due to a combination of the variability introduced when imaging an acute brain slice, lack of a pH control inside the release sites, and unknown distribution of FFN102 between the cytosol and vesicles, the following results are representative of only relative changes in pH. For analysis of the data, the rate of the ratio change during washing pre-KCl was used to create

an exponential best-fit to normalize the data between slices. Additionally, the average flash that occurred after release was used to normalize the magnitude of the ratios between different animals. We noticed that during the observed dip in fluorescence, there was a significant protonation of FFN102 within the frame. The magnitude of this acidification was 24.2% compared to the total alkalization that occurred when KCl depolarization led to complete emptying of the vesicles (2-3 slices per animal, 5 different animals). We initially had hoped to be able to analyze individual puncta to identify release sites that did or did not exhibit this acidification (potentially indicating release sites with or without VGLUT), but at the current imaging rate and resolution, the ratio data from this analysis were extremely noisy. I am confident that future optimization of this experimental setup could lead to less noise and improved quantification of individual release sites.

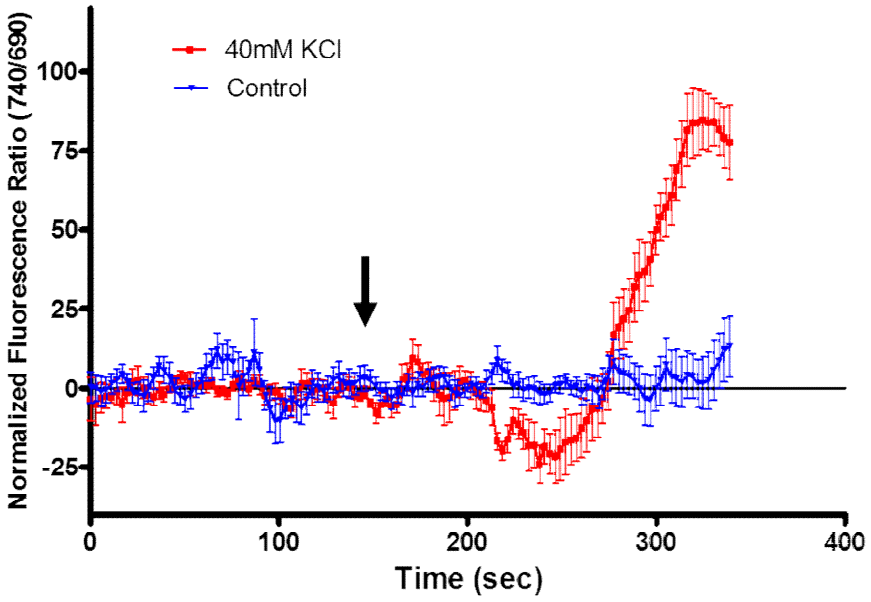

Figure 17. Plot of the normalized fluorescence ratio of the protonated versus deprotonated forms of FFN102 in ventral striatum of acute slice, before and after treatment with 40mM KCl. This was measured using interlaced two-photon imaging with two lasers set at either 690nm (protonated) or 740nm (deprotonated). There was a decrease in this ratio (acidification, magnitude: 24.2%) observed after KCl was applied (black arrow), but before exocytosis occurred (large increase in ratio – alkalization). The ratio for untreated acute slices remained relatively constant.

To further assess whether VGLUT2 was responsible for the acidification observation, these experiments were repeated in mice with a viral knockdown of the transporter. A mouse line with VGLUT2 flanked by LoxP genetic sequences (floxed) were injected in the ventral tegmental area (VTA, the source of dopaminergic neurons that project to the ventral striatum) with a virus that either led to the expression of cre recombinase or mCherry. Cre recombinase identifies LoxP sites and can lead to site-specific recombination. In this case, expression of cre recombinase in the dopaminergic neurons of the floxed VGLUT2 mouse line resulted in specific reduction in the expression of the VGLUT2 gene in those neurons. Additionally, mCherry expression was used in this experiment as a viral and genetic background control for this mouse line. Cre recombinase and mCherry expression levels in dopaminergic neurons (VTA) and projections (striatum) were confirmed through immunohistochemistry on each acute brain slice post-FFN imaging (**Figure 18**).

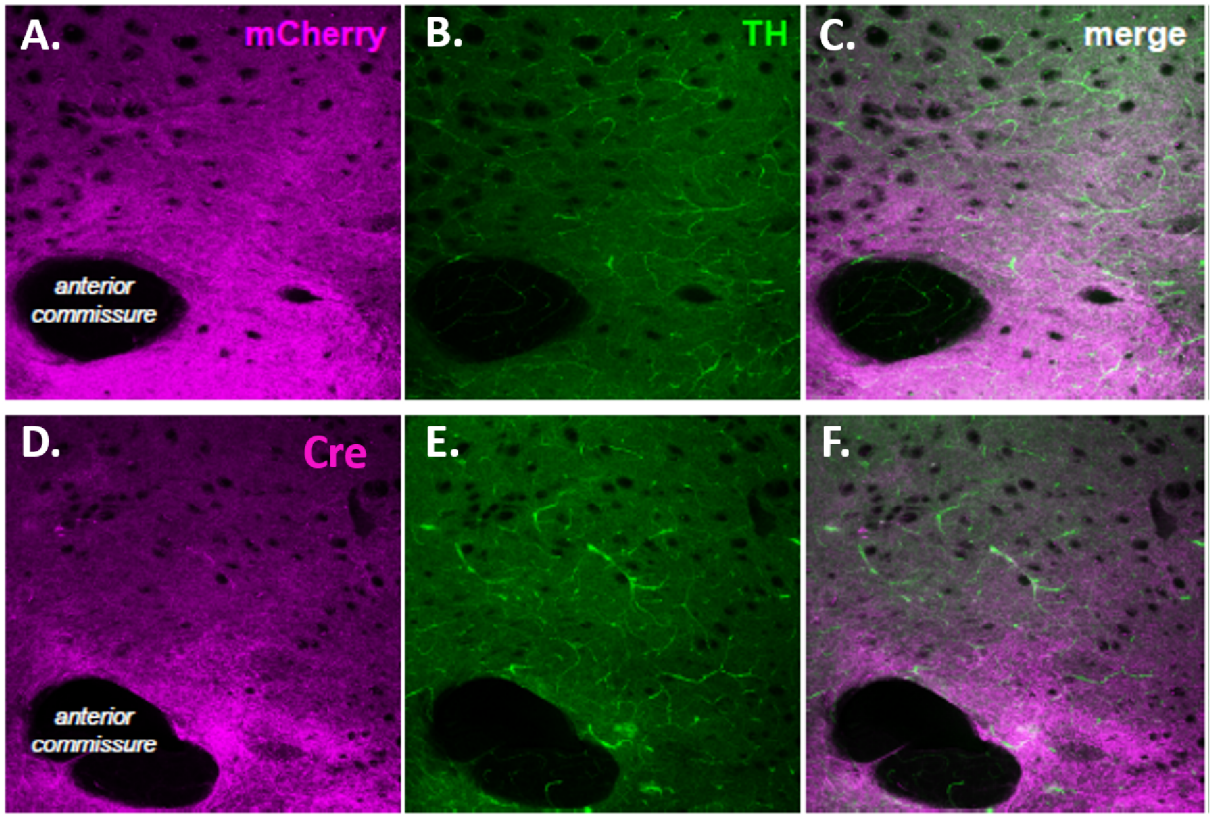

Figure 18. Confirmation of virally injected protein expression in the dopaminergic projections in the ventral striatum of acute murine brain slices. Mice with a floxed-VGLUT2 gene were either injected in the ventral tegmental area (VTA, location of dopaminergic cell bodies) with a mCherry or Cre recombinase virus 2 weeks prior to imaging with FFN102. After imaging with FFN102, acute slices from the striatum were collected and immunostained for either mCherry (A) or Cre (D), and the dopaminergic marker, tyrosine hydroxylase (TH, B and E). A strong colocalization of mCherry (panels A-C) or Cre recombinase (panels D-F) expression and dopaminergic projections is observed.

When imaging the FFN102-loaded brain slices from these mice, we were able to detect pH changes in the mCherry injected control mice with a similar acidification magnitude (41.2%) as in wild-type (WT) conditions (**Figure 19A**). In VGLUT2-knockdown conditions, however, there was a significant reduction in the magnitude and duration of the acidification dip. The local acidification maximum in the knockdown condition was 13.6%, only slightly larger than the standard deviation of the baseline signal (2-3 slices per animal, 3 different animals) (**Figure 19A**). We further quantified each of these conditions (WT, WT+KCl, Cre+KCl, and mCherry+KCl) to incorporate the duration factor into the quantification of the dip in

fluorescence ratio. This was done by measuring the total area under the curve (AUC) between the time KCl reached the brain slice and the time exocytosis started to occur (**Figure 19B**). We observed an 83% reduction in the acidification AUC between WT mice and mice without VGLUT, indicating a potentially important role of VGLUT in the observed acidification phenomenon.

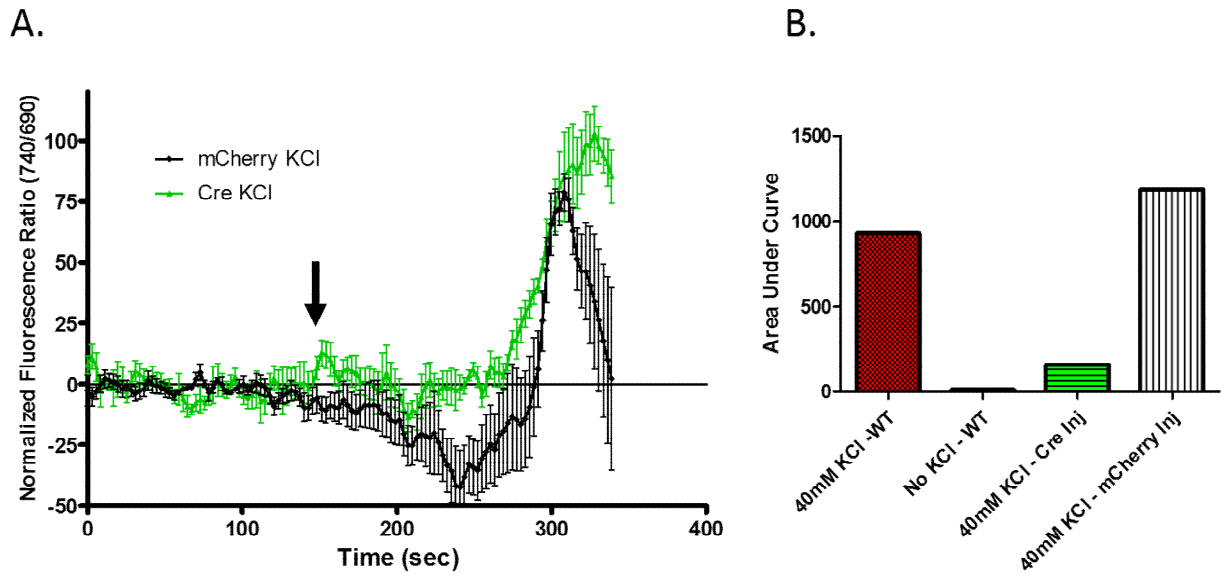

Figure 19. A) Comparison of the FFN102 fluorescence ratios over the 40mM KCl treatment in mice of the same genetic background that had either a mCherry control viral injection, or a Cre recombinase viral injection into the VTA. The acidification dip pre-exocytosis was almost completely abolished in the Cre injected condition. B) Quantification of all 4 total conditions (WT mice with KCl, WT mice without KCl, floxed-VGLUT2 mice with Cre and KCl, and floxed-VGLUT2 mice with mCherry and KCl). There was an 83% reduction in the pre-exocytosis acidification when Cre was expressed in the floxed-VGLUT2 mouse line.

In summary, using the pH-sensitive FFN102, we were able to identify KCl-dependent changes in dopaminergic vesicular loading and further develop the speculated role of glutamatergic co-transmission in regulating DA quantal size[64]. Further work is needed to fully understand this mechanism, and to determine whether this phenomenon occurs under physiologically relevant release conditions. In general, these results are an exciting step forward for the FFN program, as we were able to successfully demonstrate the use of a pH-sensitive FFN

to measure intracellular vesicular loading changes, another example of a novel functional application of FFNs, and one that would not be possible currently with other tools in the field.

2.4 Conclusions

2.4.1 Summary

This chapter explored the potential of the pH-sensitive DA-specific FFN, FFN102, in fulfilling two important goals of the FFN program. These goals were to develop a fluorescent tool that could measure changes in presynaptic plasticity through quantifying both the release probability and changes in vesicular content of individual release sites. In order to quantify changes in release probability, we measured the fluorescence increase (FFN flash) created when FFN102 was released from an acidic vesicle into the neutral extracellular space. We also demonstrated that this FFN flash correlated well with DA release, as measured by well-established electrochemical and microdialysis techniques in the field. Subsequently, we demonstrated that the FFN flash was also observable under phasic firing conditions and could be modulated as expected with pharmacological agents or genetic modification. Further, we observed that in the acute brain slice, the FFN flash was measurable from just a single EP; however, identifying the relationship between the flash and an individual release site remains to be established.

Ongoing efforts to measure the FFN flash from a particular DA release site focused on using imaging parameters with the fastest temporal resolution that were still able to produce significant signal changes. However, due to the nature of how the FFN flash works, and the speed at which FFN102 diffuses, it may not be possible to demonstrate definitely whether a particular release site fired, but with enough data we may start to draw conclusions based on probability. Although we have not definitively demonstrated a measurable release from a single

DA release site, the experiments performed towards this goal have already started to elucidate potential mechanisms behind silent puncta, as observed with a bi-modality of release detected near individual puncta after only individual EPs. Additionally, the much higher probability of detecting release after the first EP, could be used to provide insight behind the massive striatal DA release observed following the first EP in the acute brain slice.

The second major FFN102 result described in this chapter was the demonstration of the utility of FFNs to measure another method of presynaptic neurotransmitter regulation, changes in vesicular loading. By simultaneously measuring changes in the relative concentrations of protonated and deprotonated FFN102, we were able to demonstrate a change of the intracellular vesicular equilibrium of dopaminergic release sites loaded with the FFN102 tracer in acute murine brain slice. This data, supported by evidence generated in fly brain experiments, demonstrated the hypothesized role of glutamatergic co-transmission in regulating quantal size in *ex vivo* experimental systems[64]. These experiments represent the first demonstration of the ability of FFN to measure intracellular vesicular pH changes within acute murine brain slices by leveraging the pH-sensitivity and functionality of FFN102. Combined with the ability to also quantify neurotransmitter release, FFN102 represents the first FFN with distinct improvements in functionality over currently availed technologies capable of only measuring pH. It is our hope that the demonstration of the FFN102 functionality described throughout Chapter 2 will serve as the proof of concept for the value that FFNs will provide to studying the presynaptic changes that contribute to the regulation of neurotransmission in the brain.

2.4.2 FFN102 - Future Directions

As described above, we have demonstrated that the flash of FFN102 fluorescence occurring after vesicular release is directly correlated to DA release. However, identifying the

exact individual release sites responsible for that change in fluorescence has been problematic. To tackle this challenge we have planned two future experimental improvements. First, the two-photon microscope will be upgraded with a Resonant Galvanometer. Controlling the scanning mirrors of the microscope using a resonant galvanometer can result in up to a six-fold improvement in the rate of imaging an x-y plane compared to standard galvo imaging[65]. Resonant scanning decreases the amount of time wasted focusing the mirrors on each pixel in the field of view, while leaving the quality of the image unaffected. As discussed previously, due to the constant problem of FFN102 diffusion, any temporal improvements in image acquisition will allow for better separation between the individual release site signal and neighboring background signal contributing to the flash. Second, as will be discussed in more detail in Chapter 4, we now have access to a pH-sensitive FFN that labels the sparse noradrenergic release sites in the cortex. In addition to the imaging rate, the magnitude of the background signal when trying to measure changes from an individual release sites in this system will be equally important. Also, repeating these experiments in an area with sparse innervation may lower the background signal due to release from neighboring puncta, which may lead to an improved quantification of the individual release site signal.

Lastly, as will be discussed further in Chapter 4, it is our goal to move from the acute brain slice experimental system to measurements that take place *in vivo* in the intact brain. As such, we hope to be able to further test FFN functionality in an *in vivo* experimental system without the artifacts present in acute brain slices. It would be interesting to see if the magnitude of the flash is still significant when working with living, intact brain tissue. It would also be important for the FFN program to evaluate whether some of the conclusions drawn with FFNs in acute brain slice, such as silent puncta, will still hold true when tested *in vivo*. In conclusion, the

extensive joint laboratory effort that established the foundation for the FFN program has generated some truly unique research opportunities. In this chapter I describe the functional experiments I performed using the first DA-specific and pH-sensitive FFN, FFN102; hopefully laying the foundation for use in future presynaptic regulation studies.

2.5 References:

1. Rodriguez, P. C. *et al.* Fluorescent dopamine tracer resolves individual dopaminergic synapses and their activity in the brain. *Proc. Natl. Acad. Sci. U. S. A.* **110,** 870–5 (2013).

2. Gubernator, N. G. *et al.* Fluorescent false neurotransmitters visualize dopamine release from individual presynaptic terminals. *Science* **324,** 1441–4 (2009).

3. Lee, M., Gubernator, N. G., Sulzer, D. & Sames, D. Development of pH-responsive fluorescent false neurotransmitters. *J. Am. Chem. Soc.* **132,** 8828–30 (2010).

4. Fink, D. W. & Koehler, W. R. pH Effects on fluorescence of umbelliferone. *Anal. Chem.* **42,** 990–993 (1970).

5. Pereira, D. B. Imaging fluorescent false neurotransmitter release and Ca2+ at individual striatal dopaminergic boutons reveals a low density of active release sites. *Submitted*

6. Hyland, B. ., Reynolds, J. N. ., Hay, J., Perk, C. . & Miller, R. Firing modes of midbrain dopamine cells in the freely moving rat. *Neuroscience* **114,** 475–492 (2002).

7. Tsai, H.-C. *et al.* Phasic firing in dopaminergic neurons is sufficient for behavioral conditioning. *Science* **324,** 1080–4 (2009).

8. Schmitz, Y., Benoit-Marand, M., Gonon, F. & Sulzer, D. Presynaptic regulation of dopaminergic neurotransmission. *J. Neurochem.* **87,** 273–289 (2003).

9. Rice, M. E. Distinct regional differences in dopamine-mediated volume transmission. *Prog. Brain Res.* **125,** 277–90 (2000).

10. Nicholson, C. Volume transmission in the year 2000. *Prog. Brain Res.* **125,** 437–46 (2000).

11. Nirenberg, M. J. *et al.* The dopamine transporter: comparative ultrastructure of dopaminergic axons in limbic and motor compartments of the nucleus accumbens. *J. Neurosci.* **17,** 6899–907 (1997).

12. Yung, K. K. *et al.* Immunocytochemical localization of D1 and D2 dopamine receptors in the basal ganglia of the rat: light and electron microscopy. *Neuroscience* **65,** 709–30 (1995).

13. Freeman, A. S. & Bunney, B. S. Activity of A9 and A10 dopaminergic neurons in unrestrained rats: further characterization and effects of apomorphine and cholecystokinin. *Brain Res.* **405,** 46–55 (1987).

14. Schultz, W., Dayan, P. & Montague, P. R. A neural substrate of prediction and reward. *Science* **275,** 1593–9 (1997).

15. Cooper, R. L., Harrington, C. C., Marin, L. & Atwood, H. L. Quantal release at visualized terminals of a crayfish motor axon: intraterminal and regional differences. *J. Comp. Neurol.* **375,** 583–600 (1996).

16. Silver, R. A., Momiyama, A. & Cull-Candy, S. G. Locus of frequency-dependent depression identified with multiple-probability fluctuation analysis at rat climbing fibre-Purkinje cell synapses. *J. Physiol.* **510 (Pt 3,** 881–902 (1998).

17. Hessler, N. A., Shirke, A. M. & Malinow, R. The probability of transmitter release at a mammalian central synapse. *Nature* **366,** 569–72 (1993).

18. Walmsley, B., Edwards, F. R. & Tracey, D. J. Nonuniform release probabilities underlie quantal synaptic transmission at a mammalian excitatory central synapse. *J. Neurophysiol.* **60,** 889–908 (1988).

19. Koester, H. J. & Johnston, D. Target cell-dependent normalization of transmitter release at neocortical synapses. *Science* **308,** 863–6 (2005).

20. Granseth, B., Odermatt, B., Royle, S. J. & Lagnado, L. Clathrin-mediated endocytosis is the dominant mechanism of vesicle retrieval at hippocampal synapses. *Neuron* **51,** 773–86 (2006).

21. Wenner, P. Mechanisms of GABAergic homeostatic plasticity. *Neural Plast.* **2011,** 489470 (2011).

22. Parrish, J. Z. *et al.* Krüppel mediates the selective rebalancing of ion channel expression. *Neuron* **82,** 537–44 (2014).

23. Balaji, J. & Ryan, T. A. Single-vesicle imaging reveals that synaptic vesicle exocytosis and endocytosis are coupled by a single stochastic mode. *Proc. Natl. Acad. Sci. U. S. A.* **104,** 20576–81 (2007).

24. Murthy, V. N., Sejnowski, T. J. & Stevens, C. F. Heterogeneous Release Properties of Visualized Individual Hippocampal Synapses. *Neuron* **18,** 599–612 (1997).

25. Branco, T., Staras, K., Darcy, K. J. & Goda, Y. Local dendritic activity sets release probability at hippocampal synapses. *Neuron* **59,** 475–85 (2008).

26. Davis, G. W. & Müller, M. Homeostatic control of presynaptic neurotransmitter release. *Annu. Rev. Physiol.* **77,** 251–70 (2015).

27. Turrigiano, G. G., Leslie, K. R., Desai, N. S., Rutherford, L. C. & Nelson, S. B. Activity-dependent scaling of quantal amplitude in neocortical neurons. *Nature* **391,** 892–6 (1998).

28. Edwards, R. H. The neurotransmitter cycle and quantal size. *Neuron* **55,** 835–58 (2007).

29. Turrigiano, G. G. Homeostatic plasticity in neuronal networks: the more things change, the more they stay the same. *Trends Neurosci.* **22,** 221–7 (1999).

30. Turrigiano, G. G. & Nelson, S. B. Homeostatic plasticity in the developing nervous system. *Nat. Rev. Neurosci.* **5,** 97–107 (2004).

31. Plomp, J. J., van Kempen, G. T. & Molenaar, P. C. Adaptation of quantal content to decreased postsynaptic sensitivity at single endplates in alpha-bungarotoxin-treated rats. *J. Physiol.* **458,** 487–99 (1992).

32. Harata, N. C., Aravanis, A. M. & Tsien, R. W. Kiss-and-run and full-collapse fusion as modes of exo-endocytosis in neurosecretion. *J. Neurochem.* **97,** 1546–1570 (2006).

33. Staal, R. G. W., Mosharov, E. V & Sulzer, D. Dopamine neurons release transmitter via a flickering fusion pore. *Nat. Neurosci.* **7,** 341–346 (2004).

34. Wightman, R. M. & Haynes, C. L. Synaptic vesicles really do kiss and run. *Nat. Neurosci.* **7,** 321–2 (2004).

35. Federici, M. *et al.* Paradoxical abatement of striatal dopaminergic transmission by cocaine and methylphenidate. *J. Biol. Chem.* **289,** 264–74 (2014).

36. Kuhar, M. J., Ritz, M. C. & Boja, J. W. The dopamine hypothesis of the reinforcing properties of cocaine. *Trends Neurosci.* **14,** 299–302 (1991).

37. Ruetsch, Y. A., Böni, T. & Borgeat, A. From cocaine to ropivacaine: the history of local anesthetic drugs. *Curr. Top. Med. Chem.* **1,** 175–82 (2001).

38. Caudle, W. M. *et al.* Reduced vesicular storage of dopamine causes progressive nigrostriatal neurodegeneration. *J. Neurosci.* **27,** 8138–48 (2007).

39. Mooslehner, K. A. *et al.* Mice with very low expression of the vesicular monoamine transporter 2 gene survive into adulthood: potential mouse model for parkinsonism. *Mol. Cell. Biol.* **21,** 5321–31 (2001).

40. Gabor, G. & Walt, D. R. Sensitivity enhancement of fluorescent pH indicators by inner filter effects. *Anal. Chem.* **63,** 793–796 (1991).

41. Schmitz, Y., Schmauss, C. & Sulzer, D. Altered Dopamine Release and Uptake Kinetics in Mice Lacking D2 Receptors. *J. Neurosci.* **22,** 8002–8009 (2002).

42. Wightman, R. M. *et al.* Dopamine release is heterogeneous within microenvironments of the rat nucleus accumbens. *Eur. J. Neurosci.* **26,** 2046–54 (2007).

43. Castro, D. C. & Berridge, K. C. Opioid hedonic hotspot in nucleus accumbens shell: mu, delta, and kappa maps for enhancement of sweetness 'liking' and 'wanting'. *J. Neurosci.* **34,** 4239–50 (2014).

44. Svingos, A. L., Clarke, C. L. & Pickel, V. M. Localization of the delta-opioid receptor and dopamine transporter in the nucleus accumbens shell: implications for opiate and psychostimulant cross-sensitization. *Synapse* **34,** 1–10 (1999).

45. Arbuthnott, G. W. & Wickens, J. Space, time and dopamine. *Trends Neurosci.* **30,** 62–9 (2007).

46. Altrock, W. D. *et al.* Functional inactivation of a fraction of excitatory synapses in mice deficient for the active zone protein bassoon. *Neuron* **37,** 787–800 (2003).

47. Rosenmund, C. *et al.* Differential control of vesicle priming and short-term plasticity by Munc13 isoforms. *Neuron* **33,** 411–24 (2002).

48. Moulder, K. L. *et al.* Plastic elimination of functional glutamate release sites by depolarization. *Neuron* **42,** 423–35 (2004).

49. Kannenberg, K., Sieghart, W. & Reuter, H. Clusters of GABAA receptors on cultured hippocampal cells correlate only partially with functional synapses. *Eur. J. Neurosci.* **11,** 1256–64 (1999).

50. Losonczy, A., Biró, A. A. & Nusser, Z. Persistently active cannabinoid receptors mute a subpopulation of hippocampal interneurons. *Proc. Natl. Acad. Sci. U. S. A.* **101,** 1362–7 (2004).

51. Moulder, K. L., Jiang, X., Taylor, A. A., Olney, J. W. & Mennerick, S. Physiological activity depresses synaptic function through an effect on vesicle priming. *J. Neurosci.* **26,** 6618–26 (2006).

52. Jiang, X. *et al.* A role for the ubiquitin-proteasome system in activity-dependent presynaptic silencing. *J. Neurosci.* **30,** 1798–809 (2010).

53. Venton, B. J. Cocaine Increases Dopamine Release by Mobilization of a Synapsin-Dependent Reserve Pool. *J. Neurosci.* **26,** 3206–3209 (2006).

54. Tao, L. & Nicholson, C. Diffusion of albumins in rat cortical slices and relevance to volume transmission. *Neuroscience* **75,** 839–47 (1996).

55. Kress, G. J. *et al.* Fast phasic release properties of dopamine studied with a channel biosensor. *J. Neurosci.* **34,** 11792–802 (2014).

56. Jones, S. R. *et al.* Profound neuronal plasticity in response to inactivation of the dopamine transporter. *Proc. Natl. Acad. Sci. U. S. A.* **95,** 4029–34 (1998).

57. Giros, B., Jaber, M., Jones, S. R., Wightman, R. M. & Caron, M. G. Hyperlocomotion and indifference to cocaine and amphetamine in mice lacking the dopamine transporter. *Nature* **379,** 606–12 (1996).

58. Krueger, B. K. Kinetics and Block of Dopamine Uptake in Synaptosomes from Rat Caudate Nucleus. *J. Neurochem.* **55,** 260–267 (1990).

59. Accardi, A. & Miller, C. Secondary active transport mediated by a prokaryotic homologue of ClC Cl- channels. *Nature* **427,** 803–7 (2004).

60. Johnson, R. G. Accumulation of biological amines into chromaffin granules: a model for hormone and neurotransmitter transport. *Physiol. Rev.* **68,** 232–307 (1988).

61. Schuldiner, S., Shirvan, A. & Linial, M. Vesicular neurotransmitter transporters: from bacteria to humans. *Physiol. Rev.* **75,** 369–92 (1995).

62. Hu, G. *et al.* New fluorescent substrate enables quantitative and high-throughput examination of vesicular monoamine transporter 2 (VMAT2). *ACS Chem. Biol.* **8,** 1947–54 (2013).

63. Stuber, G. D., Hnasko, T. S., Britt, J. P., Edwards, R. H. & Bonci, A. Dopaminergic terminals in the nucleus accumbens but not the dorsal striatum corelease glutamate. *J. Neurosci.* **30,** 8229–33 (2010).

64. Hnasko, T. S. *et al.* Vesicular glutamate transport promotes dopamine storage and glutamate corelease in vivo. *Neuron* **65,** 643–56 (2010).

65. Callamaras, N. & Parker, I. Construction of a confocal microscope for real-time x-y and x-z imaging. *Cell Calcium* **26,** 271–9 (1999).

Chapter 3: APP+ is a Marker of Catecholamine Neurons in Brain Tissue, but not a Fluorescent False Neurotransmitter[1]

3.1 Introduction

3.1.1 More than just Dopamine

While the Fluorescent False Neurotransmitter (FFN) project is already being used to study dopamine (DA) neurotransmission in a way previously impossible, if this tool concept is going to provide a broader and more lasting impact on the field of neuroscience, then it needs to be applicable to more than just the DA system. Studying the direct effect of only one type of pre-synaptic neuron on its target cannot provide a comprehensive understanding of neuronal regulation. Instead, this type of understanding will require systematic studies that explore a wide range of potential neurotransmission inputs. The interconnections that comprise and control the circuits of the brain are exceptionally difficult to study because of the number of signaling pathways that are involved. This is exactly why, to be most impactful, FFNs must also be developed that can support the study of other, non-DA, neurotransmitter signaling systems. Although several examples of potential FFN functional uses were highlighted in Chapter 2, FFN102 is limited to studying the role of DA. Thus, our ultimate goal is to establish a multi-functional platform of selective FFN probes for all different types of neurotransmitters. Ideally, this would expand the possible application of FFNs to a much broader group of research questions across multiple brain regions, and allow a more complete elucidation of the role of

each type of neurotransmitter input in each of these systems. Due to the success of our DA-FFNs, we embarked on this new project by first exploring highly related members in the monoamine family; norepinephrine (NE) and serotonin (5-HT).

At the origin of the FFN project, our group screened a series of potential small fluorescent cores that could be potential FFNs. While this screen identified the coumarin core, which led to many successful DA-FFN probes[2–4], reviews of the literature highlighted the potential for fluorescent phenylpyridiniums as substrates for monoamine transporters (MATs) other than just the dopamine transporter (DAT). Particular examples of this group that were absent from our initial screening libraries appeared to be highly promising (discussed in 3.1.3). Therefore, combined with the resources and previous laboratory experience in developing and testing DA-FFNs, we sought to evaluate this additional fluorescent core as a potential FFN candidate for the NE and 5-HT systems.

3.1.2 Origins of MPP+ and the MAT link

The link between phenylpyridiniums and monoamines originates from the non-fluorescent 1-methyl-4-phenylpyridium (MPP+), which stems from medical observations collected from a group of recreational drug users[5,6]. An impure synthesis of the μ-opioid receptor agonist, 1-Methyl-4-phenyl-4-propionoxypiperidine (MPPP), led to the significant generation of 1-Methyl-4-phenyl-1,2,3,6-tetrahydropyridine (MPTP) as an undesired side product. The 23-year-old patient who inadvertently took MPTP developed severe Parkinsonism symptoms within days, which lasted for 18 months[6]. This degeneration was ultimately attributed to the metabolite of MPTP, 1-methyl-4-phenylpyridinium (MPP+). First, MPTP crosses the blood brain barrier, after which it metabolizes to MPP+ through monoamine oxidase-B (MAO-B)[7]. MPP+ is then taken up in monoaminergic neurons specifically, as it is a substrate of the MATs: the dopamine

transporter (DAT)[8,9], the norepinephrine transporter (NET)[10], and the serotonin transporter (SERT)[11]. After entering the cell, MPP+ is then concentrated in the matrix of the mitochondria, driven by the electrical gradient of the mitochondrial membrane and the positive charge on the pyridinium[7]. Once inside, MPP+ inhibits the electron transport chain through the binding of Complex I[12], which leads to ATP depletion and cell death.

Our group was further drawn to this molecule as a potential structural scaffold due to the discovered protective nature of the vesicular monoamine transporter (VMAT) in cells exposed to MPP+[13]. Increased VMAT2 expression can help rescue cells from MPP+ neurotoxicity, while inhibition of VMAT2 leads to increased neurotoxicity of the compound[14]. It is believed that by sequestering the compound into vesicles, VMAT2 limits the available MPP+ in the cytosol capable of entering the mitochondria and harming ATP production. For the FFN project, this compound posed an interesting potential lead, as it is a substrate for three monoamine transporters, it is sequestered into vesicles, and through slight chemical modifications, could be highly fluorescent.

3.1.3 Selection of APP+, a Fluorescent MPP+ Analogue

One of the first and most widely characterized fluorescent MPP+ analogues is 4-(4-(dimethylamino)styryl)-1-methylpyridinium (ASP+). ASP+ was first identified as a substrate for the low affinity and polyspecific transporter, organic cation transporter (OCT)[15]. In the brain, OCT-3 can transport monoamines, but with much less specificity and higher concentrations required compared to the respective MATs[16]. More recently, however, it was discovered that ASP+ is also a weak substrate of the three MATs (DAT, NET, and SERT), similar to MPP+[17]. In fact, ASP+ was one of the first successful examples of a fluorescent reporter of MAT activity. ASP+ has been used in this capacity to label cells expressing DAT, NET, or SERT, as well as to

study MAT binding and transport kinetics[18]. Although, the widespread use of ASP+ has been limited by the high binding constant and very slow catalytic turnover observed for MAT activity. A screen of ASP+ analogues led to the identification of (E)-4-[2-(6-hydroxy-2-naphthalenyl)ethenyl]-1-methyl-pyridinium iodide (HNEP+), which showed a promising increase in MAT activity[19]. However, like ASP+, HNEP+ is also highly lipophilic and had high non-specific uptake when used at concentrations required for studying MAT activity[18].

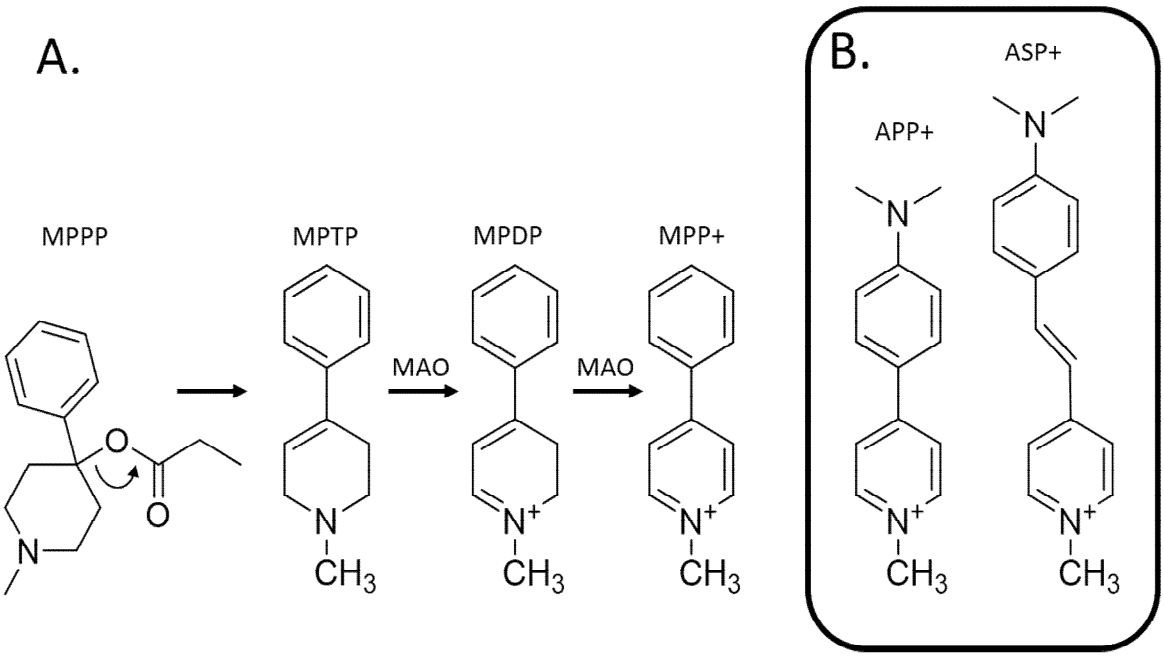

Figure 1. A) Elimination of the propanoyloxy group from the opioid agonist, MPPP, leads to formation of the undesirable compound, MPTP. In the brain, MPTP is oxidized by monoamine oxidase (MAO) to MPP+, which is a potent DAT, NET, and SERT substrate. B) Fluorescent MPP+ analogues, APP+ and ASP+, are potential FFNs for monoamine-systems other than DA.

The previous generation of fluorescent MPP+ analogues were improved upon by using the smaller and less lipophilic compound 4-(4-dimethylamino)phenyl-1-methylpyridium (APP+) (**Figure 1**). This compound is much closer in size and structure to MPP+, only deviating by a single dimethylamine electron donating group. While this fluorescent molecule had previously been used in photophysical chemistry, it was not until recently that its potential utility in

neuroscience become realized[20]. In tandem with our own research interests with this potential molecule, APP+ was shown to be a substrate for DAT, NET, and SERT, and identified as the fluorescent reporter in the commercial Neurotransmitter Transporter Uptake Assay Kit[21,22]. As a result, we decided to explore APP+ as a potential FFN lead, and a potential scaffold that could generate NE or 5HT selective FFNs. This chapter describes the characterization of this compound's utility as a labeling tool in both cell culture and *ex vivo* acute mouse brain slices, as well as the functional characterization of this probe as a potential reporter of monoaminergic neurotransmission.

3.2 Results and Discussion

3.2.1 APP+ is a DAT, NET, and SERT Substrate in Cell Culture

After identifying the most promising fluorescent analogue lead, APP+, we first wanted to confirm the observations that it was in fact a substrate of the three primary MATs: DAT, NET, and SERT. For these experiments, we used transfected cell cultures (either EM4 or HEK cell lines) overexpressing one of the MATs. APP+ (2μM) was bath applied to the cells (10min) and then cell fluorescence was measured. I would like to thank Dr. Rich Karpowicz, a former graduate student of Dr. Sames' laboratory, for his collaborative help with these initial cell-based screens.

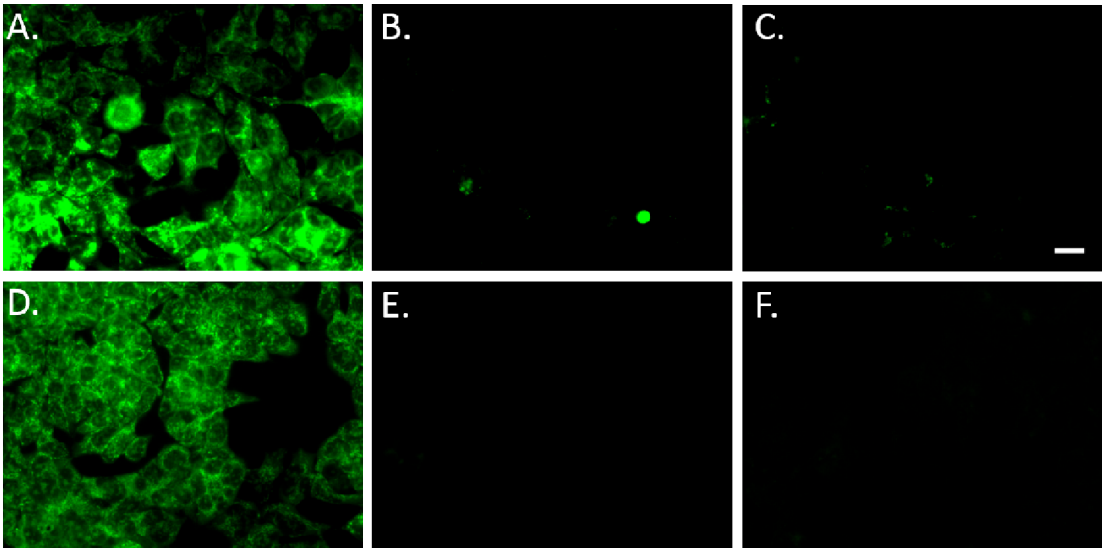

Figure 2. A) Representative fluorescent images of APP+ uptake (2µM for 10min) in hDAT-EM4 cells, compared to nomifensine (2µM) inhibited (B), or null-transfected EM4 cells (C). D) Representative fluorescent images of APP+ uptake (2µM for 10min) in hNET-HEK cells, compared to nomifensine inhibited (E), or null-transfected HEK cells (F). Scale bar: 15µm.

In hDAT-EM4 cells, treatment with APP+ resulted in significant punctated accumulation that was not present in null-transfected or DAT-inhibited (nomifensine, 2µM) EM4 cells (**Figure 2A-C**). Based on the charged nature of the APP+ dye and the previous MPP+ literature, we suspected that these intracellular puncta were most likely mitochondria. We confirmed this by the high degree of colocalization of APP+ fluorescence with that of Mitotracker Deep Red (**Figure 3**). These experiments were repeated with similar results in both hNET-HEK (**Figure 2D-F**) and hSERT-HEK[23]. During these experiments we also observed very low extracellular background fluorescence signal. This is consistent with the poor spectroscopic properties of the dye in aqueous environments, due to the twisted intramolecular change transfer (TICT) that occurs in polar environments (**Figure 4**)[24,25]. If the dihedral angle between the two ring systems is too great, the excited electron will decay in a nonradiative manner. Nonpolar environments or geometric restriction, such as when bound to a protein binding pocket, limit this rotation, which results in the highly fluorescent planar form of the molecule being favored[26].

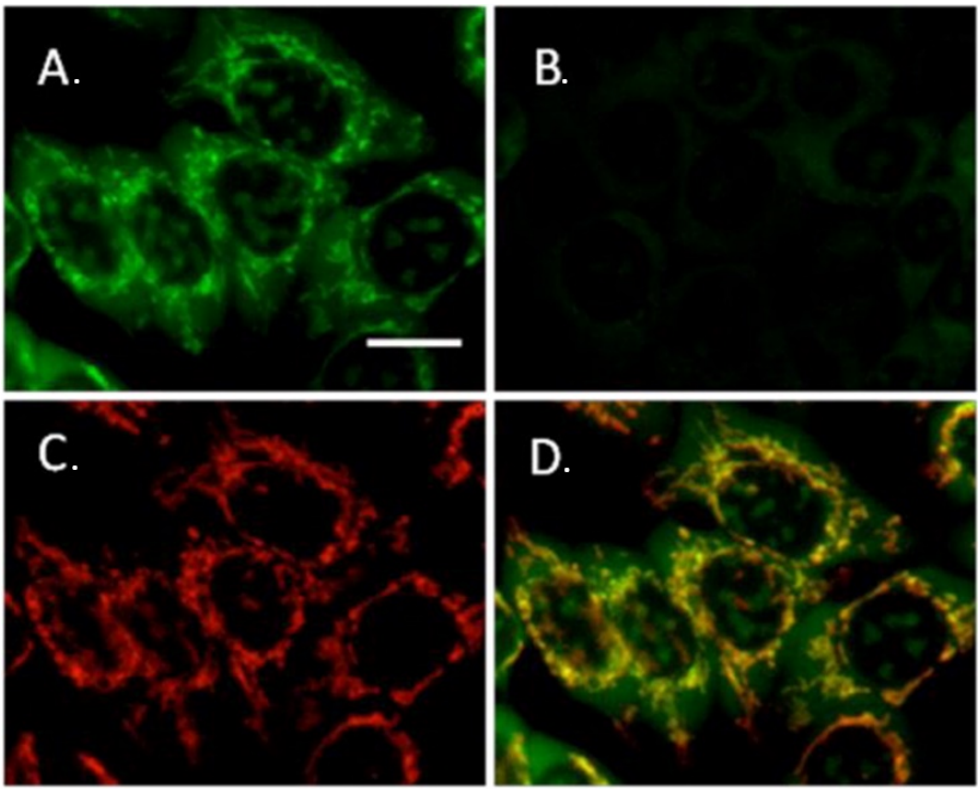

Figure 3. A) Higher magnification representative image of the APP+ fluorescence pattern in hDAT-EM4 cells. B) A comparable image in null-transfected EM4 cells. C) Mitotracker Deep Red (20nM for 10min) fluorescence pattern in the same hDAT-EM4 cells. D) Colocalization of APP+ and Mitotracker Deep Red in hDAT-EM4 cells. Scale bar: 15µm.

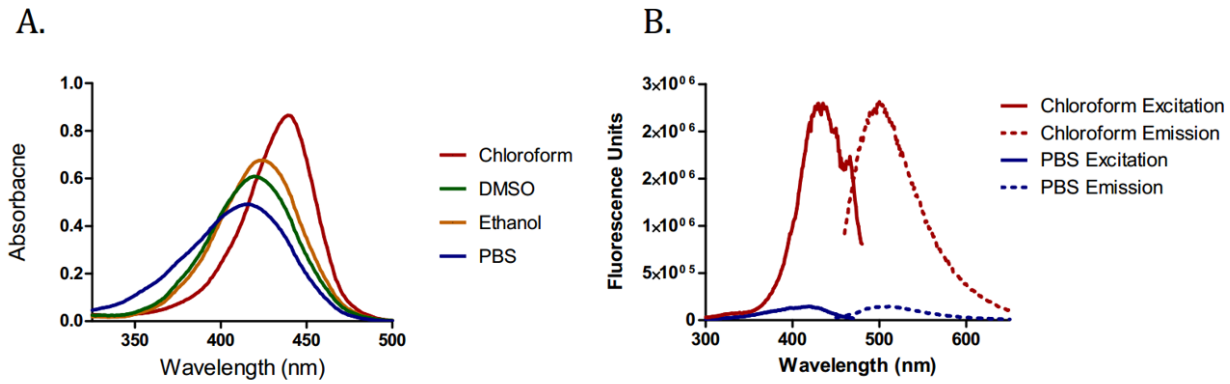

Figure 4. A) APP+ absorbance spectra in solvents of variable polarity. Highest absorbance was observed in chloroform, the least polar solvent out of the group. B) APP+ fluorescence excitation and emission spectra in either chloroform or phosphate buffered saline (PBS). Very little fluorescence was observed in PBS, a polar solvent, compared to chloroform.

3.2.2 APP+ is a VMAT2 Substrate in Cell Culture

After confirming the broad MAT substrate scope, we next tested APP+ for VMAT2 activity. These experiments were performed in HEK cells overexpressing rodent VMAT2 (VMAT2-HEK)[27]. Unlike the previous lines, VMAT2-HEK cells do not overexpress a monoamine transporter. As a result, for these experiments we used much longer incubation times (2μM for 60min) to allow APP+ to cross the membrane through other slower or less selective means. Interestingly, we observed that there was significantly less fluorescence accumulation in VMAT2-HEK cells than that of their null-transfected HEK cell counterpart (**Figure 5**). Similar to the DAT-EM4 cells, null-transfected HEK cells showed a strong punctated staining pattern, while VMAT2-HEK cells had much dimmer puncta. Using Mitotracker Deep Red we saw no apparent difference in the mitochondrial labeling between the two cell lines, ruling out potential differences in the number, or membrane potential, of the mitochondria between the two cell lines (**Figure 5**). Similar to what is known about MPP+ and VMAT2, we believe that this result is due to a second potential APP+ concentration sink in acidic compartments generated by VMAT2 that competes with APP+ accumulation in mitochondria. Due to the previously discussed photophysical properties of this fluorophore, APP+ is potentially only weakly fluorescent in these compartments compared to when mitochondrial bound.

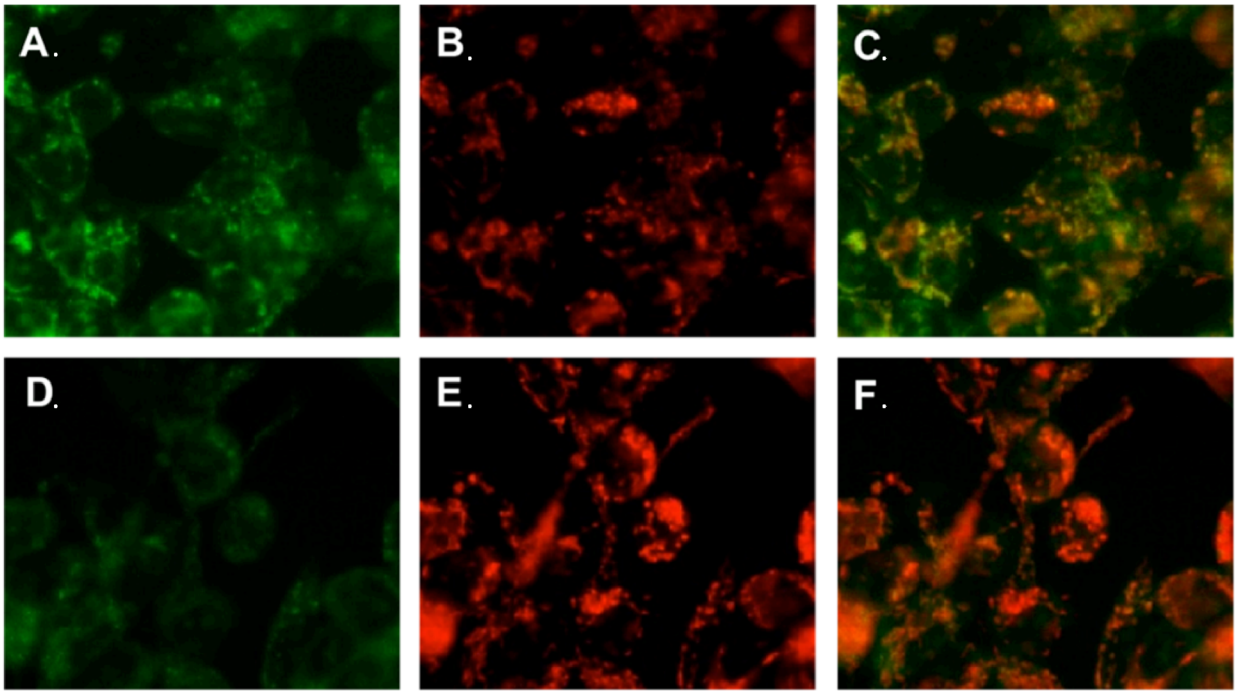

Figure 5. A) In TetR-HEK control cells, APP+ (2µM) fluorescence signal strength and pattern was comparable to observations in hDAT-EM4, and hNET-HEK cells. The incubation time required to reach comparable fluorescence was considerably longer without expression of a MAT (60min). Mitotracker Deep Red (B) still had a high degree of colocalization (C) in TetR-HEK cells. D) APP+ fluorescence signal, under the same loading conditions, in VMAT2-HEK cells was significantly reduced. Using Mitotracker Deep Red (E), we confirmed that the decrease in fluorescence signal was not due to an absence of mitochondria or degradation of the mitochondrial membrane potential.

We explored this hypothesis further using two different VMAT2 inhibitors, dihydrotetrabenazine (dTBZ, 2µM) and reserpine (1µM). Surprisingly, these inhibitors did not consistently rescue the bright punctated mitochondrial labeling as observed in the controls (**Figure 6**). Results from this experiment were quite variable, but inevitably did not lead to a quantifiably significant change between uninhibited and inhibited VMAT2-HEK cells. In trying to explain this result, we had to look more closely at the VMAT2-HEK system and the properties of APP+. First, unlike our potential neuronal targets, the VMAT2-HEK cells have no surface MAT activity and there may have been only a very low concentration of APP+ that crossed the membrane. This intracellular concentration could still be sequestered into acidic compartments if a small percentage of VMAT2 were still active, or it could be pumped out of the cytosol through

an efflux transporter. Since MPP+ was used as a method of selective pressure in generating this VMAT2-HEK cell line, an efflux transporter capable of transporting APP+ might even be upregulated in this cell line[27].

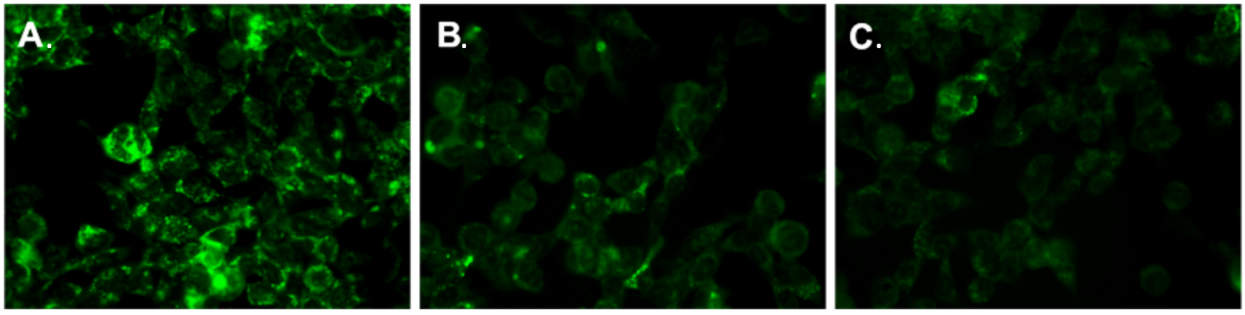

Figure 6. APP+ uptake (2μM for 60min) in TetR-HEK cells (A) resulted in a strong fluorescence signal and mitochondrial punctated pattern, compared to APP+ fluorescence in VMAT2-HEK cells (B), as observed in **Figure 5**. C) Inhibition of VMAT2 with reserpine (1μM) did not significantly restore APP+ fluorescence.

During our experimentation, however, it was independently reported in Dr. Miller's laboratory that APP+ could be used as a reporter to assay VMAT2 activity[28]. While this report was promising for confirming that APP+ was a VMAT2 substrate, the problems faced during our experimentation with APP+ and VMAT2-HEK cells highlighted potential problems of using this dye as an FFN. Although the system is far removed from that of an actual neuronal synapse, potential sequestering of APP+ into the vesicular lumen of neuronal synapses would need to result in a measurable amount of fluorescence if we hoped to observe activity-dependent changes as with other FFNs. Some of this concern was again dissuaded by follow-up results published by Dr. Miller's laboratory, where they were able to show fluorescence overlap between VMAT2-mCherry and APP+, which could be reduced with TBZ (20μM) inhibition[29]. Therefore, we thought the probe was interesting enough to pursue for further experimentation in brain tissue.

3.2.3 APP+ Labels Catecholamine Neurons in Brain Tissue

The next set of experiments describe the first use of APP+ dye in *ex vivo* acute murine brain slices. At the time, use of this dye had only been previously characterized in cell culture and the peripheral nervous system[30]. Based on our previous familiarity with the DA system, and available genetic markers within the laboratory, we first looked at APP+ uptake in DA cells and projections. Using mice that express GFP under the catecholamine specific tyrosine hydroxylase promoter (TH-GFP), APP+ cellular uptake was colocalized with GFP signal in the substantia nigra (SN) and ventral tegmental area (VTA), areas rich with DA neurons (**Figure 7**). For these experiments, the brain slice was perfused with 500 nanomolar APP+ for 30 minutes, followed by a 10 minute wash period. This resulted in a significant number of cell bodies that had fluorescent signal from each fluorophore, as well as a large degree of nonspecific punctated structures (~2-3μm) only observed in the channel collecting APP+ fluorescence. When counting the number of cells with GFP that were also APP+ positive, as determined by a fluorescence intensity two fold greater than the background, we observed a 76 percent colocalization (84/110 cells from 6 different mice). Importantly, when comparing colocalization in the other direction, I was unable to find any APP+ positive cells that did not also have TH-GFP, suggesting that APP+ cellular uptake was specific to dopaminergic neurons, but uptake by all dopaminergic neurons was not complete. It is possible that some of the TH-GFP positive neurons may not have accumulated detectable levels of APP+ due to poor overall health or lower DAT expression compared with their neighbors. To confirm that this uptake was DAT dependent, the experiment was repeated using a pretreatment (15min) with the DAT-inhibitor nomifensine (2μM). This resulted in a significant reduction in the number of colocalized cells, from 76 percent to 7 percent (3/43 cells from 3 different mice) (**Figure 7**). However, the use of this DAT-inhibitor did not affect the punctated APP+ staining surrounding the cells, and while the APP+ cellular labeling in this area

seemed to be strongly dopaminergic and DAT-dependent, the scattered puncta staining seemed non-specific. Discussed later in this chapter will be our hypothesis on the cause for this scattered punctated background labeling. As for the cell bodies, a higher magnification revealed that unlike what we had observed with our coumarin-based FFNs, the labeling was perinuclear with puncta in the soma. This is consistent with our observations in cell culture, and it is likely that a significant portion of the fluorescence in neuronal cell bodies was from mitochondrial bound APP+.

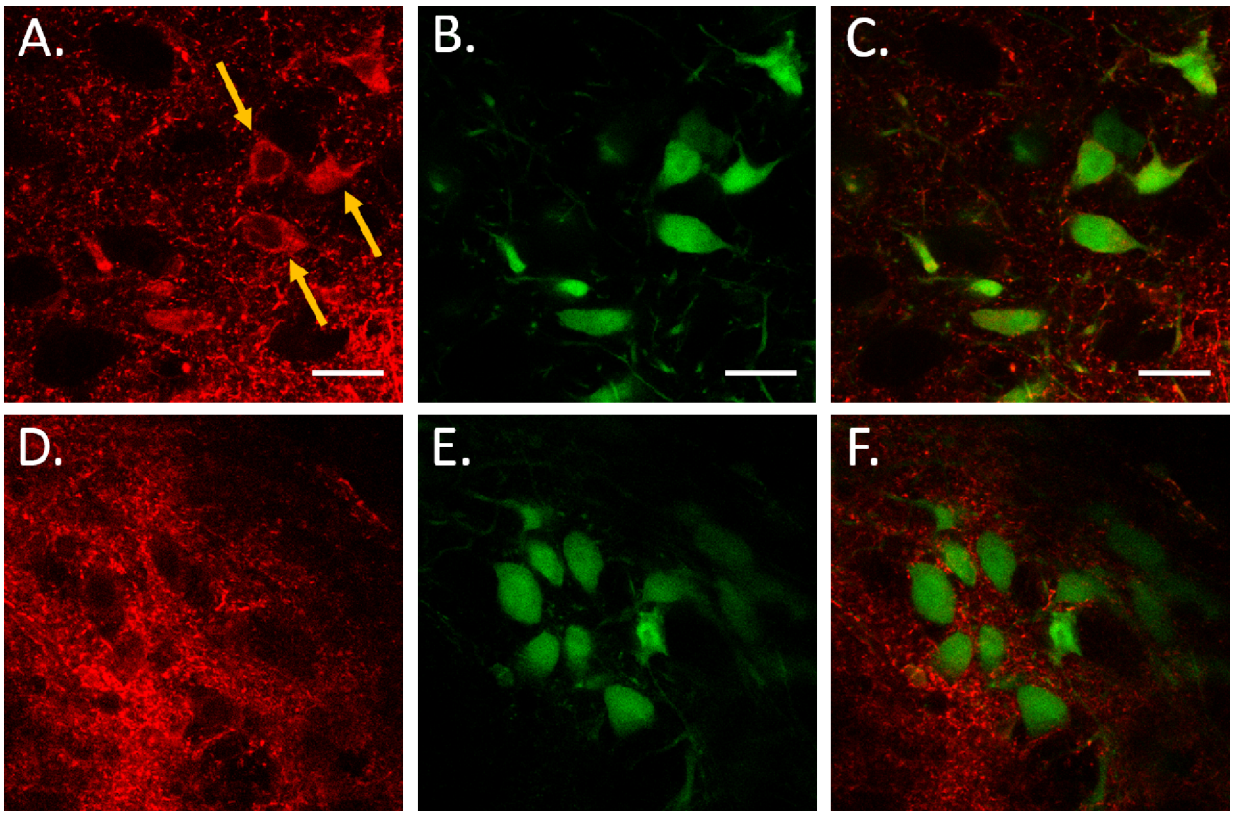

Figure 7. Colocalization of APP+ and dopaminergic neurons of the ventral tegmental area (VTA) and substantia nigra (SN) that express GFP under the catecholamine-specific tyrosine hydroxylase promoter (TH-GFP). A) APP+ (500nM) loaded cell bodies in this area after 30min. B) TH-GFP from the dopaminergic neurons in the same field of view. C) Overlay of the two fluorophores resulted in a 76% colocalization between APP+ and dopaminergic cell bodies. We observed significant background signal, although labeled cell bodies were visible, as highlighted with yellow arrows. D-F) This experiment was repeated in the presence of the DAT-inhibitor, nomifensine (2μM), which significantly decreased APP+ uptake in cell bodies, but not the background. The resulting colocalization of cell bodies for this experiment was 7%. Scale bar: 20μm.

In addition to DA cells, TH-GFP also labels NE cells. Therefore, with this genetic marker we also measured APP+ uptake in the locus coeruleus (LC), which is the primary location of NE cell bodies in the brain. Initial results of this colocalization experiment performed in adult mice showed very little APP+ uptake. Further literature research into the LC showed that NET expression drastically changes with age, with dramatic decreases observed in the LC upon reaching adulthood[31,32]. Repeating colocalization in young mice (21-30d postnatal) yielded much more promising results (**Figure 8**). Similar to what was observed in the SN/VTA, all APP+ positive cells also had TH-GFP, and 59% of TH-GFP positive cells also had APP+ (74/126 cells from 3 different mice). We believe that this increase in the amount of colocalization when using young animals was due to the greater NET expression responsible for actively transporting APP+. The colocalization percentage might have been higher if the animals used were at peak NET expression (10d postnatal), but collecting slices from animals younger than 3 weeks would have been much more challenging. Lastly, we briefly looked for serotonergic labeling in the dorsal raphe (DR), but at the time we did not have a genetic marker for serotonergic neurons. Also, measuring SERT-specific APP+ labeling in this area was made more difficult by dopaminergic neurons (A10c), which are also present in this area and were also labeled by APP+[33].

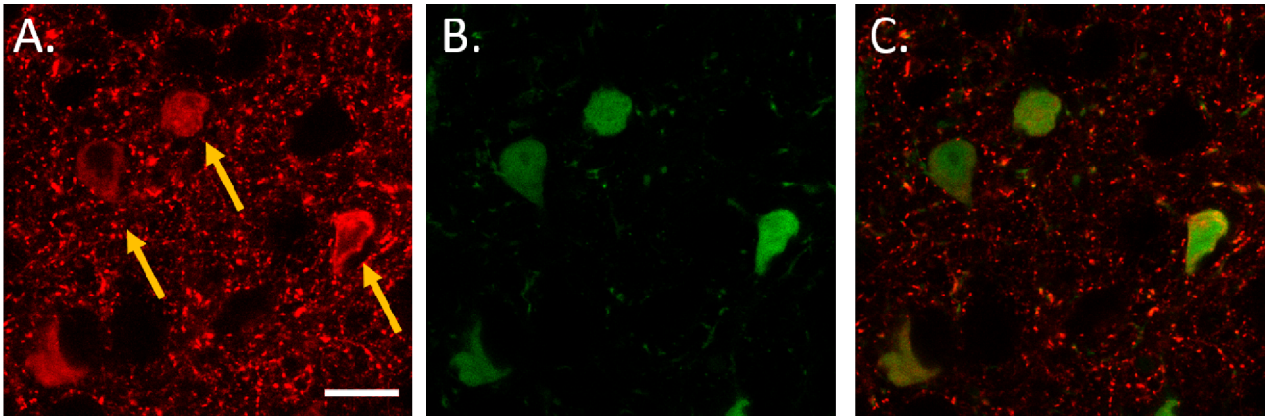

Figure 8. Colocalization of APP+ and noradrenergic neurons of the locus coeruleus (LC) that express GFP under the catecholamine-specific tyrosine hydroxylase promoter (TH-GFP). A) APP+ (500nM) loaded cell bodies in this area after 30min. B) TH-GFP from the dopaminergic neurons in the same field of view. C) Overlay of the two fluorophores resulted in a 76% colocalization between APP+ and dopaminergic cell bodies, as labeled by yellow arrows. Scale bar: 20µm.

3.2.4 APP+ Labels Dopaminergic Projections

In addition to labeling cell bodies, we were also interested in examining the projections of those neurons, and, in particular, potential release sites. We chose to perform these experiments in the dorsal striatum (DS) and study the same dopaminergic projections as described in Chapter 2, due to the familiarity with the area and the availability of colocalization markers. When loading the projections in this area with the APP+ dye, a lower concentration (100nM) and shorter incubation time (15min) were sufficient to observe bright APP+ puncta (**Figure 9B**). Additionally, because of the low concentrations used, and the low background signal present due to the aqueous photophysical properties of the dye, very little washing was required to achieve a strong signal/background ratio. Colocalization of APP+ puncta with TH-GFP resulted in a high degree of overlap, with a quantification of 83.4 ± 6.9% of APP+ puncta that colocalized with TH-GFP (mean ± SD, 2-3 slices per animal, 3 different animals) (**Figure 9**). Unlike what was observed in cell bodies, 10.1 ± 5.7% of APP+ puncta were actually bright enough to cause significant florescent bleedthrough and be detected in the GFP channel when using WT animals without GFP as a control (mean ± SD, 2-3 slices per animal, 3 different

animals) (**Figure 10**). While the two-photon excitation spectra are fairly well separated, the similar emission wavelengths of GFP and APP+ resulted in this small percentage of bleedthrough.

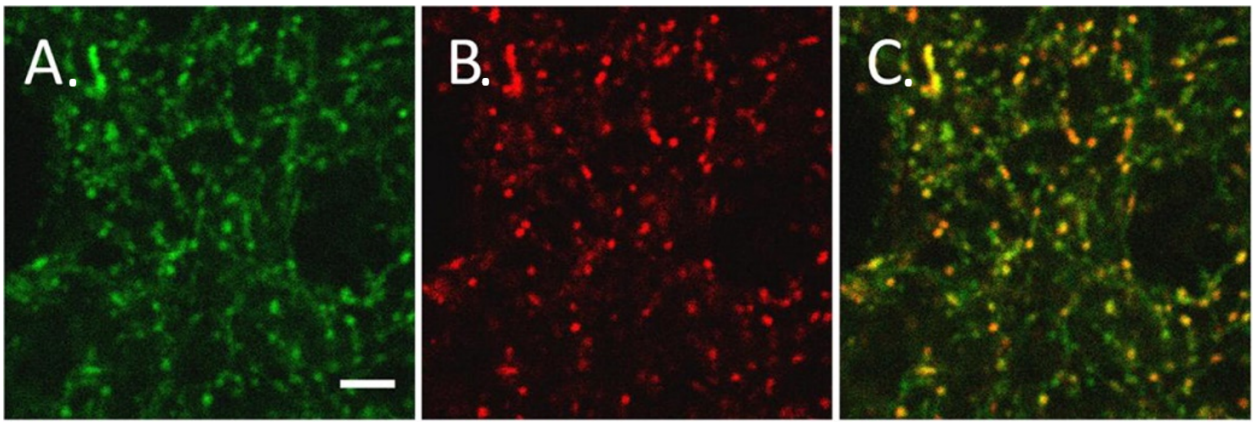

Figure 9. A) Representative image of GFP signal in the dorsal striatum of acute murine brain slices driven by the catecholamine-specific promoter tyrosine hydroxylase (TH-GFP) B) APP+ (100nM for 15min) fluorescence in the same area. C) There was a strong colocalization between the two fluorophores, and an 83.4% colocalization of APP+ puncta with TH-GFP. Scale bar: 5µm.

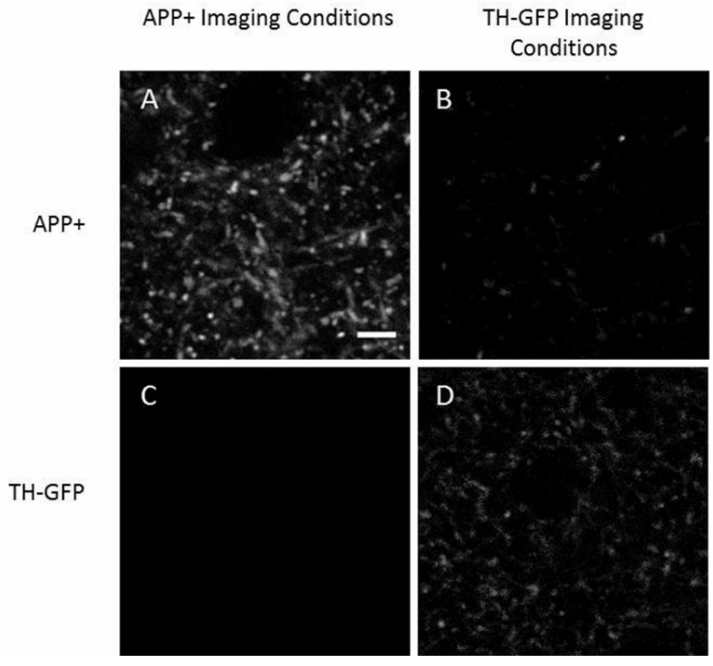

Figure 10. Overlap of APP+ and GFP fluorescence emission resulted in small amount of APP+ fluorescence entering the GFP imaging channel (B). This fluorescence bleedthrough led to a potential increase in falsely identified colocalized puncta by 10.1%. Scale bar: 5µm.

In light of this bleedthrough issue with GFP, we used a second independent confirmation of dopaminergic labeling, FFN102. We have already demonstrated that FFN102 has greater than a 90% colocalization with TH-GFP, and has photophysical properties that can be well separated from APP+ (FFN102 is described and characterized in Chapter 2)[2]. Colocalization between these two fluorescent probes was performed in wild type animals, and resulted in a 74.1 ± 6.9% of APP+ puncta colocalizing with FFN102 puncta (mean ± SD, 2-3 slices per animal, 3 different animals) (**Figure 11**). These results are consistent with the TH-GFP and bleedthrough control experiments, and highlight that >70% of APP+ puncta in the dorsal striatum are dopaminergic.

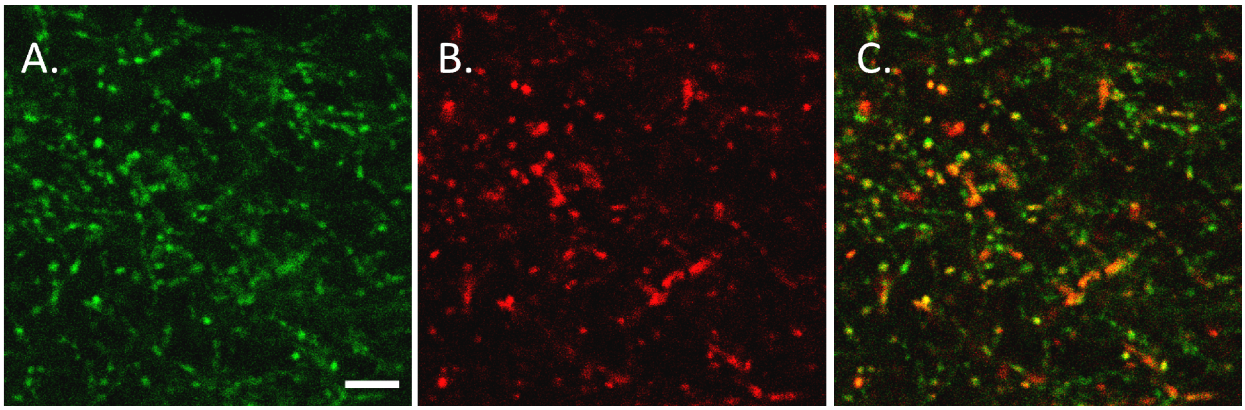

Figure 11. A) Representative image of FFN102 (10µM for 30min) signal in the dorsal striatum of acute murine brain slices. B) APP+ (100nM for 15min) fluorescence in the same area. C) There was strong colocalization between the two fluorophores, and 74.1% colocalization of APP+ puncta with FFN102. Scale bar: 5µm.

To further confirm dopaminergic projection labeling by APP+, inhibiting DAT with a nomifensine (1µM) pretreatment led to a 2.3-fold reduction in the number of APP+ puncta (**Figure 12**). While the reduction was statistically significant, we noticed that the majority of the remaining puncta were very large (>1µm). While these puncta were still within the maximum observed size range, typical dopaminergic release sites are usually less than 0.5µm, suggesting that these structures were most likely not dopaminergic synapses[34]. It is possible that when the high-affinity DAT activity was blocked, weaker and competing transport mechanisms on non-

dopaminergic structures contributed more to the staining pattern. We thought it was possible that APP+, like MPP+ and ASP+, might also be transported by low-affinity and high-capacity transporters, such as OCT-3. This theory was confirmed in our laboratory with hOCT3-transfected HEK cells and corticosterone inhibition[35]. These results could also explain the high non-specific background observed in the cellular-uptake experiments in the VTA/SN and LC, where the amount of DAT expression relative to the field area was much lower[36,37]. In conclusion, however, APP+ fluorescence in the dorsal striatum seemed to be fairly specific for dopaminergic projections under normal experimental conditions, and could lead to a potential FFN if that staining pattern changed upon neuronal activity.

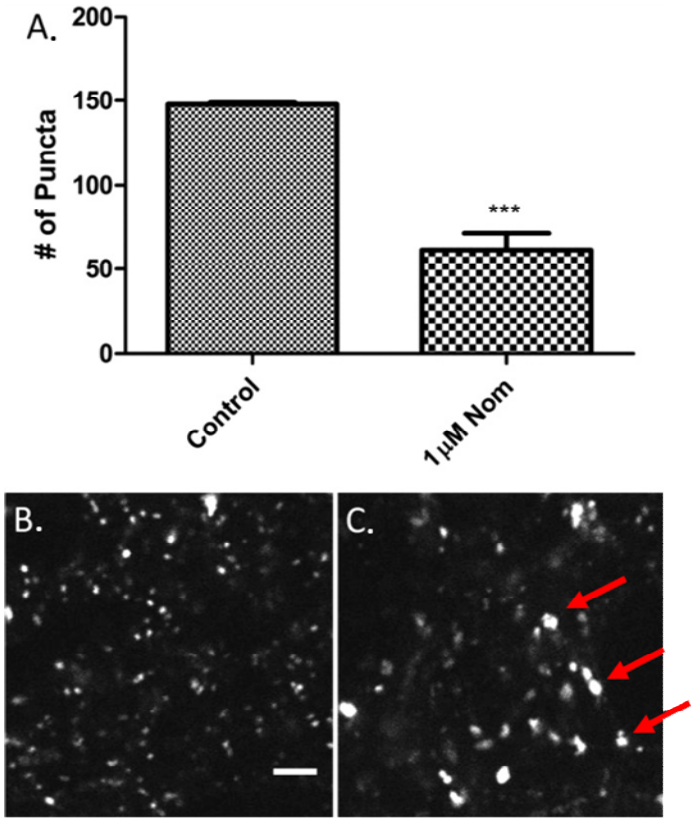

Figure 12. A) Quantification of the number of APP+ puncta in the dorsal striatum of acute brain slices with and without the DAT-inhibitor, nomifensine (1μM). Nomifensine resulted in a 2.3 fold reduction in the number of puncta. B) Representative image of APP+ fluorescence in this area under normal conditions. C) Representative image of APP+ fluorescence in the presence of nomifensine. We noted an increase in very large puncta that are most likely not dopaminergic in the presence of nomifensine (red arrows). Scale bar: 5μm.

3.2.5 APP+ is not an FFN

One of the defining characteristics of an FFN is that it can be used as a measure of neurotransmission. This means that the probe must be packaged into vesicles and show a quantifiable change upon vesicular exocytosis. While APP+ seemed to be relatively selective at entering dopaminergic synapses, and it is suspected to be a VMAT2 substrate, we next needed to assess potential changes to the APP+ puncta fluorescence using two different neuronal stimulation protocols in acute slices. The first protocol involved perfusing the slice with an increased K^+ concentration (40mM KCl) to chemically depolarize the membranes. This is a very harsh method of inducing exocytosis that for our previous FFNs caused almost complete destaining of all labeled puncta within ~3 minutes, as well as significant movement of the slice due to global neuronal activation. It was first noticed that continual imaging of a small area of APP+ puncta over time led to rapid destaining that was not dependent on the arrival of the change in K^+ concentration. The same imaging protocols and similar laser power used for measuring release over time of FFN102 and other probes in our lab, led to rapid photobleaching of the APP+ probe[2]. This was confirmed by imaging APP+ washing/bleaching kinetics over time at different imaging frequencies. The probe fluorescence was very stable over 15 minutes when imaged every 1 minute, but showed a 73% decrease when imaged every 15 seconds. When 40mM KCl stimulation experiments were repeated at this slower imaging rate there was a 15.3 ± 2.5% decrease in the APP+ puncta fluorescence after 8 minutes (mean ± SD, 2-3 slices per animal, 3 different animals). Although the 40mM KCl perfused slices showed a significant reduction in APP+ staining versus untreated slices just 1 minute after increased K^+ concentrations reached the slice (t-test, $p < 0.05$), the extent of the total destaining observed did not mimic the almost complete FFN102 depletion observed after ~3 minutes under similar conditions (**Figure 13**).

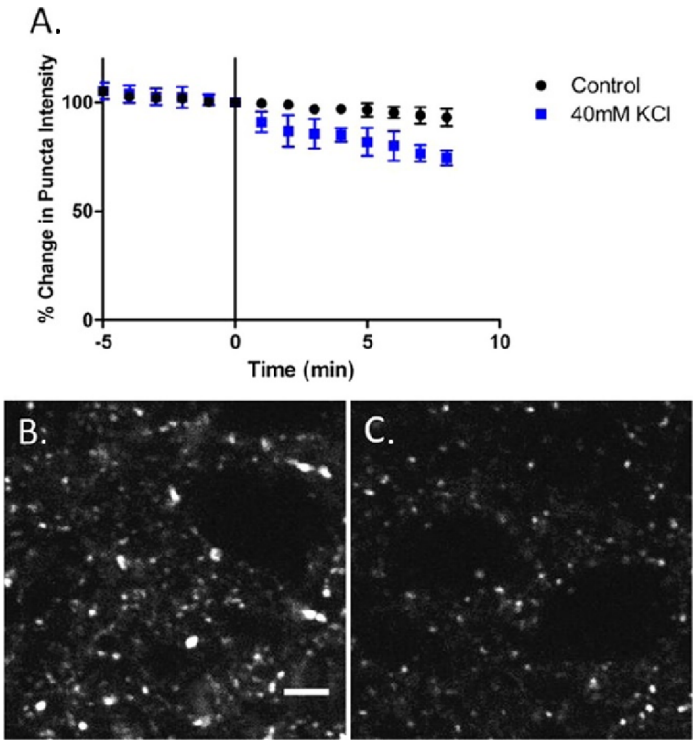

Figure 13. A) Change in average puncta intensity over time in the presence or absence of 40mM KCl depolarization conditions. We observed a significant decrease in fluorescence intensity of APP+ puncta, but only to a very small degree (15.3%). Representative images of APP+ fluorescence before (B) and 8min after (C) KCl depolarization. We observed a large number of puncta still present after KCl, compared to the complete elimination observed with FFN102 puncta after a KCl treatment[2]. Scale bar: 5µm.

One limitation of using 40mM KCl is that there are drastic spatial deformations of the acute slice that occur when every single neuron is triggered to fire. This leads to slice shifts that change the microscope field of view and make tracking individual puncta over a long time course problematic. As a result, it is impossible to definitively identify the source of that 15% reduction in APP+ fluorescence using this method. We hypothesized that there were two likely possibilities based on our previous experiments with this probe. First, the APP+ signal from different dopaminergic projections was primarily from APP+ in hydrophobic environments, such as mitochondrial membranes, and not from the probe that is sequestered into vesicles. This type of staining pattern would then be relatively uniform across the whole population of APP+ positive dopaminergic terminals, and would result in a small and equal change in fluorescence

from every puncta. The second possibility is that there is some heterogeneity between the puncta and that some might have a much higher proportion of fluorescence that is contributed by the vesicular population. These puncta might not have a nearby mitochondria or other favorable hydrophobic environment that overwhelms the fluorescent signal. As a result, these puncta, which are a small portion of the total population (~15%), might completely destain, while the others would show a very weak change in fluorescence.

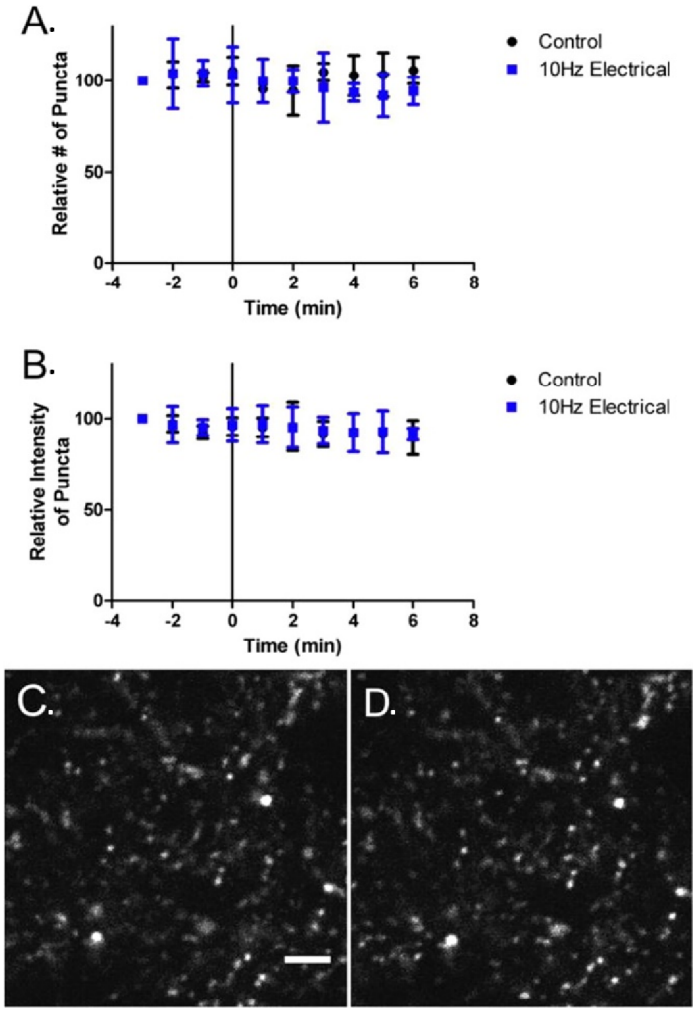

Figure 14. Quantification of the percent change in puncta number (A) and relative intensity (B) during the course of tonic electrical stimulation (local 10Hz stimulation for 600pulses). We observed no significant change in either parameter by the end of the stimulation, as well as no individual puncta that were identified to fully destain. Representative images of APP+ fluorescence in the same field of view before (C) and 6min after (D) electrical stimulation. Scale bar: 5µm.

To test these hypotheses we switched to an electrical stimulation protocol similar to the protocol described in Chapter 2 (2.2.1), which is known with other FFNs to result in significant fluorescent changes in some release sites. Local electrical stimulation is a milder and more physiologically relevant way to activate neurons than 40mM KCl perfusion, and therefore does not cause drastic changes in the field of view. Again, imaging every 15 seconds, 3600 pulses (10Hz) were delivered locally to the striatum and the specific fluorescence of individual puncta was measured over time (**Figure 14**). This stimulation protocol led to no significant change in the number of puncta, 94.6 ± 11.8% for unstimulated vs. 86.7 ± 9.7% for stimulated, or average fluorescence of a puncta, 89.6 ± 9.2% for unstimulated vs. 91.6 ± 3.1% for stimulated (mean ± SD, 2-3 slices per animal, 3 different animals, ANOVA: $p > .05$). Additionally, no puncta were identified by our selection criteria similar as described in Chapter 2 (2.1.3) to have decreased in intensity sufficiently to be considered destained.

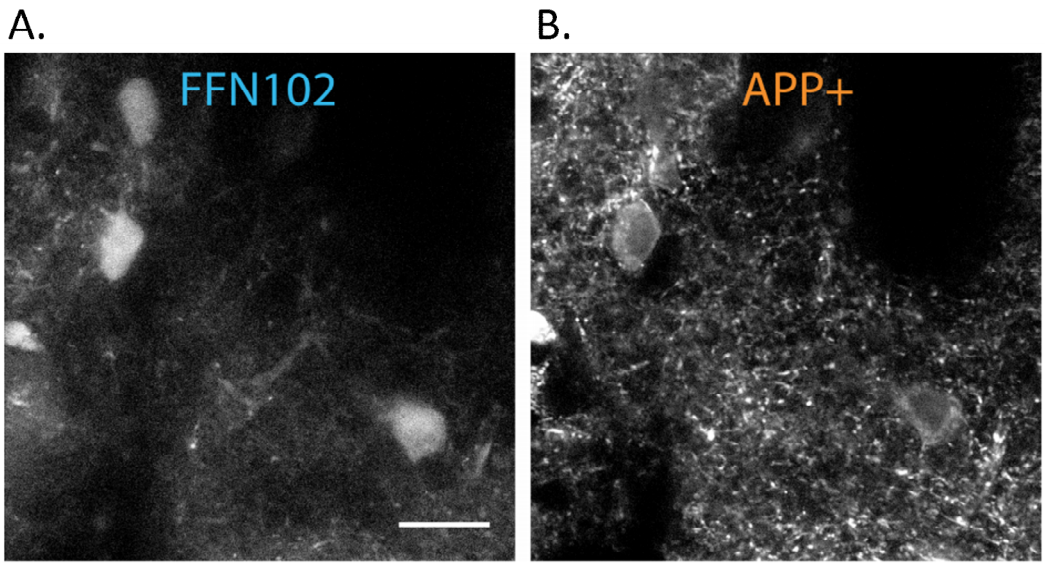

Figure 15. Representative images of FFN102 (A) and APP+ (B) fluorescence from loaded dopaminergic neurons in the ventral tegmental area. To determine if APP+ was acutely toxic, APP+ was loaded into these neurons first (500nM for 45min), then FFN (10µM) was added to the APP+ solution for the following 30min. We did not observe

any qualitative changes in FFN102 loading, or morphological changes to the cell bodies, over this time period. Scale bar: 20μm.

These results suggest that the releasable vesicular APP+ only accounted for a small percentage of the total fluorescence from each puncta. Therefore, APP+ might not be the next broad spectrum FFN that we originally were seeking, but its interesting properties could be useful for other experiments, such as *in vivo* changes in mitochondrial density or membrane potential of monoaminergic neurons. As a result, we wanted to test for acute toxicity of this probe for relatively short exposures similar to the experiments described above, a potentially important parameter when considering the future applications of APP+. This was tested by conducting a 45 minute pretreatment of APP+ (500nM) in SN/VTA neurons in acute brain slice, followed by standard FFN102 loading over 30 minutes[2]. Imaging at the end of the 75 minute time course showed the typical APP+ labeling as previously described, as well as, typical FFN102 labeling as previously observed in our group (2-3 slices per animal, 2 different animals) (**Figure 15**). On this time scale, APP+ did not seem to have a detrimental effect on DAT activity, although this evidence is simply supportive and not conclusive. If APP+ was negatively impacting mitochondria and ATP production on this time scale, it is expected that DAT activity would be impaired after the sodium potassium pump lost its energy source[38]. This also suggests that the small changes in simulated release we observed with 40mM KCl and electricity were not due to APP+ toxicity. Additionally, this supports the conclusion that APP+ could be used as a monoaminergic neuronal marker for functional assays within a time window before MPP+-like toxicity starts to occur (estimated 18h for MPP+)[39].

3.3 Conclusion

In this chapter, the monoamine specific application of APP+, a fluorescent analogue of the MPP+ toxin, was explored in the search for new FFNs. We confirmed reports that APP+ was

a substrate of the three monoamine transporters, DAT, NET and SERT, a first for a fluorescent probe in our assays. Testing for VMAT2 activity suggested that APP+ was also a substrate, which was independently confirmed during our experimentation[28]. Based on the results obtained in these preliminary cell culture assays, we then tested this compound in *ex vivo* acute mouse brain slices to determine its behavior in neurons.

These *ex vivo* experiments showed that there was selective accumulation of the APP+ probe in both dopaminergic and noradrenergic cell bodies through monoamine transporter function, but that there was also surrounding puncta staining through a DAT/NET-independent uptake mechanism. Additionally, as observed in cell culture, staining in these cell bodies was punctated and perinuclear, which is likely to be mitochondrial. This highlights a potential use of APP+ as a monoaminergic cellular marker similar to GFP, but without requiring genetic manipulation. Further, due to its accumulation in mitochondria, this probe could also be used as a monoamine selective mitochondrial reporter, or in assays elucidating the connection between MPP+ toxicity and Parkinsonism.

APP+ was also tested in dopaminergic projections to further access its potential viability as an FFN. The APP+ punctated staining pattern observed in the dorsal striatum showed high colocalization with both TH-GFP and FFN102 dopaminergic markers (~75%). However, this staining remained largely stable after both 40mM KCl and electrical stimulation conditions (<15% fluorescence change). This was thought to be due to the relatively small percentage of fluorescence signal that came from APP+ inside the vesicular lumen relative to the total synapse. This was in part due to the poor photophysical properties of the probe in hydrophilic compared to hydrophobic environments, and the competing sequestering of this charged molecule in

mitochondrial membranes. We therefore concluded that APP+ was suitable for labeling studies, but it was not applicable for further pursuit as a new, functional NE or 5HT-FFN lead.

3.4 References

1. Karpowicz, R. J., Dunn, M., Sulzer, D. & Sames, D. APP+, a fluorescent analogue of the neurotoxin MPP+, is a marker of catecholamine neurons in brain tissue, but not a fluorescent false neurotransmitter. *ACS Chem. Neurosci.* **4,** 858–69 (2013).

2. Rodriguez, P. C. *et al.* Fluorescent dopamine tracer resolves individual dopaminergic synapses and their activity in the brain. *Proc. Natl. Acad. Sci. U. S. A.* **110,** 870–5 (2013).

3. Gubernator, N. G. *et al.* Fluorescent false neurotransmitters visualize dopamine release from individual presynaptic terminals. *Science* **324,** 1441–4 (2009).

4. Hu, G. *et al.* New fluorescent substrate enables quantitative and high-throughput examination of vesicular monoamine transporter 2 (VMAT2). *ACS Chem. Biol.* **8,** 1947–54 (2013).

5. Langston, J. W., Ballard, P., Tetrud, J. W. & Irwin, I. Chronic Parkinsonism in humans due to a product of meperidine-analog synthesis. *Science* **219,** 979–80 (1983).

6. Davis, G. C. *et al.* Chronic Parkinsonism secondary to intravenous injection of meperidine analogues. *Psychiatry Res.* **1,** 249–54 (1979).

7. Singer, T. P., Ramsay, R. R., McKeown, K., Trevor, A. & Castagnoli, N. E. Mechanism of the neurotoxicity of 1-methyl-4-phenylpyridinium (MPP+), the toxic bioactivation product of 1-methyl-4-phenyl-1,2,3,6-tetrahydropyridine (MPTP). *Toxicology* **49,** 17–23 (1988).

8. Javitch, J. A., D'Amato, R. J., Strittmatter, S. M. & Snyder, S. H. Parkinsonism-inducing neurotoxin, N-methyl-4-phenyl-1,2,3,6 -tetrahydropyridine: uptake of the metabolite N-methyl-4-phenylpyridine by dopamine neurons explains selective toxicity. *Proc. Natl. Acad. Sci.* **82,** 2173–2177 (1985).

9. Bougria, M., Vitorica, J., Cano, J. & Machado, A. Implication of dopamine transporter system on 1-methyl-4-phenylpyridinium and rotenone effect in striatal synaptosomes. *Eur. J. Pharmacol. Mol. Pharmacol.* **291,** 407–415 (1995).

10. Pifl, C., Hornykiewicz, O., Giros, B. & Caron, M. G. Catecholamine transporters and 1-methyl-4-phenyl-1,2,3,6-tetrahydropyridine neurotoxicity: studies comparing the cloned human noradrenaline and human dopamine transporter. *J. Pharmacol. Exp. Ther.* **277,** 1437–43 (1996).

11. Pifl, C., Schingnitz, G. & Hornykiewicz, O. Effect of 1-methyl-4-phenyl-1,2,3,6-tetrahydropyridine on the regional distribution of brain monoamines in the rhesus monkey. *Neuroscience* **44,** 591–605 (1991).

12. Murphy, M. P., Krueger, M. J., Sablin, S. O., Ramsay, R. R. & Singer, T. P. Inhibition of complex I by hydrophobic analogues of N-methyl-4-phenylpyridinium (MPP+) and the use of an ion-selective electrode to measure their accumulation by mitochondria and electron-transport particles. *Biochem. J.* **306 (Pt 2,** 359–65 (1995).

13. Liu, Y. *et al.* A cDNA that suppresses MPP+ toxicity encodes a vesicular amine transporter. *Cell* **70,** 539–51 (1992).

14. Staal, R. G. & Sonsalla, P. K. Inhibition of brain vesicular monoamine transporter (VMAT2) enhances 1-methyl-4-phenylpyridinium neurotoxicity in vivo in rat striata. *J. Pharmacol. Exp. Ther.* **293,** 336–42 (2000).

15. Hohage, H., Stachon, A., Feidt, C., Hirsch, J. R. & Schlatter, E. Regulation of organic cation transport in IHKE-1 and LLC-PK1 cells. Fluorometric studies with 4-(4-dimethylaminostyryl)-N-methylpyridinium. *J. Pharmacol. Exp. Ther.* **286,** 305–10 (1998).

16. Duan, H. & Wang, J. Selective transport of monoamine neurotransmitters by human plasma membrane monoamine transporter and organic cation transporter 3. *J. Pharmacol. Exp. Ther.* **335,** 743–53 (2010).

17. Schwartz, J. W., Blakely, R. D. & DeFelice, L. J. Binding and transport in norepinephrine transporters. Real-time, spatially resolved analysis in single cells using a fluorescent substrate. *J. Biol. Chem.* **278,** 9768–77 (2003).

18. Schwartz, J. W., Novarino, G., Piston, D. W. & DeFelice, L. J. Substrate binding stoichiometry and kinetics of the norepinephrine transporter. *J. Biol. Chem.* **280,** 19177–84 (2005).

19. Brown, A. S., Bernal, L.-M., Micotto, T. L., Smith, E. L. & Wilson, J. N. Fluorescent neuroactive probes based on stilbazolium dyes. *Org. Biomol. Chem.* **9,** 2142–8 (2011).

20. Coe, B. J. *et al.* Quadratic Optical Nonlinearities of N-Methyl and N-Aryl Pyridinium Salts. *Adv. Funct. Mater.* **13,** 347–357 (2003).

21. Blakely, R. D., Mason, J., Tomlinson, I. D. & Rosenthal, S. J. Fluorescent substrates for neurotransmitter transporters. US7947255 B2 (2011).

22. Jørgensen, S., Nielsen, E. Ø., Peters, D. & Dyhring, T. Validation of a fluorescence-based high-throughput assay for the measurement of neurotransmitter transporter uptake activity. *J. Neurosci. Methods* **169,** 168–76 (2008).

23. Solis, E. *et al.* 4-(4-(dimethylamino)phenyl)-1-methylpyridinium (APP+) is a fluorescent substrate for the human serotonin transporter. *J. Biol. Chem.* **287,** 8852–63 (2012).

24. Kharlanov, V. & Rettig, W. Excited-state relaxation of bridged and unbridged anilino-pyridinium dyes. *Chem. Phys.* **332,** 17–26 (2007).

25. Fromherz, P. & Heilemann, A. Twisted internal charge transfer in (aminophenyl)pyridinium. *J. Phys. Chem.* **96,** 6864–6866 (1992).

26. Wilson, J. N., Ladefoged, L. K., Babinchak, W. M. & Schiøtt, B. Binding-induced fluorescence of serotonin transporter ligands: A spectroscopic and structural study of 4-(4-(dimethylamino)phenyl)-1-methylpyridinium (APP(+)) and APP(+) analogues. *ACS Chem. Neurosci.* **5,** 296–304 (2014).

27. Adam, Y., Edwards, R. H. & Schuldiner, S. Expression and function of the rat vesicular monoamine transporter 2. *Am. J. Physiol. Cell Physiol.* **294,** C1004–11 (2008).

28. Bernstein, A. I., Stout, K. A. & Miller, G. W. A fluorescent-based assay for live cell, spatially resolved assessment of vesicular monoamine transporter 2-mediated neurotransmitter transport. *J. Neurosci. Methods* **209,** 357–66 (2012).

29. Bernstein, A. I., Stout, K. A. & Miller, G. W. The vesicular monoamine transporter 2: an underexplored pharmacological target. *Neurochem. Int.* **73,** 89–97 (2014).

30. Parker, L. K., Shanks, J. A., Kennard, J. A. G. & Brain, K. L. Dynamic monitoring of NET activity in mature murine sympathetic terminals using a fluorescent substrate. *Br. J. Pharmacol.* **159,** 797–807 (2010).

31. Murrin, L. C., Sanders, J. D. & Bylund, D. B. Comparison of the maturation of the adrenergic and serotonergic neurotransmitter systems in the brain: implications for differential drug effects on juveniles and adults. *Biochem. Pharmacol.* **73,** 1225–36 (2007).

32. Sanders, J. D., Happe, H. K., Bylund, D. B. & Murrin, L. C. Development of the norepinephrine transporter in the rat CNS. *Neuroscience* **130,** 107–17 (2005).

33. Stratford, T. R. & Wirtshafter, D. Ascending dopaminergic projections from the dorsal raphe nucleus in the rat. *Brain Res.* **511,** 173–176 (1990).

34. Freund, T. F., Powell, J. F. & Smith, A. D. Tyrosine hydroxylase-immunoreactive boutons in synaptic contact with identified striatonigral neurons, with particular reference to dendritic spines. *Neuroscience* **13,** 1189–1215 (1984).

35. Karpowicz, R. J. Advanced Fluorescent False Neurotransmitters for the study of Monoamine Transporter Activity and Synaptic Transmission. *Columbia Univ. Ph.D Thesis* (2014).

36. Arbuthnott, G. W. & Wickens, J. Space, time and dopamine. *Trends Neurosci.* **30,** 62–9 (2007).

37. Lorang, D., Amara, S. G. & Simerly, R. B. Cell-type-specific expression of catecholamine transporters in the rat brain. *J. Neurosci.* **14,** 4903–14 (1994).

38. Giros, B. & Caron, M. G. Molecular characterization of the dopamine transporter. *Trends Pharmacol. Sci.* **14,** 43–49 (1993).

39. Nakai, M., Mori, A., Watanabe, A. & Mitsumoto, Y. 1-methyl-4-phenylpyridinium (MPP+) decreases mitochondrial oxidation-reduction (REDOX) activity and membrane potential (Deltapsi(m)) in rat striatum. *Exp. Neurol.* **179,** 103–10 (2003).

Chapter 4: FFN270: A New pH-sensitive Optical Tracer of Norepinephrine that Resolves Individual Noradrenergic Synapses and Their Activity *in vivo*

4.1 Introduction

4.1.1 Studying Norepinephrine Neurotransmission

In the initial search for a norepinephrine (NE) specific fluorescent false neurotransmitter (FFN), the phenylpyridinium core appeared promising initially (Chapter 3), but did not meet all the criteria of a true FFN. To trace neurotransmission, a FFN must load into specific release sites, get packaged into vesicles, and most importantly, be released upon vesicle fusion. Undaunted, we continued to search for fluorescent compounds that could accumulate in noradrenergic neurons and be used to trace NE release, in other words, a NE-FFN. The critical need to develop new methods for studying NE neurotransmission in particular is due to the severe limitations of the currently available tools combined with existing evidence highlighting the importance of NE as a global modulator of neuronal activity across many brain area. Additionally, because the exogenous substrate scope of NET is sufficiently promiscuous (**Figure 1**, see also discussion in Chapter 3.1), we believed further pursuit of a NET-driven NE-FFN would be a fruitful endeavor with a reasonable chance for success[1–3].

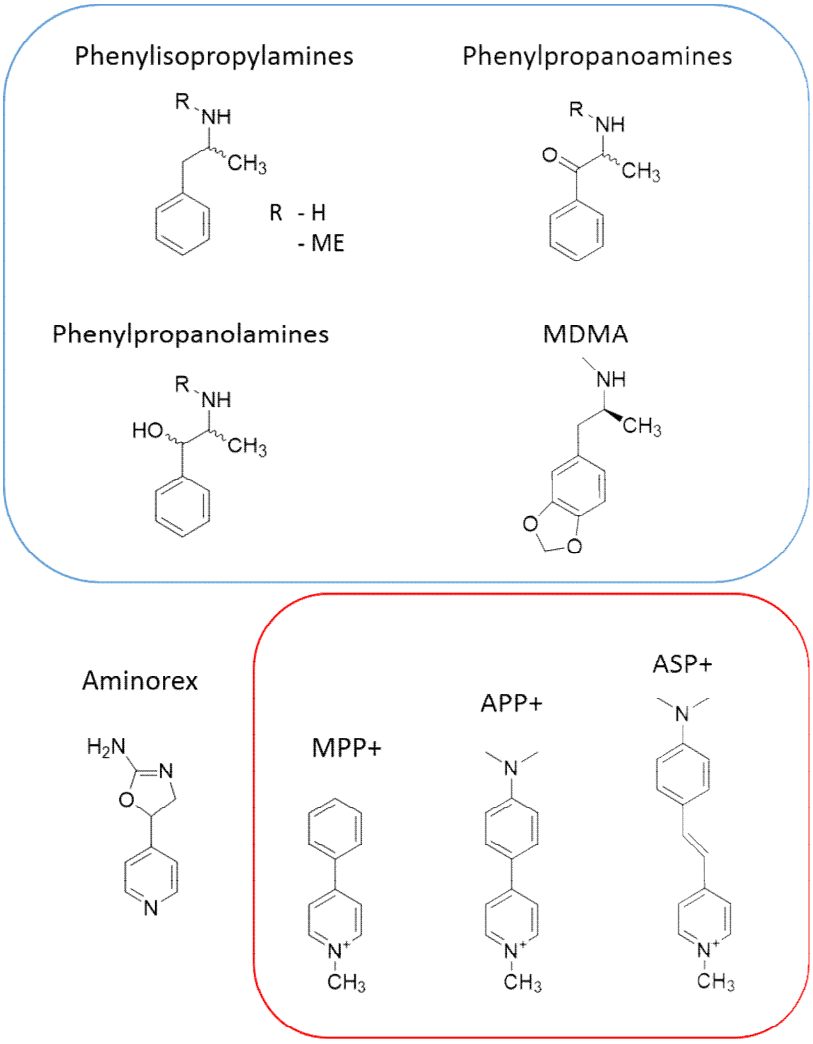

Figure 1. Representative NET substrates. Highlighted in blue are a series of phenethylamines with varying degrees of oxidation that are all NET substrates (EC_{50} < 500nM, except for (1R,2R)-2-methylamino-1-phenylpropan-1-ol). Aminorex is a similarly structured NET substrate (~50nM). Highlighted in red are the series of compounds discussed in Chapter 3 that have all been shown to be NET substrates.

As briefly covered in Chapter 1, the current tools to study catecholamine neurotransmission have room for improvement, but the deficiency of the toolkit is greater for NE transmission in comparison to dopamine (DA) transmission. This lack of adequate tools has made studying the role of NE in the brain particularly challenging and highlights a rationale for the development of a NE-FFN. It is only recently that advancements in electrochemical techniques and electrodes have enabled the functional distinguish between NE from DA or other analytes, but many of these techniques have yet to be usefully applied beyond an *in vitro*

setting[4–6]. Traditionally, electrochemical NE detection has only been correlative to extracellular NE concentrations when applied to specific brain areas with low DA levels, when combined with microdialysis[7], or when relative changes in metabolite concentrations are measured[8]. Recent adaptations of cell-based neurotransmitter fluorescent engineered reporters (CNiFERs) to the NE system has improved the ability to specifically detect extracellular NE concentrations in relevant time scales[9]. However, both CNiFER and electrochemical methods still lack sufficient spatial resolution to resolve individual synapses.

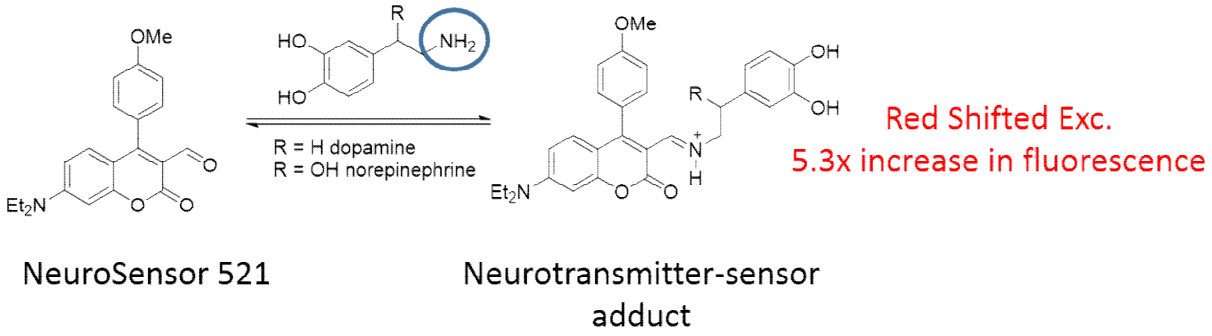

Figure 2. The aldehyde of NeuroSensor 521 reacts with the primary amine of NE to form an iminium ion. This dehydration reaction is driven forward by the high concentrations of NE found within the vesicles. The maximum excitation wavelength of the product is significantly red shifted, and can result in fluorescence increases of 5.3 fold when saturated with NE. As highlighted with a blue circle, this chemosensor is not specific for NE and can react with any concentrated primary amine[10].

Development of fluorogenic chemosensors, such as the coumarin-based NeuroSensor 521 (**Figure 2**), have enabled high-spatial resolution imaging of norepinephrine containing large dense core vesicles (LDCV) in chromaffin cells[10]. NeuroSensor 521 reacts with the primary amine of NE, forming an iminium ion, which results in a significant red shift in the excitation wavelength of the fluorophore. Unlike previous norepinephrine imaging techniques that require fixation, it is possible to use NeuroSensor 521 in living systems. However, its application has been limited to cell culture. Furthermore, although this sensor demonstrates selectivity for the primary amine of norepinephrine over the secondary amine of epinephrine, it is also highly

reactive with many other important neurotransmitters with primary amines, including dopamine, glutamate, and glycine[10]. As a result of this lack of specificity, the potential utility for this sensor in dissecting the role of individual neurotransmission pathways in brain tissue is limited.

Overall, due to the limitations of the techniques recently developed for measuring NE release, they have not yet played an important role in elucidating the function of NE in the brain. The vast majority of research in this area has been performed by measuring large scale changes in bulk NE release. This includes, but is not limited to, measuring with microdialysis[11], electroencephalogram (EEG)[12], or recording the collective firing of the main nucleus of noradrenergic cell bodies[13], the locus coeruleus (LC). While these methods are well-established and have led to many advancements in understanding the role of NE, they have extremely poor spatial or temporal resolution. One of the most popular methods, recording from noradrenergic neurons in the LC, has excellent temporal resolution, but is correlated with global extracellular NE levels. Spatial resolution can be improved to levels approaching electrochemistry when using microdialysis, but the poor temporal resolution remains a large are problem (seconds timescale)[11]. A more complete and detailed understanding of the roles and regulation of NE in the brain can only be realized by introducing robust new methods for studying NE neurotransmission that have improved spatial and temporal resolution.

4.1.2. Norepinephrine Functions in the Brain

NE produces its effect on target neurons via activation of G-protein coupled receptors (GPCRs). This specific group of GPCRs, called adrenergic receptors, has 3 sub-families, α-1, α-2, and β adrenergic receptors. Each subtype has been shown to have variations in substrate binding or particular G-protein coupled signal transmission[14]. Depending on the adrenergic receptor subtype, NE binding can lead to activation of either the G_s (stimulation of adenylate

cyclase), G_i (inhibition of adenylate cyclase), or G_q (activation of phospholipase-C) proteins[15]. Modulation of adenylate cyclase leads to changes in cyclic-AMP production, which has an extensive range of intracellular downstream effects depending on neuronal type. Activation of phospholipase-C leads to increased intracellular calcium levels, which can increase the probability of neuronal firing, discussed in more detail in 4.3.8. The varying, and sometimes competing, effects of these adrenergic receptors means that NE modulation does not always have the same pre- or post-synaptic effect, making studying the role of the NE system in neuromodulation even more complex.

Despite drawbacks with current methods of studying NE neurotransmission, and the complicated nature of adrenergic receptors, a large body of evidence supports the connections between NE regulation and numerous cognitive functions and psychiatric disorders. Primarily originating from the locus coeruleus (LC), noradrenergic neurons widely project to many areas of the brain and central nervous system, including the cortex, hippocampus, hypothalamus, amygdala, spinal cord, and others[16]. Having a regulatory impact on such diverse group of brain regions has led to implicating NE dysregulation in an equally diverse group of disorders, including depression[17,18], attention deficit hyperactivity disorder[19], post-traumatic stress disorder[20], drug addiction/withdrawal[21–23], and autism[24,25]. Additionally, in Parkinson's disease, degeneration of NE neurons is observed prior to DA depletion and is thought to be responsible for the cognitive disorders that are present in the prodromal stage before the onset of motor disturbances[26]. However, the exact mechanism by which NE dysregulation plays a role in each of these diseases and disorders has not yet been clearly established, because the normal function of NE in the brain is still poorly understood. This is in part due to the lack of adequate research

tools (as discussed above) to assess how each NE-synaptic connection contributes to the functioning of this important neurotransmission pathway.

Traditionally, NE was believed to be a global regulator of tonic brain activity. Because the neuronal projections of the LC innervate more brain regions than any other described nucleus, it was believed that NE must be having a general regulatory effect on brain activity[27]. Experiments using iontophoretically applied NE to specific neurons or brain areas generally demonstrated a decrease in spontaneous neuronal activity, while either enhancing or suppressing evoked activity of targeted neurons[28,29]. Combined with data that showed drastic changes in NE brain levels from sleep to awake[30] and from normal to stressed[31] behaviors, NE was thought to globally modulate brain activity for heightened sensory responsiveness. Particular increases in LC neuronal firing were observed when a stimulus interrupted the animal's ongoing activity, suggesting that NE plays an important role in attention and arousal, helping to determine the importance of a stimulus and coordinate the brain's appropriate functional response[32]. However, recent evidence suggests that the role of NE is more complicated. First, the neurons of the LC are not all phenotypically equal, nor are they distributed homogenously within this nucleus. The LC has its own sub-regional organization, with four phenotypically distinguishable groups of noradrenergic cell types that project to specific brain regions[33]. The LC neurons that project into different brain regions can also have different firing rates and different morphological axonal arborization patterns, presumably due to the differences in NE-driven neuromodulation occurring in different terminal fields[33,34].

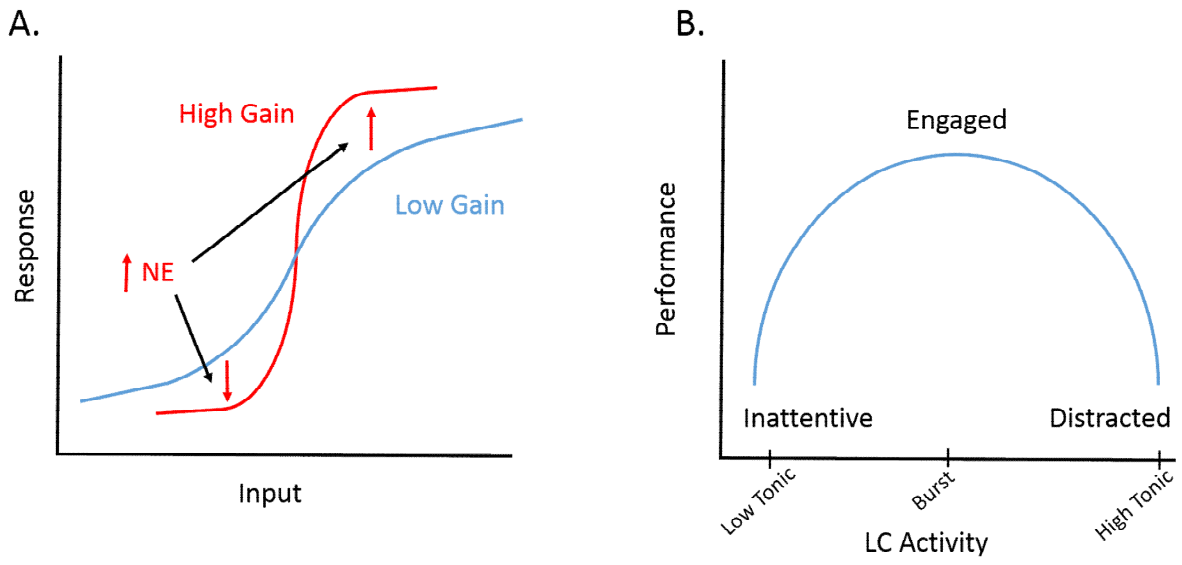

Figure 3. A) Visual representation of the "adaptive-gain" theory. NE neuronal targets can be differentially modulated by NE input. An increase in gain caused by NE neuromodulation leads to an increase in contrast of the excitatory or inhibitory response of the target neuron, leading to a more binary behavior. B) Animal behavioral performance follows an inverted-U pattern with levels of LC activity. Low LC activity leads to inattentiveness, while periods of burst firing lead to active engagement with the task. However, consistently high activity leads to poor task performance and an easily distracted behavior[35].

From this evidence, a current hypothesis in the field states that NE modulates its neuronal targets by either increasing the activity of units receiving excitatory input or decreasing activity of those receiving inhibitory inputs[36]. This "adaptive-gain" hypothesis helps explain why increased levels of NE can have conflicting modulating effects on the firing rates of different neurons within the same population (**Figure 3**). This increased modulating function of NE during arousal actually has an inverted-U-shaped relationship to functional behavior. Low tonic LC activity results in a careless and inattentive behavior. Low tonic firing with periods of increased LC phasic firing facilitates the evaluation and exploration of a particular new task as important or rewarding. However, continuously high LC activity leads to a distractible behavior where the ongoing activity is no longer novel or engaging[37]. Therefore, it is hypothesized that NE-driven "arousal" plays an important role in decision making, and acts as a filter to determine which task is worth exploring and engaging further, while simultaneously allowing for a currently engaged

and ongoing task to be modified with the addition of new information[35]. This role in behavior is believed to be accomplished by the LC exerting regulating control over multiple brain areas simultaneously, and modulating the firing of particular regions in-sequence.

Related to input processing, there is also a link between the NE-system and cognition. The normal quiescent behavior of LC neurons during slow-wave sleep is interrupted by transient increases that are observed only if there was a recent intensive learning experience[38]. It is believed this NE release plays a role in memory consolidation by modulating long-term potentiation or depression (LTP or LTD) through activation of β-noradrenergic receptors and the downstream cyclic-AMP cascade[39]. Additionally, the NE-system has been deemed to be important in memory retrieval. Animals that had forgotten a previously learned memory task would show drastic memory improvements when the LC was remotely stimulated[40] or when extracellularly NE levels were increased pharmacologically[41]. Mice lacking the noradrenergic-specific protein used to synthesize NE (and epinephrine), dopamine β-hydroxylase (DBH), showed the ability to remember tasks up to 48 hours later, but showed poor retrieval of long-term memories[42]. Furthermore, in humans, fMRI has been used to show that increased LC activity strongly correlates with memory retrieval, especially during the retrieval of memories linked to a strong emotional response[43].

In summary, the NE-system appears to play critical roles in regulating arousal of the brain and in coordinating the firing patterns of different brain regions to appropriately evaluate particular sensory information, consolidate memories, or retrieve memories. The majority of the research in this area, especially behavioral, has relied on global LC firing patterns or artificial NE increases to connect the NE-system to a particular response. However, the various regions of the LC and its projections are not uniform, and the particular firing patterns and axonal

arborization vary for individual noradrenergic neurons. As will be discussed in more detail later in this chapter, FFNs would provide a unique opportunity to study native NE neurotransmission on the micro-anatomical scale. The ability to determine how individual noradrenergic release sites affect neighboring neurons or postsynaptic targets may provide insights into how the macroscopic NE-driven neuromodulation leads to the associated functional behaviors.

4.2 Results and Discussion

4.2.1 Initial NET Substrate Leads

The story of developing our first NE-FFN is one that comes full circle. It begins *in vivo* with preliminary observations from two of our DA-FFNs (FFN102 and FFN202)[44,45], rapidly progressing to chemical optimization of related core molecules using NET-transfected cell culture screens, followed by characterization of the optimized fluorescent probes in acute murine brain slices, and finally, returning *in vivo* to demonstrate the utility of the resultant NE-FFN (FFN270) in examining NE transmission in living rodent.

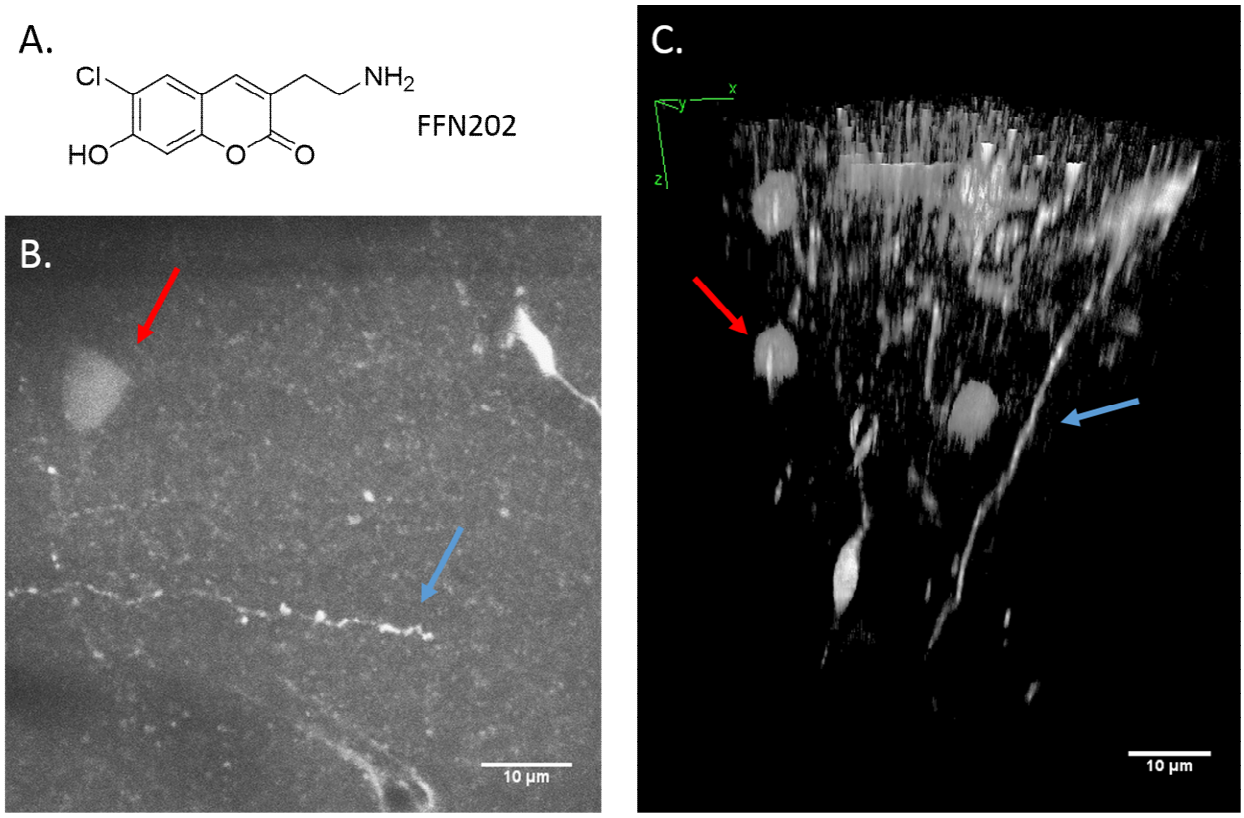

Figure 4. A) Structure of FFN202, the first FFN to be tested *in vivo*. B) Two-photon fluorescence image of FFN202 taken in Layer 1 of the somatosensory cortex. Red arrow: cell body, Blue arrow: axonal structure. C) 3-D reconstruction of FFN202 labeling in the outer 100µm of somatosensory cortex. More axonal structures are observed traveling in the z-plane. Scale Bar: 10µm.

Thanks to the collaborative help of Dr. Wenbiao Gan (New York University), we had the opportunity to explore the uptake of FFN102 and FFN202 into the outer layers of the somatosensory and motor cortex *in vivo* (**Figure 4**). With FFN102, we did not observe any specific uptake into axons or release sites in this preliminary *in vivo* experiment. Although, with the 3-ethylamine structural isomer, FFN202, we observed a few fluorescent strings that looked axonal. Due to the comparative lack of FFN102 uptake, we suspected that the FFN202 uptake was most likely not into dopaminergic structures, but may represent the sparse, structurally similar, noradrenergic projections that are present throughout the cortex. As a result, we decided to screen our coumarin library for any NET-specific uptake using the same hNET-transfected HEK cells described in Chapter 3 (3.2.1). I would like to thank Dr. Adam Henke, a former post-

doctoral member of Dr. Sames' laboratory, for his collaborative help with these initial cell-based screens, as well as the chemical synthesis of new leads described below.

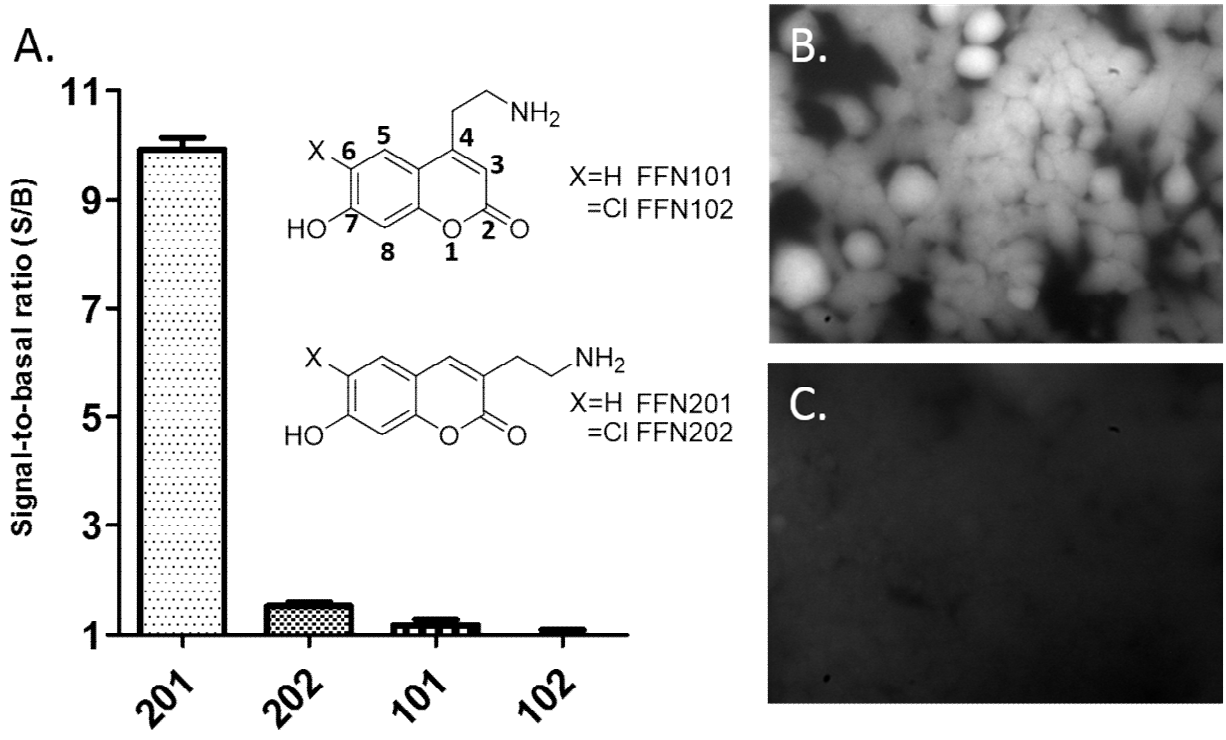

Figure 5. A) Total cellular fluorescence after loading of 3- and 4-series 7-hydroxycoumarins (5µM) in hNET-HEK cells. Signal to Basal ratio (S/B) was determined by comparing FFN fluorescence in the presence and absence of 2µM nomifensine after a 30min incubation period. Included are the structures of each FFN used in the experiment and the structural numbering for the coumarin core. Representative images of FFN201 without inhibitor (B) and with inhibitor (C). In panel B, loaded-FFN201 exhibits diffuse distribution throughout hNET-HEK cells, but this loading was blocked with nomifensine in panel C.

When FFN102 and FFN202 were initially applied to hNET-HEK cells (5µM for 30min), with and without NET-inhibition (nomifensine, 2µM), FFN102 showed no NET-specific uptake and FFN202 showed slight NET-specific uptake. Intrigued by these results, we also screened the structural core molecules of each of these FFNs: the 3-aminoethyl-7-hydroxycoumarin (FFN201) for FFN202 and the 4-aminoethyl-7-hydroxycoumarin (FFN101) for FFN102. This was in hope of better understanding what structural features may be driving the difference in NET-specific uptake. Similar to FFN102, the 4-series core showed no NET-specific uptake, suggesting that the

ethylamine side chain in the 4-position prevents NET transport. In contrast, we observed a very strong NET-specific uptake with the 3-series core, FFN201 (S/B Ratio: 9.9±0.2, mean ± SEM, n = 3). The signal-to-basal ratio of FFN201 was over five-fold greater than that of FFN202 (**Figure 5**). This suggested that the 3-position for the ethylamine side chain is tolerated by NET, but that the chlorine on the 6-position for FFN202 was limiting NET activity. The electron withdrawing group (EWG) chlorine was originally added to this position to modulate the pKa of the 7-hydroxy group[45]. In the absence of the EWG that pulls electron density from the ring, the pKa of the 7-hydroxyl on FFN201 is 8.0, well outside of the range required for measuring a change in fluorescence when transported between the vesicular lumen (pH: 5.5) and the extracellular space (pH: 7.4). Addition of the chlorine to the 6-position, as seen in FFN202, lowered the pKa to 6.4, making possible its use in functional release studies, similar to those described in Chapter 2. With FFN201 now identified as our new lead NE-FFN core, a series of pH-sensitive analogues were synthesized and tested for hNET activity.

4.2.2 Identification of FFN270 in hNET-HEK Cell Culture Screens

Based on the observations from the initial transfected cell-based screens above, a second-generation set of 3-aminoethyl-7-hydroxycoumarin compounds were synthesized and tested in hNET-HEK cells (5μM for 30min). These compounds, depicted in **Figure 6A**, either include the smaller (than chlorine) EWG, fluorine, on the 6-position, or an EWG (Cl or F) on the 8-position. 7-hydroxycoumarins were also synthesized with the aminoethyl group in 6- and 8-positions around the coumarin core, but none of these were active at hNET (not shown). The results from screening these compounds in hNET-HEK cells are included in **Figure 6B**, which showed that increased bulk at either the 6- (FFN202) or 8-position (FFN269) drastically reduced hNET activity. However, unlike what was observed at the 6-position, a fluorine was well tolerated at

the 8-postion (FFN270), and retained 86 percent of the activity observed with FFN201 (S/B FFN270: 8.5±0.5, FFN201: 9.9±0.2, mean ± SEM, n = 3). The spectroscopic properties of the 8-fluoro analogue, FFN270, were then measured to confirm a pH-dependent ratiometric fluorescence with a pKa in the desired range (5.5-7.4). Consistent with other 7-hydroxycoumarins, FFN270 showed a stronger fluorescence at higher pH values, with an isosbestic point at pH 6.1, which is suitable for future functional pH-sensitive experiments.

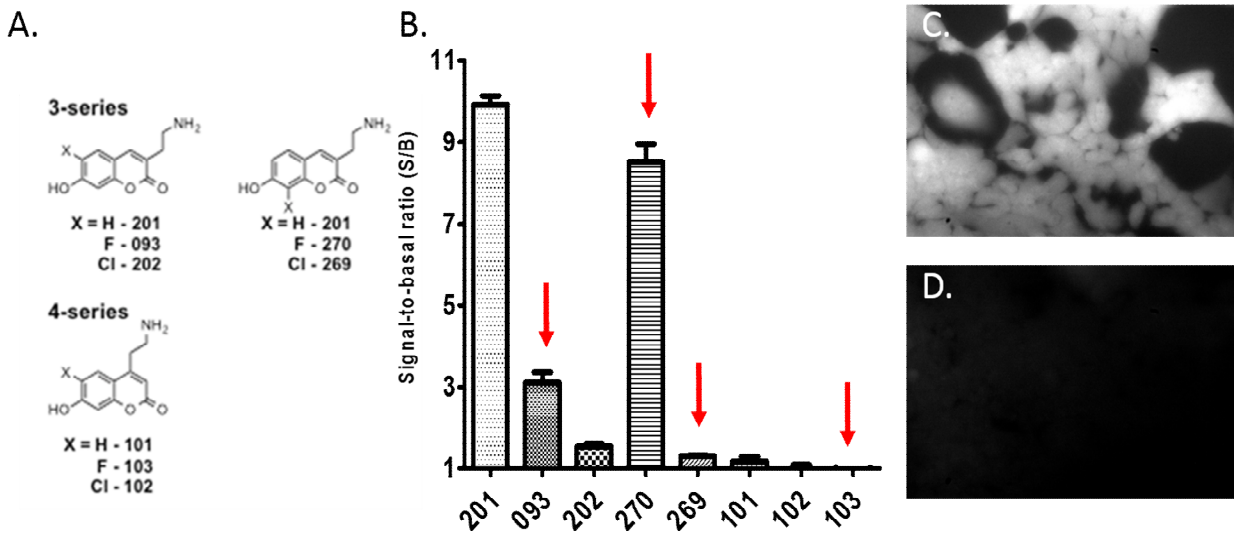

Figure 6. A) Chemical structures of selected 7-hydroxycoumarins tested for hNET activity with hNET-HEK cells. B) S/B ratios for each fluorophore collected as described in **Figure 5**. Highlighted with red arrows are the newly synthesized compounds to complete the series. C) Representative images of FFN270 without inhibitor (C) and with inhibitor (D).

4.2.3 Assessing FFN270 Transport in VMAT2-HEK Cell Culture Assays

Encouraged by the NET-specific uptake and spectrophysical properties of FFN270, we next determined whether FFN270 was actively transported by the vesicular monoamine transporter (VMAT2), using the same transfected VMAT2-HEK cells described in Chapter 3 (3.2.2). These cells were incubated with FFN270 (20μM) for two hours (**Figure 7**). Longer incubation times were required for this assay compared to the hNET-HEK screen due to the lack of a transfected plasma membrane transporter (NET) and the poor lipophilicity of the compound

(LogD: -1.5). Following the 2 hour incubation, a bright punctated staining pattern was observed, similar to that previously observed with older generation FFNs, such as FFN102 and FFN202[45].

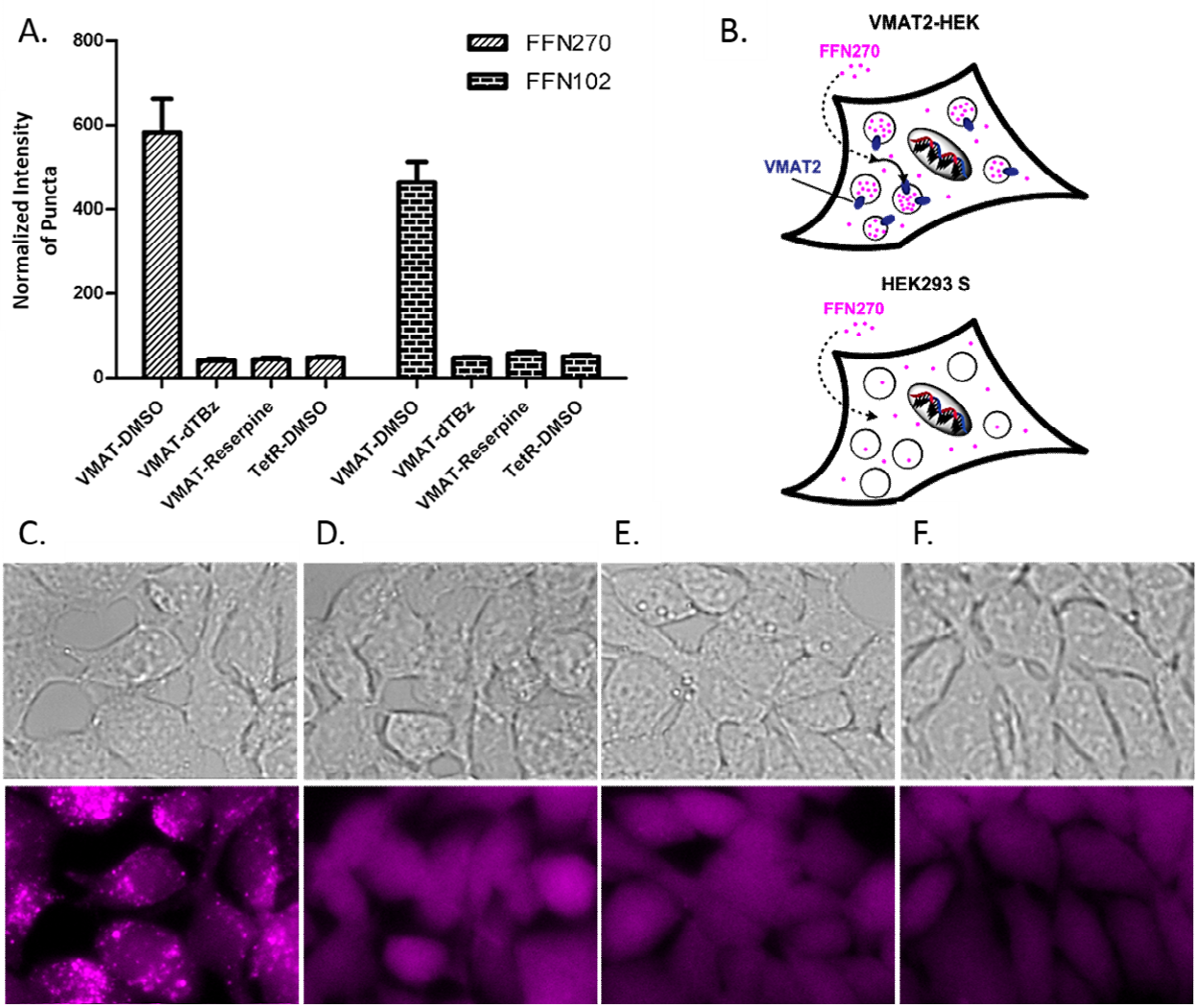

Figure 7. A) VMAT2-dependent loading of FFN102 and FFN270 were compared using the normalized intensity of puncta (number of puncta multiplied by average fluorescence intensity) in VMAT2-HEK cells after a 2h incubation (20μM) under different conditions. B) Representative schematic depicting the rationale for intracellular punctate fluorescence with active VMAT2, and general cytosolic labeling in null-transfected or inhibited conditions. The fluorescent probes passively diffuse through the plasma membrane were they are then actively concentrated in acidic compartments by VMAT2 activity. Without active VMAT2 (inhibition or null-transfected) intracellular fluorescence is only resultant from equilibrative passive diffusion. Representative images of FFN270 in (C) VMAT2-HEK cells, (D) dTBZ (2μM) inhibited or (E) reserpine (2μM) inhibited VMAT2-HEK cells, and (F) null-transfected HEK293 cells. Each image set includes a bright field image and a fluorescence image.

Using FFN102 as a benchmark VMAT2 substrate, which is known to produce robust exocytosis-dependent fluorescent changes in acute murine brain slices[44], we compared VMAT2-

dependent loading of FFN270 with that of FFN102. Loaded acidic compartments appeared as fluorescent puncta within the cells. The puncta were then selected for quantification based on their size and fluorescence intensity as compared to the background. The normalized intensity (number of puncta multiplied by average fluorescence intensity) of these puncta in FFN270- and FFN102-treated VMAT2-HEK cells were then compared with the number in null-transfected HEK cells (without VMAT2) or with cells treated with VMAT2-inhibitors: reserpine (2μM) or dihydrotetrabenazine (dTBZ, 2μM). Under any of the conditions in which VMAT2 activity was absent or inhibited, the normalized intensity of FFN270 was drastically reduced (between 88 and 90%). These results suggest that, unlike APP+ as described in Chapter 3 (3.2.2), the accumulation of FFN270 into acidic compartments due to VMAT2 activity comprised the predominant portion of total FFN270 fluorescence. Thus, FFN270 appeared to meet the cell-based screening criteria for a NE-FFN: NET-dependent uptake and VMAT2-dependent accumulation into acidic compartments. Additionally, the FFN270 VMAT2-HEK cell-culture results matched closely with those of FFN102 (FFN270: 945±173 and FFN102 733±60, mean ± SEM, not significant, n = 4), indicating that FFN270 may also have significant vesicular accumulation in the VMAT2-expressing neurons present in acute murine brain slices, as did FFN102.

4.2.4 Labeling of Noradrenergic Neurons in Acute Murine Brain Slices

After passing the transfected cell-based screening criteria for a new NE-FFN, we then sought to determine whether FFN270 would prove useful in studying NE neurotransmission in living brain tissue, by performing a series of studies in acute murine brain slices. The first step in this process necessitated that we determine whether FFN270 is a substrate for murine NET by testing the uptake of this compound by the noradrenergic cell bodies of the mouse LC. As

discussed in Chapter 3 (3.2.3), the mice used for these experiments were younger (21-30d postnatal) than the typical adolescent mice (49-70d) used in all other experimentation requiring mice, due to the decreased NET expression in adult animals[46,47]. Using the tyrosine hydroxylase (TH) promoter driven GFP as a positive label of catecholaminergic neurons, acute brain slices containing LC neurons were incubated with FFN270 (10μM) for 30 minutes, followed by a wash for 10 minutes before imaging. A significant accumulation of FFN270 fluorescence, as measured by two-photon excitation, was observed in neuronal cell bodies also containing the TH-GFP signal, as well as in the lining of blood vessels (**Figure 8**). FFN270 positive cell bodies were selected for quantification if their fluorescence was two standard deviations above the background signal. Similar to the results observed with APP+, 72 percent of the noradrenergic cell bodies in the LC labeled with GFP actively accumulated FFN270 (62/86 cells from 6 different mice). While there was also FFN270 uptake in what appeared to be the endothelial lining of the blood vessels, no uptake in other neurons or glial cells was observed in this region. As a negative control, uptake of FFN102 was also tested in this area. As expected, no significant uptake of this DA-FFN was observed in any TH-GFP positive cells of the LC. This result is consistent with the findings from our hNET-HEK cell culture experiments, and our hypothesis-generating preliminary *in vivo* experiment, in which no uptake of FFN102 was observed in the cortex (conducted in parallel with experiment from **Figure 4**).

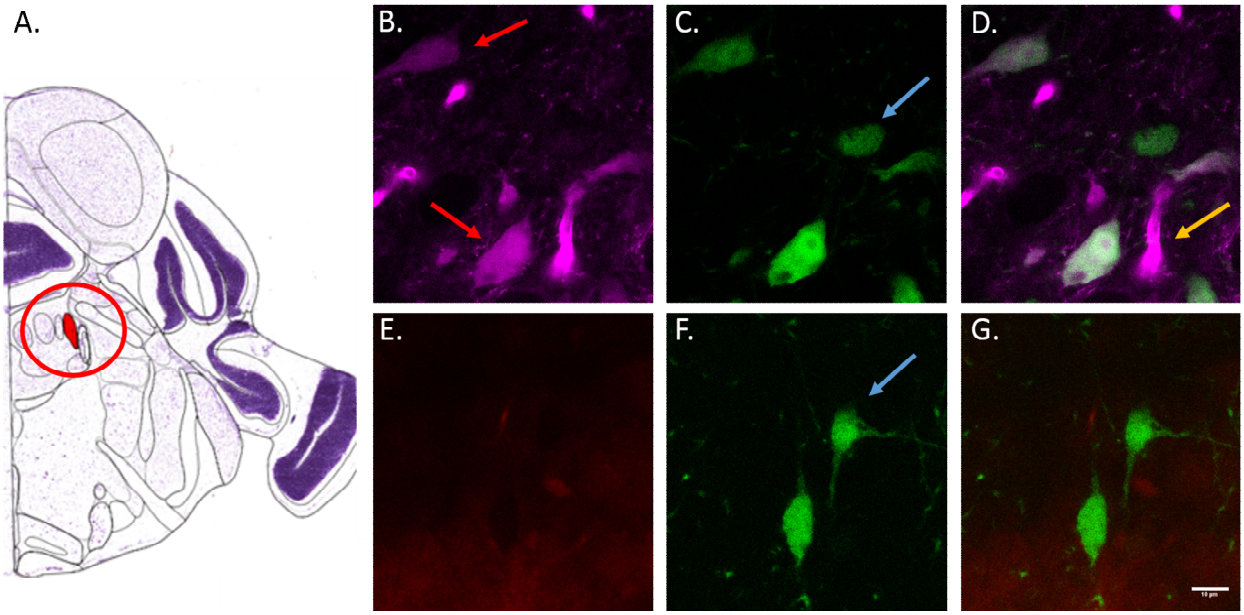

Figure 8. FFN270, but not FFN102, labels noradrenergic neurons in the locus coeruleus (LC). A) Atlas image highlighting the location of the LC in the mouse brain (Bregma: -5.5mm, Allen Brain Atlas). B-D) FFN270 (D) strongly colocalized with the noradrenergic label TH-GFP (C), resulting in a 72% colocalization of noradrenergic cell bodies (labeled by red arrows, as determined by fluorescence > 2xSD of background, 62/86 cells, 6 animals). Cells that did not colocalize are highlighted with a blue arrow, and blood vessels are highlighted with a yellow arrow. E-G) When repeated with FFN102 (E), no colocalization was observed with TH-GFP (F). Scale Bar: 10µm.

Our next steps were to confirm that the uptake of FFN202 into axons in the outer layers of the somatosensory and motor cortex, observed in our initial hypothesis-generating *in vivo* experiment (**Figure 4**), represented uptake into noradrenergic projections, and to demonstrate that FFN270 can also be actively accumulated into these noradrenergic projections. For these experiments we chose to image the noradrenergic projections in the outer layers (Layers 1 and 2/3) of the barrel cortex for 3 main reasons; 1) accessibility for future *in vivo* functional experiments, 2) the demonstrated importance of NE in this area of the brain, and 3) the potential for observable changes in fluorescence to be shown by FFNs. First, two-photon imaging in the outer 200 microns of the intact cortical layers of the barrel cortex *in vivo* is already a well-established method that has been used to image individual spine turnover[48], calcium transients[49], and changes in membrane potential[50]. Using multiphoton microscopy, it is possible to collect

images at this depth with single synapse spatial resolution and observe changes in fluorescence of only a few percentage points.

Second, NE-driven neuromodulation in the barrel cortex is linked to major changes in the sensory information processing function of the cortical networks in this area. Specifically, changes in NE release affect the strength and temporal patterns of spontaneous synaptic inputs of the barrel cortical networks[13,51], while differentially augmenting sensory induced cortical neuron firing rates during whisker deflection[52]. Depending on the firing frequency of the LC, a subset of barrel cortical neurons are maximally facilitated or suppressed, and the members of this network change as the frequency of LC input changes[13]. As discussed earlier, recent evidence no longer supports the belief of homogenous global noradrenergic activity. On a large scale, LC neurons that project to different brain regions demonstrate different firing rates, however, a more directed study of the firing patterns of specific NE synaptic connections has not been possible[34]. The intent for this experiment is to determine whether FFN270 can be used in the barrel cortex to further elucidate the role of NE inputs on specific cortical neurons by locally measuring NE neurotransmission from individual release sites, potentially during live sensory input behavior. The differences in the effects of NE on postsynaptic targets could be due to differential postsynaptic adrenergic receptor expression or a presynaptic regulatory mechanism made visible by FFNs. It is possible that with a NE-FFN we could observe presynaptic heterogeneity of noradrenergic synapses, similar to the properties of dopaminergic synapse discussed in Chapter 2. As a whole, the noradrenergic projections of the barrel cortex pose an exciting new territory with promising future potential to explore with FFN270.

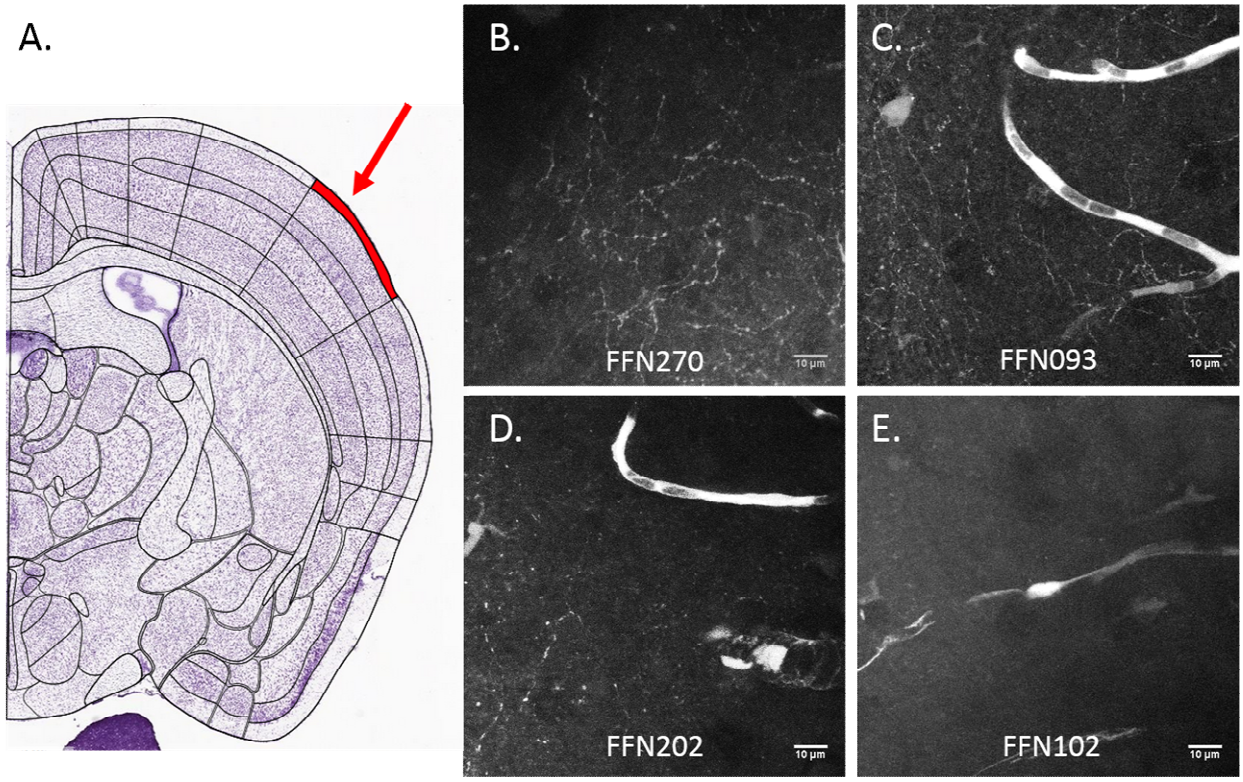

Figure 9. Representative images of different FFNs (10µM) loaded into layer 1 of the barrel cortex (A, Bregma: -1.0mm, Allen Brain Atlas) of acute murine brain slices (30min, 10min wash). A) FFN270, B) FFN093, C) FFN202, D) FFN102. For structure and expected loading based on hNET-HEK data of each FFN refer to **Figure 6**. Expected noradrenergic axons appeared as long strings with punctated release sites, while blood vessels appeared as large tubular structures. Scale Bar: 10µm.

Imaging FFN270 in the barrel cortex was performed using the same loading conditions used in the LC experiments (10µM for 30min, followed by a 10min wash). These conditions resulted in sparse FFN270 staining that resembled beads on a string, similar to what was observed in the preliminary *in vivo* experiment. For these images, 20 micron thick z-stacks were collected and then maximally z-projected into a single plane image due to the relatively sparse density of these structures. This experiment was then repeated with the second best compounds tested in the hNET-HEK screen, FFN093, as well as FFN202 and FFN102 as controls. Representative images are included in **Figure 9** and the results are consistent with the cell culture data. FFN270 had the highest density of labeled structures with the greatest signal-to-background ratio, followed closely by FFN093. Similar to what was observed initially *in vivo*,

FFN202 did have a few labeled structures, but they were less dense and had smaller signal-to-background ratios. It is possible that not all of these structures had the same level of NET expression leading to only some capable of loading enough FFN202 to be visible above background, while others were unable to transport enough of the poor substrate to be visible. Lastly, FFN102 incubation resulted in virtually no punctated structures, and less fluorescence than any of the three other FFNs tested. Like the FFN270, however, blood vessel staining was still present. It is possible that some of the limited FFN102 signal observed might be due to dopaminergic projections potentially present in the barrel cortex, but potential dopaminergic projections are primarily thought to be in the deeper layers (IV),[53] and dopaminergic projections in the cortex typically have poor DAT expression[54]. Additional experiments would be required to determine if the FFN102 fluorescence signal is sparse DAT expression or non-specific background.

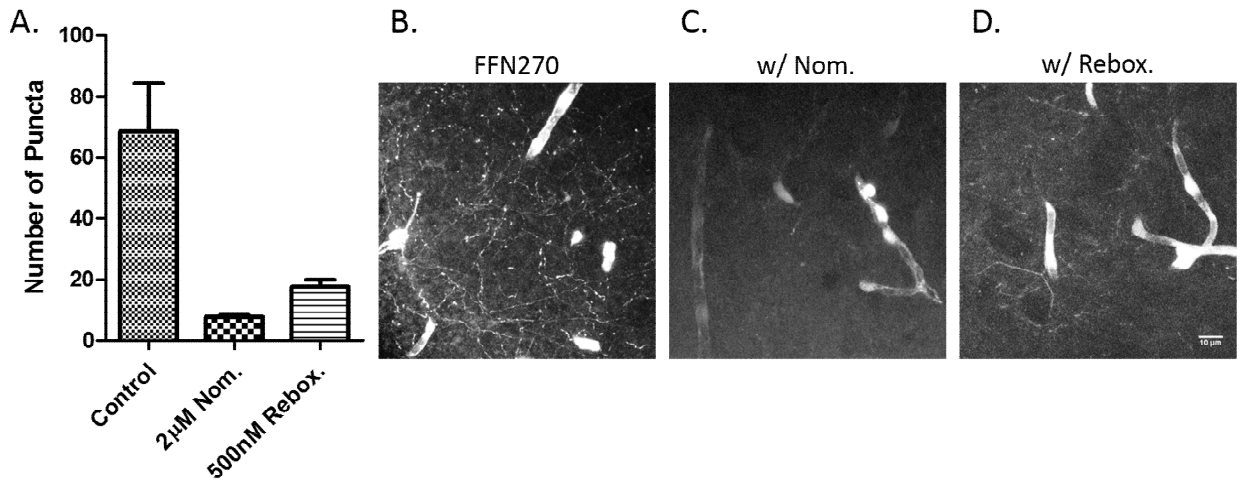

Figure 10. A) FFN270 axonal labeling in Layer 1 of the barrel cortex was inhibited with nomifensine (2μM, Nom.) or reboxetine (500nM, Rebox.). The average number of puncta along strings was significantly higher in control conditions (68.5±22) compared to Nom. (7.7±0.7) and Rebox. (17.5±3.5) conditions (n=3). Representative images of FFN270 labeling under normal loading conditions (B) or inhibited with Nom. (C) or Rebox. (D). Blood vessel labeling was not inhibited. Scale Bar: 10μm.

To confirm that the punctate fluorescence observed with FFN270 was due to NET uptake into noradrenergic projections, loading of FFN270 into the brain slices was performed in the presence of the NET inhibitors, either nomifensine (2μM) or reboxetine (500nM) (**Figure 10**). Quantification of the number of puncta along strings showed a 89.1 percent decrease of these structures when inhibited with nomifensine, and a 74.5 percent decrease when inhibited with reboxetine (Control: 68.5±16 Nom.: 7.7±0.5 Rebox.: 17.5±2.5, mean ± SEM, 2-3 slices per animal, 3 different animals per condition). As expected, nomifensine almost completely eliminated FFN uptake in these structures, but the decrease resulting from reboxetine inhibition was incomplete. It is possible that since nomifensine is both a DAT (K_i ~ 50nM) and NET (K_i ~ 25nM) inhibitor, and reboxetine is only a NET (K_i ~ 10nM) inhibitor (DAT K_i > 10μM), that some of the FFN270 labeled structures were dopaminergic[55]. Alternatively, it may be that the reboxetine concentration and pre-incubation times used (15min) were insufficient to completely block NET activity, so that some structures were still bright enough to be selected for counting.

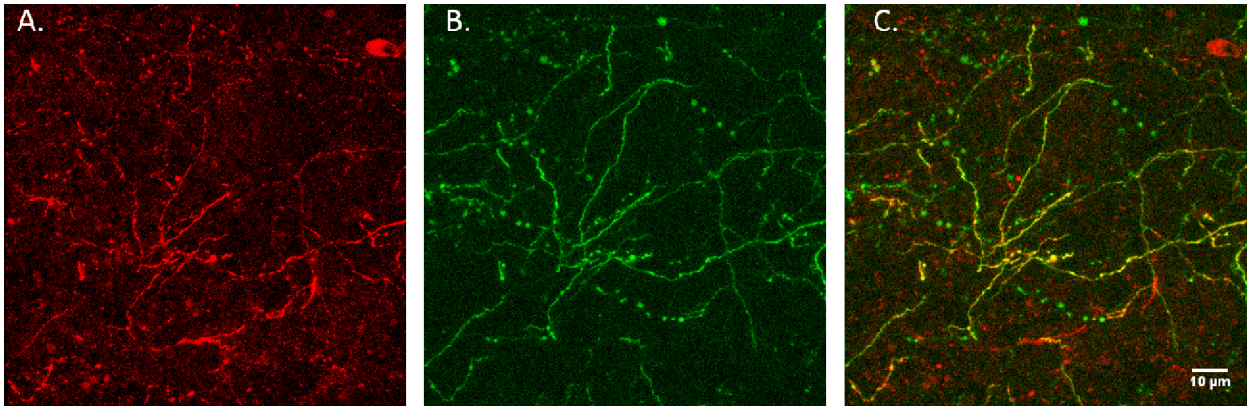

Figure 11. Representative images of noradrenergic projections in Layer 1 of the barrel cortex in TH-GFP, labeled with FFN270 (A) and TH-GFP (B). C) We observed a high level of colocalization (>80%) between the two fluorophores indicating that FFN270 labels noradrenergic projections. Scale Bar: 10μm.

To further characterize the nature of these structures, TH-GFP mice were again used for NE-neuron colocalization studies. In general, the strength of the GFP signal in the noradrenergic

projections in the cortex are much weaker than the GFP signal in the noradrenergic cell bodies in the LC, due to the axonal separation between the brain stem and these sparse distal projections. However, we were able to image TH-GFP positive structures in the barrel cortex when using longer imaging dwell times and higher laser power (see Experimental 5.3). When comparing the percent colocalization of FFN270 puncta and GFP signal found along the strings, there was greater than 80% overlap between the two channels (2-3 slices per animal, 3 different animals) (**Figure 11**). Consistent with the inhibition data, this result further supports the conclusion that FFN270 labels catecholaminergic projections in the barrel cortex, but due to the tyrosine hydroxylase promoter being active in both dopaminergic and noradrenergic neurons, this experiment alone cannot distinguish between these two neuronal types. Dopamine β-hydroxylase (DBH) is the enzyme that converts dopamine to norepinephrine through the copper cofactor catalyzed oxidation of the beta position of the aminoethyl group on DA[56,57]. Importantly, the promoter of this protein in the brain is specifically active in noradrenergic neurons and could be useful in distinguishing between dopaminergic and noradrenergic neurons in the brain. A DBH driven cre recombinase mouse line is available from the Mutant Mouse Resource and Research Center, but this line is cryopreserved[58]. It would be possible to obtain this line in the future and crossbreed with a floxed mCherry mouse line already in the laboratory, which would then activate fluorescent mCherry expression in only neurons that expressed the cre recombinase. However, the time to unfreeze the line, obtain a breeding pair, and then generate double mutants was not feasible within the timeline of this research project.

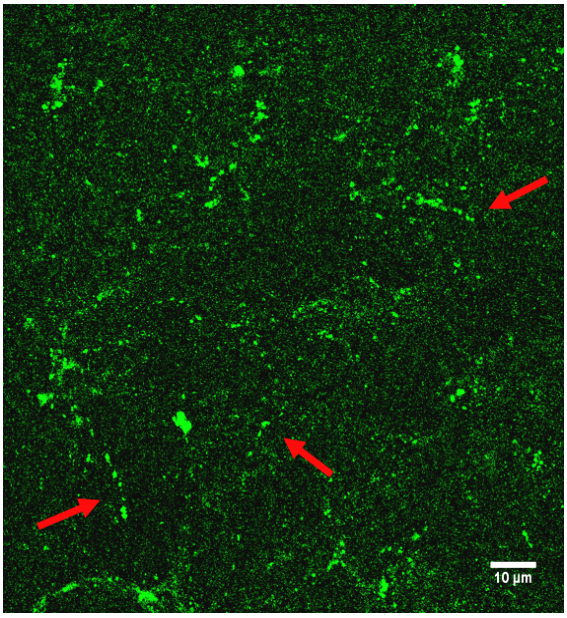

Figure 12. Representative image of staining pattern of dopamine β-hydroxylase (DBH) antibodies in Layer 1 of the barrel cortex. Note that fixation/staining was performed after imaging with FFN270 in healthy tissue, resulting in non-ideal DBH staining conditions. Colocalization with FFN270 was problematic, because a) FFN270 did not remain in the tissue after fixation and antibody conjugation steps, and b) FFN270 images collected pre-fixation were difficult to register with DBH images due to tissue deformation caused during the fixation process. However, we did observe some strings of puncta (marked by arrows) that corresponded to noradrenergic projections with a density that was similar to FFN270 puncta. Scale Bar: 10µm.

In a further attempt to confirm that noradrenergic projections were present in the exact areas where we were observing FFN270 fluorescent structures in our acute brain slice experiments, the slices were fixed after imaging and then re-imaged after immunostaining for DBH. Unfortunately, after the 4% paraformaldehyde fixation and antibody conjugation steps, none of the FFN staining remained in the slice. We attempted to use the vasculature to locate the same area after fixation, which worked reasonably well, but we were unable to re-locate the exact same axons again, possibly due to deformations of the slice that occurred during the fixation process. However, we did observe noradrenergic axons with a similar density pattern as generated with FFN270 (**Figure 12**). This is consistent with noradrenergic staining patterns collected from other researchers in similar brain regions[33]. While the collection of data in this section highly suggested that the majority of the monoaminergic projections visible in this area

with FFN270 were noradrenergic, these experiments were unable to demonstrate this definitively. Of note, in section 4.3.8, another piece of evidence is described using an *in vivo* system that would further support this conclusion and eliminate any remaining uncertainty.

4.2.5 Stimulated FFN270 Release in Acute Murine Brain Slices

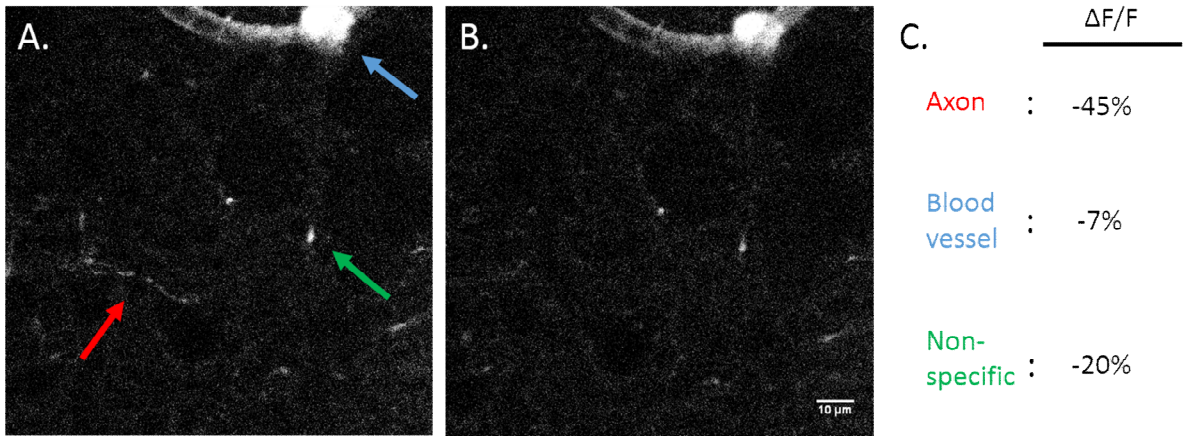

Figure 13. Representative images of FFN270 loaded noradrenergic projections in Layer 1 of the barrel cortex in acute brain slice, before (A) and 5min after (B) 40mM KCl depolarization. C) Preliminary quantification of the ΔF/F of certain FFN270 labeled objects in the field of view. Red: noradrenergic axon, Blue: blood vessel, Green: non-specific spot. Scale Bar: 10µm.

An important requirement for any NE-FFN is that it also must be able to measure the synaptic vesicle content release from noradrenergic release sites. FFN270 has been shown to label noradrenergic axons, so the next step was to examine whether this probe can be used to trace NE release. As outlined in Chapter 3, this process involved measuring fluorescence changes under both electrical and chemical release conditions. For FFN270, we first measured fluorescence changes using 40mM KCl to induce membrane depolarization. **Figure 13** includes representative images before and after (5 minutes) K^+ induced depolarization. There was visually more change in the fluorescence of the axonal strings compared to the blood vessels, but finding the same field of view before and after the treatment was problematic. The slice deformations

caused from this treatment, as discussed in more detail in Chapter 3 (3.2.5), were more pronounced when imaging the outer layers of the barrel cortex near the edge of the slice. Combined with the sparse density of these projections, we were unable to quantify the degree of release associated with this technique.

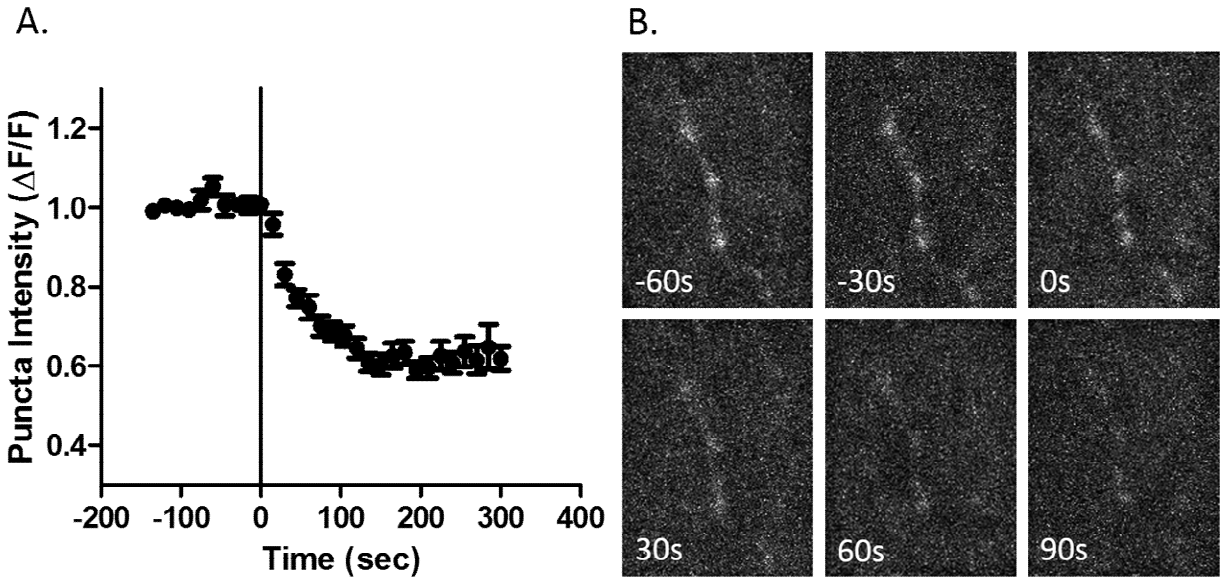

Figure 14. A) Change in FFN270 puncta fluorescence that destain over time in the barrel cortex in acute brain slice, during the course of a locally applied electrical stimulation (10Hz, 3000pulses, starts at t: 0min). B) Representative noradrenergic axon labeled with FFN270 over the course of stimulation. Scale Bar: 10µm.

Switching to electrically stimulated NE-release, the same stimulation protocol was used as described in Chapter 3 (10Hz local stimulation, 3.2.5). The sparse nature of these projections, however, made finding a good imaging area difficult. Imaging fast enough to measure release kinetics only allowed for imaging 5 z-planes, and as a result, some image sets only include a few puncta. Combined with the previous observation of "silent puncta" described in Chapter 2 (2.2.5), this led to only a very limited number of destained puncta per experiment. Destained puncta were selected from all puncta using a MATLAB script that identified fluorescent changes after initiation of electrical stimulation that were significantly different from changes that

occurred during baseline washing (see Experimental 5.3). This included both the degree of exponentiality of the detaining curve compared with the baseline curve and the magnitude of destaining relative to the standard deviation of the baseline signal. The results are included in **Figure 14** and the kinetics from the collection of all destained puncta demonstrated a destaining half-life ($t_{1/2}$) of 30.3 seconds (2-3 slices per animal, 3 different animals). This $t_{1/2}$ is comparable to the kinetics observed in dopaminergic neurons with FFN200 (~25sec at 10Hz), and glutamatergic hippocampal release sites with FM1-43 (~25sec at 10 Hz)[59].

Interestingly, due to the sparse nature of the axons in this area, it was easier to identify which puncta were along the same axons than in the striatum, and subsequently, we noticed that many of the destained puncta from a single field of view were found along the same axon. Although, we have not yet devised a quantifiable parameter to explore this preliminary observation further. As a negative control, these electrical experiments were repeated in the presence of $CdCl_2$ (200μM) to block calcium channels, which resulted in a 88.3 percent reduction in the number of FFN270 puncta that destained (2-3 slices per animal, 3 different animals)[60]. We believe that the remaining 10 percent of destained puncta are the false positives selected by the program that are primarily due to movement within the field of view. Lastly, a small "FFN flash" could be observed in these experiments, but this was much smaller than the flash observed with FFN102 in the striatum, presumably due to the differences in puncta density. As discussed in Chapter 2 (2.4.2), there is interest in exploring individually the release of sparse puncta at much higher imaging rates with individual electrical pulses to get fluorescent changes with minimal background signal contamination, but this work is not ready at this time.

In conclusion, the acute brain slice experiments demonstrated that treatment with FFN270 generated fluorescent puncta in the outer layers of the barrel cortex, and that these

puncta appeared to be in catecholaminergic projections, with the majority being noradrenergic. Thus, FFN270 appears to have potential to be a useful probe for identifying noradrenergic projections in acute mouse brain tissue. The pattern of staining generated was distinct from that of FFN102, which is DA-selective, without any detectable NET activity. Additionally, we demonstrated that FFN270 can be released from these projections by either chemical or electrical exocytosis inducing conditions, critical for a probe to be considered a functional FFN. Based on these characteristics, combined with the accessibility of imaging the outer layers of the cortex *in vivo*, we determined that FFN270 would be a prime candidate for further experimentation *in vivo*. To confirm previous *ex vivo* observations in native and undamaged neuronal networks *in vivo*, will be an important step forwards for the whole FFN program. As well, being able to demonstrate the *in vivo* utility of this new NE-FFN will support the pursuit of valuable research opportunities is the growing field of NE research.

4.2.6 Characterization of FFN270 in vivo

I would like to thank Samuel Clark, a MD/PhD student in Dr. Sulzer's laboratory, for his collaborative help with these *in vivo* experiments. His general knowledge and experience working in this experimental system was invaluable in establishing an *in vivo* protocol for the FFN project.

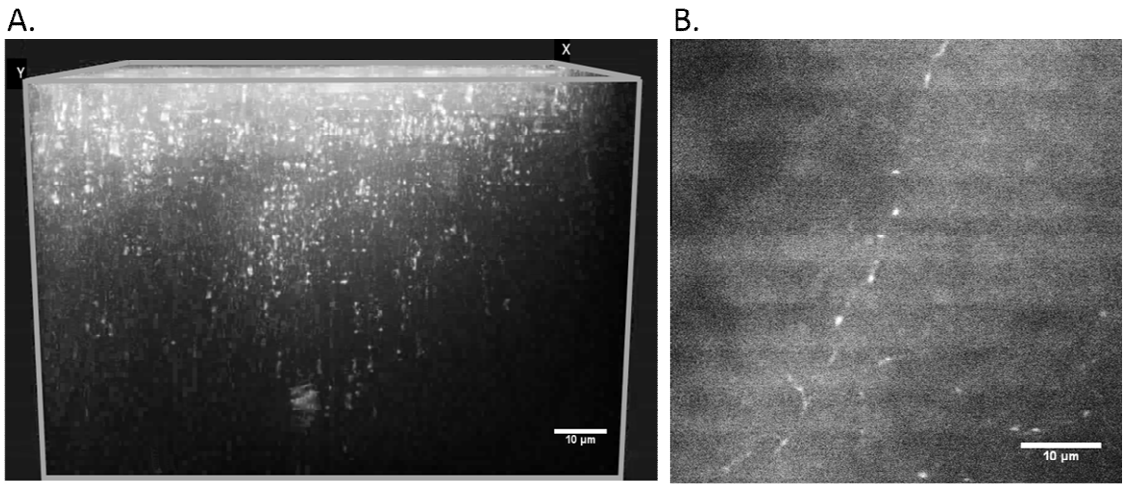

Figure 15. First *in vivo* images with FFNs acquired in our own laboratory. A) 3-D reconstruction of FFN270 labeling (50µM bath applied) in Layer 1 of the barrel cortex *in vivo.* B) Representative single x-y plane from the volume in A). Scale Bar: 10µm.

For this section, I will first discuss some of the parameters that we explored to establish an *in vivo* experimental protocol that would enable us to pursue our primary FFN270 experimental objectives, as well as allow for relatively consistent FFN experimentation over time. Initially, we set out to repeat the preliminary *in vivo* results collected with FFN202 (**Figure 4**). For this, we evaluated a method for accessing and treating the surface of the murine brain *in vivo*. This was accomplished by removing an approximately two millimeter diameter circle of skull and dura mater over the barrel cortex (stereotaxic coordinates from bregma: AP: -1.0-2.0mm, ML: 2.0-3.0mm) from an anesthetized mouse, and then surrounding this hole with a plastic well that held artificial cerebral spinal fluid (ACSF). For experimentation, the ACSF was exchanged with an ACSF solution containing FFN270 (50µM) and allowed to sit directly on the brain tissue for one hour. We used higher concentrations and longer incubation times of the FFN in the intact brain compared to the conditions used in acute brain slices, due to slice conditions resulting in suboptimal staining with a poor penetration depth. This type of "bath application" resulted in the staining pattern included in **Figure 15**. Fluorescence was highest near the surface

of the brain, and decreased as the concentration of the probe and tissue depth went down. Excitingly, there were many bright puncta along numerous axons, much more than previously observed *in vivo* with FFN202 (**Figure 4**). Depending on the wash time, the signal to background ratio of these puncta changed dramatically. Initially, there were almost no visible puncta due to the overwhelming background signal, but after a 30 minute wash, we were able to image puncta with high fluorescence compared to the background. We also observed that the puncta fluorescence decreased relatively rapidly over time when compared to the rate of similar intensity puncta in the acute brain slice. It is possible that this is due to the slow tonic firing of noradrenergic neurons even in an anesthetized state[30]. Using this FFN loading protocol, we were able to image bright puncta up to two hours post-bath application. However, while this method worked well for initial imaging of the probe, this technique would not have been suitable for much of the planned future experimentation.

The ultimate goal of FFN use *in vivo* centers around the ability to image changes in NE release over time, or under different conditions. Thus, due to the mechanism of how FFNs work, the probe would need to be reapplied for each experiment. Therefore, being able to look at the release kinetics of individual puncta before and after behavioral conditioning or disease progression would not be possible with the bath application process, as it requires exposed brain tissue. To enhance our ability to perform *in vivo* FFN experiments, we sought to establish an experimental model in which the mouse would have a long-lasting cranial window over the imaging area that would also allow for repeated FFN loading. As a result, we devised a glass window that had a small injection port in the middle. The port was sealed with a silicon sealant when not in use, and this plug was removable and sealable before and after each experiment. This is similar to plastic windows with a comparable design used to apply drugs locally to the

imaging area[61], but we have perfected this technique by making the windows out of glass with diamond drill bits. Next, we optimized the injection loading protocol for use with our fluorescent probes and the new port.

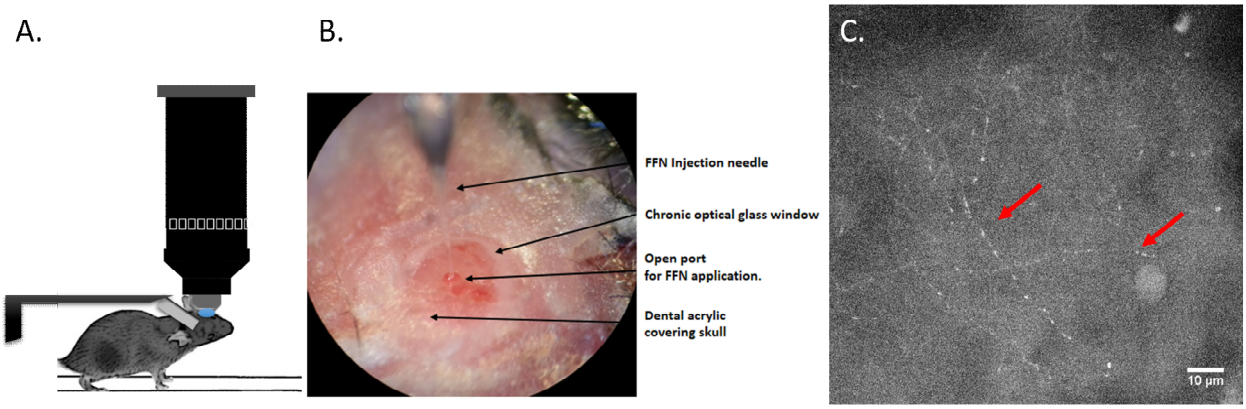

Figure 16. A) Cartoon highlighting how the mice were held for imaging. B) Diagram of the *in vivo* injection port setup. The skin was pealed back and the surface of the skull was covered in hardened dental acrylic which held the glass window in place and forms a small well to hold liquid for the water emersion objective. The glass window is the smoother circle which has a small injection port that provides direct access to the surface of the brain. The glass injection needle can then inject FFN through the port. After imaging, the port can be resealed with a silicon sealant. C) Representative image of a single x-y plane in Layer 1 of the barrel cortex from injection-loaded FFN270 (1mM) *in vivo*. Highlighted by arrows are FFN270-lebeled noradrenergic projections in a living mouse. Scale Bar: 10µm.

Small volumes of FFN270 were loaded into the brain (~100nL) through a pulled-glass injection needle and a Nanoject II injector. Injecting the same concentration that worked well for bath application (50µM) gave very little fluorescence signal, and almost no fluorescent puncta were observed. We established that loading was optimal when the FFN concentration was much higher (1mM), and spread out over 2 different injection depths (100µm and 50µm from the surface). At this injection concentration we noticed strong fluorescence background at the needle track, but greater than 50 microns from this track, the puncta were comparable to those achieved using the bath application, with similar signal to background ratios (**Figure 16**). However, the nature of using a single point source-like loading compared to continual diffusion led to an even smaller temporal window for imaging (as described in 4.2.6). We found that one hour after

injection some puncta were no longer bright enough to be identified with our puncta selection methods. However, this temporal window was sufficiently long to measure release site activity, and as such, was used as our primary method of FFN loading for the following *in vivo* experiments.

4.2.7 Amphetamine-induced Release of FFN270 in vivo

Similar to studies in acute brain slice, our interest with FFNs goes beyond neuronal labeling; we wanted to be able to use these tools to study neurotransmission and neurotransmitter concentration changes at an individual release site. This first included monitoring changes in FFN270 concentrations in noradrenergic projections after an intraperitoneal (I.P.) injection of a physiologically relevant dose of amphetamine. It is expected that amphetamine will cause neurotransmitter and FFN270 release from catecholamine release sites through redistribution of vesicle contents to the cytoplasm, reverse MAT activity, and upregulated exocytosis activity[62]. For this experiment, the FFN270 puncta in a small volume of layer 1 of the barrel cortex were monitored over the course of low (1mg/kg), high (10mg/kg), or null (PBS only) amphetamine (AMPH) doses. We observed a rapid decrease of the fluorescence intensity and number of FFN270 puncta after both the high and low AMPH doses. After a low dose of AMPH, only 31.5±9.3 percent of FFN270 puncta remained after 5 minutes post-injection, a significant difference compared to the 78.9±4.9 percent remaining in the PBS control (6 control mice, 4 mice per AMPH condition) (**Figure 17**). The approximately 21.1±5.4 percent decrease in the control was thought to be due to the slow tonic firing of noradrenergic neurons, as well as the higher degree of field of view shift that occurs when performing imaging experiments *in vivo*, as compared with acute slices. When using the higher dose, the number of puncta remaining was only 12 percent, similar to the percentage of selected structures that previously did not

colocalized with TH-GFP or were not inhibited with nomifensine in acute brain slice experiments.

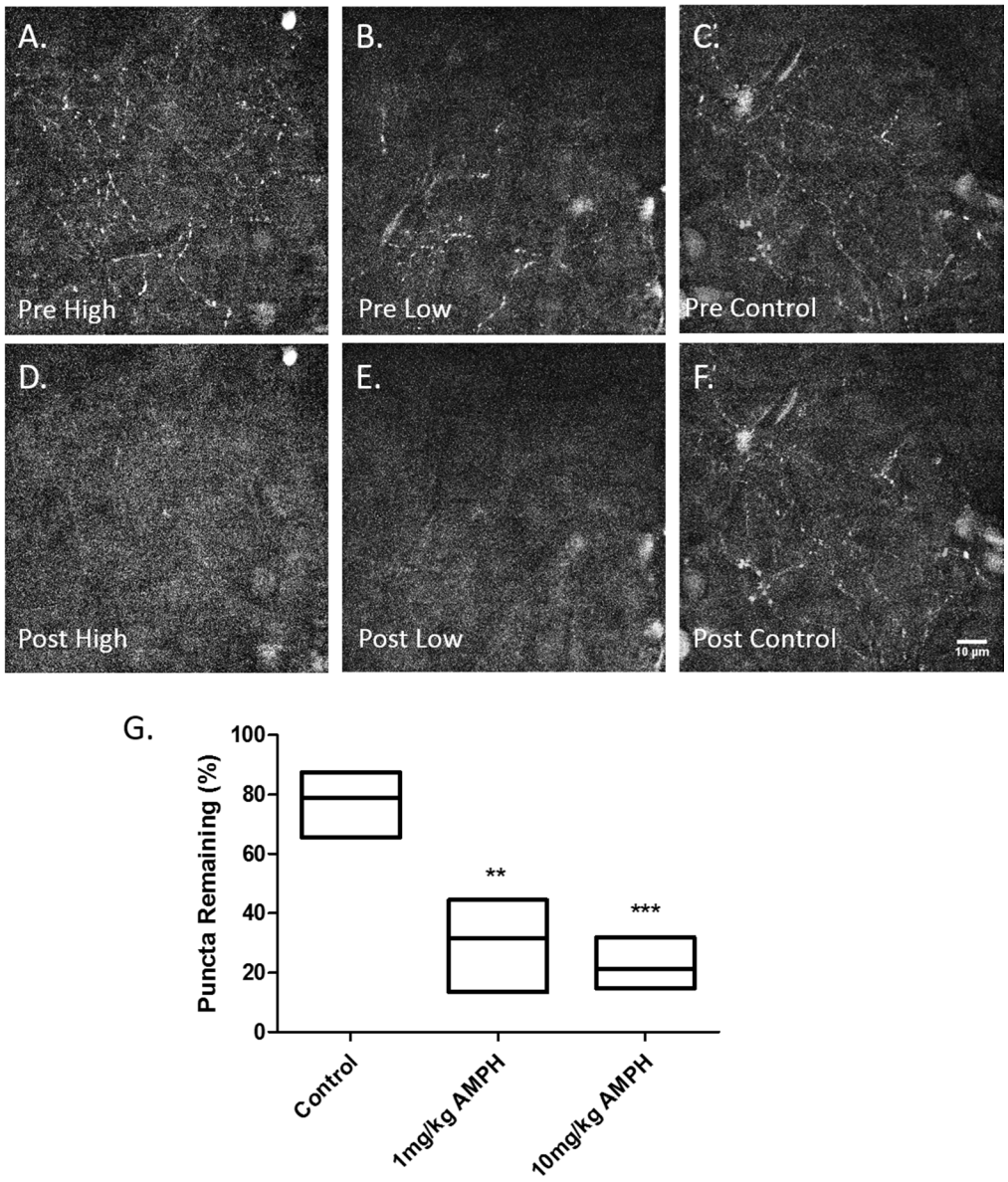

Figure 17. Representative before and 5min after injection of amphetamine (AMPH) images of FFN270 in Layer 1 of the barrel cortex. Top row includes images acquired before I.P. administration of a high dose of AMPH (10mg/kg, A), low dose of AMPH (1mg/kg, B), or control (PBS, C). D-F) Representative corresponding images acquired 5min after each injection. G) Quantification of the number of puncta before and 5min after each AMPH condition. Scale Bar: 10µm.

4.3.8 Preliminary FFN270 Release with DREADDs and Optogenetics

The next step in characterizing FFN270 *in vivo* was to measure the kinetics of exocytosis of individual terminals when specifically stimulating only the noradrenergic neurons. Since AMPH causes release from multiple types of neurotransmitter systems in mechanisms that potentially include, but are not limited to exocytosis, we moved to more recent technologies that stimulate firing and thus vesicular release in specific neurons of interest. Briefly we explored using electrical stimulation of the medium forebrain bundle (MFB), which contains the LC to cortex noradrenergic axons, but there were a couple issues associated with this technique. First, the MFB contains a massively diverse fiber network with inputs from approximately 50 different brain regions. Stimulation of this bundle would be non-specific for noradrenergic neurons and potentially activate all of these networks and their downstream targets. Second, we observed shifts of the imaging plane immediately upon initiation of the electrical stimulation. It is possible that this brain movement was a result of the widespread activation caused by stimulating this neuronal bundle. Due to these technical issues and non-specificity of using electrical stimulation, we next explored optogenic[63] and designer receptors exclusively activated by designer drugs (DREADDs)[64] techniques. I will describe both of these techniques and our preliminary work toward our goals here, but note that these experiments are still on going.

One of the many advantages of using a living system is that we can genetically target neurons of the LC, and then image the distal projections of those neurons in a network that is still intact. Through the collaboration with Dr. Gary Aston-Jones (Rutgers University), we obtained a viral construct (AAV9 PRSx8-hM3DQ DREADD) that specifically expresses the excitatory DREADDs receptor system (Gq-coupled) only in infected noradrenergic neurons by utilizing the DBH promoter (PRSx8)[12]. The Gq DREADDs works through a specially designed receptor

(hM3DQ) which binds the non-native clozapine-N-oxide (CNO) molecule. hM3DQ is a modified muscarinic G-protein-coupled receptor that is normally inactive until it binds to CNO. After binding CNO, hM3DQ, like the native muscarinic-M3 GPCR binding acetylcholine, then specifically activates the Gq-coupled G-protein pathway[64]. This then leads to phospholipase C-β activation, increasing inositol triphosphate and diacylglycerol concentration, which ultimately leads to protein kinase C activation and increased calcium release from intracellular compartments[65]. In neurons, the increased calcium caused by DREADDs activation leads to depolarization, enhanced excitability, and burst firing[66].

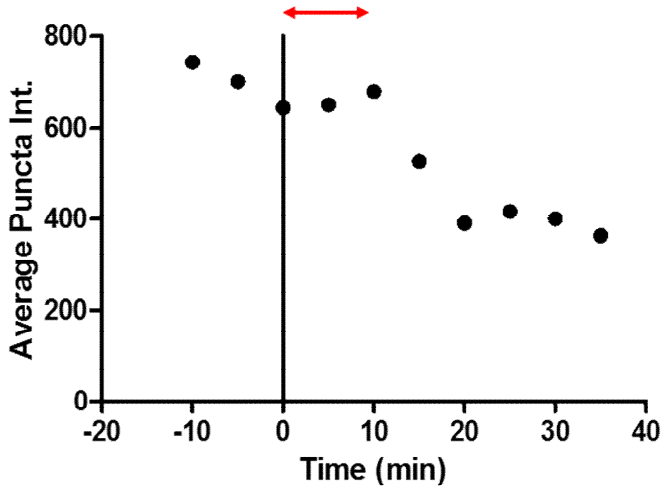

Figure 18. Preliminary FFN270 destaining from noradrenergic projection in Layer 1 of the barrel cortex, induced by a clozapine-N-oxide (CNO) injection (10mg/kg, I.P.) that leads to DREADDs activation in these neurons. The noradrenergic-specific DREADDs Gq virus (AAV9 PRSx8-hM3DQ DREADD) was injected in the LC 2 weeks prior to this experiment. Highlighted in red is the ~10min time delay between CNO injection (t=0min) and a change in the decay rate of FFN270 fluorescence.

This system was particularly appealing for our purposes due to the simplicity of the experimental design and the similarity of the protocol to the AMPH experiments, which has been demonstrated to be very robust. The CNO can be administered through I.P. injection, which does not cause changes in the imaging field of view, and the timescale of the effect is well within the hour window when the puncta are bright enough for imaging. We collected preliminary results

using the same FFN270 loading and imaging protocol as described for AMPH, but using a mouse that had been injected two weeks prior with the noradrenergic-specific DREADDs virus in the LC. Following the injection of FFN270, a time course of FFN270 puncta number and fluorescence was collected before and after the I.P. CNO injection (0.5mg/kg), and is depicted in **Figure 18**. A change in the rate of FFN270 fluorescence over time was observed at the 15 minute point, fairly consistent with the delay observed with CNO and I.P. injections by other groups[66]. These experiments will be repeated with appropriate controls, but are suggestive that FFN270 is loaded into noradrenergic neurons, and can be released through vesicular exocytosis.

In tandem with our experiments using DREADDs, we are also exploring the use of optogenetics to more precisely control LC firing. Like DREADDs, optogenetics is a technique to control intracellular calcium concentrations and cause vesicular exocytosis in neurons. Channelrhodopsin-2 (ChR2), one of the most commonly used members of the optogenetic family, is a seven-transmembrane helix channel discovered in green algae that only opens when stimulated by blue light. Inside the ChR2 is an all-trans retinol bound to the core that isomerizes when exposed to 470 nanometer light. This isomerization leads to a conformational change of ChR2 that opens a pore for cation flow. Expression of this protein in excitable cells is particularly interesting due to its ability to allow calcium to flow into the cell, mimicking the normal function of voltage-gated calcium channels on neurons[67]. Using this system with neurons, it is possible to turn flashes of blue light into a sequence of firing spikes of up to 50 hertz[68]. Optogenetics has an advantage over the DREADDs system in the precision with which neuronal firing can be controlled. Using a fiber optic cable implanted into the LC it is possible to locally deliver discrete durations of blue light and control noradrenergic firing *in vivo* with millisecond temporal control[69].

In preparation for these experiments, we injected the AAV9-CAG-ChR2-mCherry virus into the LC, but have not yet begun the imaging portion of the experiment. In addition to using this virus to elicit ChR2 expression, the vector also contains GFP, which would allow for *in vivo* colocalization of noradrenergic projections over dopaminergic ones. Communication with members of the Dr. Aston-Jones laboratory determined that it is necessary to wait at least two to three months after injection before viral protein expression from the cell bodies reaches the long range projections in the cortex, however, we are in the process of confirming this. Waiting for expression to reach the cortex would also allow for local activation of the ChR2 if activation with a fiber optic cable in the LC is problematic. A cohort of these mice have been injected, and we are currently waiting until expression of ChR2 and GFP in the cortex is sufficient.

4.3 Conclusions

4.3.1 Summary

Inspired by preliminary evidence of FFN activity *in vivo*, our laboratories pursued the use of the coumarin core as a potential NE-FFN in tandem with other fluorescent motifs described in Chapter 3. Through the use of hNET-HEK cell culture screens we identified the most promising lead for noradrenergic labeling, FFN201. However, FFN201 was not pH-sensitive in the range appropriate for allowing the measurement of fluorescent changes associated with pH differences between the synaptic vesicles and extracellular space. As a result, a series of analogues with pKa modifying groups were synthesized, and FFN270 was found to be a sufficient hNET substrate while having a desirable pKa. Further, FFN270 was identified as a VMAT2 substrate, fulfilling the stringent FFN design requirements (fluorescent dual substrate for both NET and VMAT2). Evaluation of this compound in acute murine brain slices confirmed that it is actively transported into both noradrenergic cell bodies in the LC and axonal projections in the barrel cortex.

Additionally, this loading can be inhibited by both of the NET-inhibitors, nomifensine and reboxetine.

After confirming that FFN270 is a NET substrate and a noradrenergic neuronal label in brain tissue, we further demonstrated that this probe could also be used as a tracer for NE. FFN270 release from noradrenergic terminals was observed through depolarization induced by high potassium concentrations as well as local electrical stimulation. Release due to electrical stimulation could be quantified and subsequently inhibited using the calcium channel blocker, cadmium ions (Cd^{2+}). Due to the accessible nature of the labeled projections in the outer layers of the barrel cortex, and satisfied that FFN270 met all the required characteristics of a successful FFN, we decided to move on to *in vivo* experimentation.

For *in vivo* experimentation in intact murine brains, the FFN loading protocol was first optimized to allow repeated and consistent use of the FFN in the same mouse over an extended study. This was possible through the design of a novel glass cranial window with a sealable injection pore, allowing for repeated local FFN injections. This method resulted in consistent imaging of FFN270 labeled noradrenergic projections *in vivo*, and using this protocol we demonstrated for the first time optical imaging of monoamine release from individual release sites *in vivo* (using an amphetamine injection trigger). Additionally, we are currently developing protocols for eliciting specific noradrenergic release with the DREADDs and optogenetics systems. Initial results with the DREADDs system are promising, but need to be repeated and with appropriate controls, and the foundation for optogenetics has been established.

4.3.2 Future Directions

After the full *in vivo* characterization of FFN270, our future goal, and the culminating pinnacle of years of work spread over multiple researchers, is to apply this FFN probe to

elucidating the role of presynaptic neurotransmitter release regulation in the normal and abnormal functioning of the brain and associated behaviors. By combining this new NE-FFN probe with the knowledge gained about the functional uses of other pH-sensitive FFNs (Chapter 2), we want to use FFN270 to explore the regulation of localized NE release *in vivo*. Critically, we want to assess whether the heterogeneity in catecholamine neurotransmitter release observed in acute brain slice (the "silent" puncta that remain after tonic electrical stimulation, or the bi-modality of release observed from single electrical pulses) is reproduced *in vivo*. Further, we want to understand any potential links between the observed heterogeneity and biological significance in the form of animal behavior *in vivo*, something never before possible within the FFN program. FFN270 could be particularly important in understanding how the roles of individual NE release sites in the barrel cortex and the adaptive-gain theory relate to specific behavioral changes. For example, when the animal is introduced to a new engaging task, do all noradrenergic release sites react harmoniously, or is there more localized control of NE release? During memory formation, are there lasting changes that can be observed in particular NE release sites? If we observe silent puncta *in vivo*, we can use FFNs to determine, using intact circuitry, whether or not they can be switched to active releasers after certain types of conditioning. In ultimate conclusion, I hope this work has helped establish a new and exciting research approach that will have a lasting impact on how the field comes to understand the interconnected roles between presynaptic regulation of neurotransmission and functional behavior, and I offer my sincere thanks to all who have helped this research along the way.

4.4 References

1. Rothman, R. B. *et al.* In vitro characterization of ephedrine-related stereoisomers at biogenic amine transporters and the receptorome reveals selective actions as norepinephrine transporter substrates. *J. Pharmacol. Exp. Ther.* **307,** 138–45 (2003).

2. Rothman, R. B. *et al.* Amphetamine-type central nervous system stimulants release norepinephrine more potently than they release dopamine and serotonin. *Synapse* **39,** 32–41 (2001).

3. Schwartz, J. W., Blakely, R. D. & DeFelice, L. J. Binding and transport in norepinephrine transporters. Real-time, spatially resolved analysis in single cells using a fluorescent substrate. *J. Biol. Chem.* **278,** 9768–77 (2003).

4. Bian, C., Zeng, Q., Xiong, H., Zhang, X. & Wang, S. Electrochemistry of norepinephrine on carbon-coated nickel magnetic nanoparticles modified electrode and analytical applications. *Bioelectrochemistry* **79,** 1–5 (2010).

5. Lu, L.-P., Wang, S.-Q. & Lin, X.-Q. Fabrication of layer-by-layer deposited multilayer films containing DNA and gold nanoparticle for norepinephrine biosensor. *Anal. Chim. Acta* **519,** 161–166 (2004).

6. Perry, M., Li, Q. & Kennedy, R. T. Review of recent advances in analytical techniques for the determination of neurotransmitters. *Anal. Chim. Acta* **653,** 1–22 (2009).

7. Mao, L., Li, G. & Abdel-Rahman, A. A. Effect of Ethanol on Reductions in Norepinephrine Electrochemical Signal in the Rostral Ventrolateral Medulla and Hypotension Elicited by I1-Receptor Activation in Spontaneously Hypertensive Rats. *Alcohol. Clin. Exp. Res.* **27,** 1471–1480 (2003).

8. Tibirica, E., Mermet, C., Feldman, J., Gonon, F. & Bousquet, P. Correlation between the inhibitory effect on catecholaminergic ventrolateral medullary neurons and the hypotension evoked by clonidine: a voltammetric approach. *J. Pharmacol. Exp. Ther.* **250,** 642–7 (1989).

9. Muller, A., Joseph, V., Slesinger, P. A. & Kleinfeld, D. Cell-based reporters reveal in vivo dynamics of dopamine and norepinephrine release in murine cortex. *Nat. Methods* **11,** 1245–52 (2014).

10. Hettie, K. S., Liu, X., Gillis, K. D. & Glass, T. E. Selective catecholamine recognition with NeuroSensor 521: a fluorescent sensor for the visualization of norepinephrine in fixed and live cells. *ACS Chem. Neurosci.* **4,** 918–23 (2013).

11. Fernández-Pastor, B., Mateo, Y., Gómez-Urquijo, S. & Javier Meana, J. Characterization of noradrenaline release in the locus coeruleus of freely moving awake rats by in vivo microdialysis. *Psychopharmacology (Berl).* **180,** 570–9 (2005).

12. Vazey, E. M. & Aston-Jones, G. Designer receptor manipulations reveal a role of the locus coeruleus noradrenergic system in isoflurane general anesthesia. *Proc. Natl. Acad. Sci. U. S. A.* **111,** 3859–64 (2014).

13. Devilbiss, D. M. & Waterhouse, B. D. The effects of tonic locus ceruleus output on sensory-evoked responses of ventral posterior medial thalamic and barrel field cortical neurons in the awake rat. *J. Neurosci.* **24,** 10773–85 (2004).

14. Strosberg, A. D. Structure, function, and regulation of adrenergic receptors. *Protein Sci.* **2,** 1198–209 (1993).

15. Scarpace, P. J. & Abrass, I. B. Alpha- and beta-adrenergic receptor function in the brain during senescence. *Neurobiol. Aging* **9,** 53–8

16. Schroeter, S. *et al.* Immunolocalization of the cocaine- and antidepressant-sensitive l-norepinephrine transporter. *J. Comp. Neurol.* **420,** 211–32 (2000).

17. Moret, C. & Briley, M. The importance of norepinephrine in depression. *Neuropsychiatr. Dis. Treat.* **7,** 9–13 (2011).

18. Stahl, S. M. *et al.* A Review of the Neuropharmacology of Bupropion, a Dual Norepinephrine and Dopamine Reuptake Inhibitor. *Prim. Care Companion J. Clin. Psychiatry* **6,** 159–166 (2004).

19. Zhou, J. Norepinephrine transporter inhibitors and their therapeutic potential. *Drugs Future* **29,** 1235–1244 (2004).

20. Geracioti, T. D. CSF Norepinephrine Concentrations in Posttraumatic Stress Disorder. *Am. J. Psychiatry* **158,** 1227 (2001).

21. Rothman, R. B. & Baumann, M. H. Monoamine transporters and psychostimulant drugs. *Eur. J. Pharmacol.* **479,** 23–40 (2003).

22. Ventura, R., Cabib, S., Alcaro, A., Orsini, C. & Puglisi-Allegra, S. Norepinephrine in the Prefrontal Cortex Is Critical for Amphetamine-Induced Reward and Mesoaccumbens Dopamine Release. *J. Neurosci.* **23,** 1879–1885 (2003).

23. Amara, S. G. & Sonders, M. S. Neurotransmitter transporters as molecular targets for addictive drugs. *Drug Alcohol Depend.* **51,** 87–96 (1998).

24. Mehler, M. F. & Purpura, D. P. Autism, fever, epigenetics and the locus coeruleus. *Brain Res. Rev.* **59,** 388–92 (2009).

25. Cheslack-Postava, K. *et al.* beta2-Adrenergic receptor gene variants and risk for autism in the AGRE cohort. *Mol. Psychiatry* **12,** 283–91 (2007).

26. Vazey, E. M. & Aston-Jones, G. The emerging role of norepinephrine in cognitive dysfunctions of Parkinson's disease. *Front. Behav. Neurosci.* **6,** 1–6 (2012).

27. Aston-Jones, G., Rajkowski, J. & Cohen, J. Role of locus coeruleus in attention and behavioral flexibility. *Biol. Psychiatry* **46,** 1309–1320 (1999).

28. Segal, M. & Bloom, F. E. The action of norepinephrine in the rat hippocampus. IV. The effects of locus coeruleus stimulation on evoked hippocampal unit activity. *Brain Res.* **107,** 513–25 (1976).

29. Waterhouse, B. D., Moises, H. C. & Woodward, D. J. Noradrenergic modulation of somatosensory cortical neuronal responses to iontophoretically applied putative neurotransmitters. *Exp. Neurol.* **69,** 30–49 (1980).

30. Aston-Jones, G. & Bloom, F. E. Activity of norepinephrine-containing locus coeruleus neurons in behaving rats anticipates fluctuations in the sleep-waking cycle. *J. Neurosci.* **1,** 876–86 (1981).

31. Korf, J., Aghajanian, G. K. & Roth, R. H. Increased turnover of norepinephrine in the rat cerebral cortex during stress: Role of the locus coeruleus. *Neuropharmacology* **12,** 933–938 (1973).

32. Foote, S. L., Aston-Jones, G. & Bloom, F. E. Impulse activity of locus coeruleus neurons in awake rats and monkeys is a function of sensory stimulation and arousal. *Proc. Natl. Acad. Sci. U. S. A.* **77,** 3033–7 (1980).

33. Robertson, S. D., Plummer, N. W., de Marchena, J. & Jensen, P. Developmental origins of central norepinephrine neuron diversity. *Nat. Neurosci.* **16,** 1016–23 (2013).

34. Chandler, D. J., Gao, W.-J. & Waterhouse, B. D. Heterogeneous organization of the locus coeruleus projections to prefrontal and motor cortices. *Proc. Natl. Acad. Sci. U. S. A.* **111,** 6816–21 (2014).

35. Aston-Jones, G. & Cohen, J. D. Adaptive gain and the role of the locus coeruleus-norepinephrine system in optimal performance. *J. Comp. Neurol.* **493,** 99–110 (2005).

36. Aston-Jones, G. & Cohen, J. D. Adaptive gain and the role of the locus coeruleus-norepinephrine system in optimal performance. *J. Comp. Neurol.* **493,** 99–110 (2005).

37. Aston-Jones, G. & Cohen, J. D. An integrative theory of locus coeruleus-norepinephrine function: adaptive gain and optimal performance. *Annu. Rev. Neurosci.* **28,** 403–50 (2005).

38. Eschenko, O. & Sara, S. J. Learning-dependent, transient increase of activity in noradrenergic neurons of locus coeruleus during slow wave sleep in the rat: brain stem-cortex interplay for memory consolidation? *Cereb. Cortex* **18,** 2596–603 (2008).

39. Kemp, A. & Manahan-Vaughan, D. The hippocampal CA1 region and dentate gyrus differentiate between environmental and spatial feature encoding through long-term depression. *Cereb. Cortex* **18,** 968–77 (2008).

40. Sara, S. J. & Devauges, V. Priming stimulation of locus coeruleus facilitates memory retrieval in the rat. *Brain Res.* **438,** 299–303 (1988).

41. Sara, S. J. & Devauges, V. Idazoxan, an alpha-2 antagonist, facilitates memory retrieval in the rat. *Behav. Neural Biol.* **51,** 401–11 (1989).

42. Murchison, C. F. *et al.* A Distinct Role for Norepinephrine in Memory Retrieval. *Cell* **117,** 131–143 (2004).

43. Sterpenich, V. *et al.* The locus ceruleus is involved in the successful retrieval of emotional memories in humans. *J. Neurosci.* **26,** 7416–23 (2006).

44. Rodriguez, P. C. *et al.* Fluorescent dopamine tracer resolves individual dopaminergic synapses and their activity in the brain. *Proc. Natl. Acad. Sci. U. S. A.* **110,** 870–5 (2013).

45. Lee, M., Gubernator, N. G., Sulzer, D. & Sames, D. Development of pH-responsive fluorescent false neurotransmitters. *J. Am. Chem. Soc.* **132,** 8828–30 (2010).

46. Sanders, J. D., Happe, H. K., Bylund, D. B. & Murrin, L. C. Development of the norepinephrine transporter in the rat CNS. *Neuroscience* **130,** 107–17 (2005).

47. Murrin, L. C., Sanders, J. D. & Bylund, D. B. Comparison of the maturation of the adrenergic and serotonergic neurotransmitter systems in the brain: implications for differential drug effects on juveniles and adults. *Biochem. Pharmacol.* **73,** 1225–36 (2007).

48. Lendvai, B., Stern, E. A., Chen, B. & Svoboda, K. Experience-dependent plasticity of dendritic spines in the developing rat barrel cortex in vivo. *Nature* **404,** 876–81 (2000).

49. O'Connor, D. H., Peron, S. P., Huber, D. & Svoboda, K. Neural activity in barrel cortex underlying vibrissa-based object localization in mice. *Neuron* **67,** 1048–61 (2010).

50. Petersen, C. C. H., Grinvald, A. & Sakmann, B. Spatiotemporal Dynamics of Sensory Responses in Layer 2/3 of Rat Barrel Cortex Measured In Vivo by Voltage-Sensitive Dye Imaging Combined with Whole-Cell Voltage Recordings and Neuron Reconstructions. *J. Neurosci.* **23,** 1298–1309 (2003).

51. Constantinople, C. M. & Bruno, R. M. Effects and mechanisms of wakefulness on local cortical networks. *Neuron* **69,** 1061–8 (2011).

52. Motaghi, S., Sheibani, V., Farazifard, R. & Joneidi, H. Electrical stimulation of locus coeruleus strengthens the surround inhibition in layer V barrel cortex in rat. *Neurosci. Lett.* **401,** 280–4 (2006).

53. Gurevich, E. V & Joyce, J. N. Dopamine D(3) receptor is selectively and transiently expressed in the developing whisker barrel cortex of the rat. *J. Comp. Neurol.* **420,** 35–51 (2000).

54. Sesack, S. R., Hawrylak, V. A., Matus, C., Guido, M. A. & Levey, A. I. Dopamine Axon Varicosities in the Prelimbic Division of the Rat Prefrontal Cortex Exhibit Sparse Immunoreactivity for the Dopamine Transporter. *J. Neurosci.* **18,** 2697–2708 (1998).

55. Besnard, J. & Roth, B. PDSP - NIMH Psychoactive Drug Screening Program. *Nature* 215–220 (2012). at <https://pdspdb.unc.edu/pdspWeb/>

56. Stewart, L. C. & Klinman, J. P. Dopamine beta-hydroxylase of adrenal chromaffin granules: structure and function. *Annu. Rev. Biochem.* **57,** 551–92 (1988).

57. Weinshilboum, R. M., Thoa, N. B., Johnson, D. G., Kopin, I. J. & Axelrod, J. Proportional Release of Norepinephrine and Dopamine-beta-Hydroxylase from Sympathetic Nerves. *Science (80-.).* **174,** 1349–1351 (1971).

58. Gong, S. *et al.* Targeting Cre recombinase to specific neuron populations with bacterial artificial chromosome constructs. *J. Neurosci.* **27,** 9817–23 (2007).

59. Zakharenko, S. S., Zablow, L. & Siegelbaum, S. A. Visualization of changes in presynaptic function during long-term synaptic plasticity. *Nat. Neurosci.* **4,** 711–7 (2001).

60. Huang, Y., Quayle, J. M., Worley, J. F., Standen, N. B. & Nelson, M. T. External cadmium and internal calcium block of single calcium channels in smooth muscle cells from rabbit mesenteric artery. *Biophys. J.* **56,** 1023–1028 (1989).

61. Kaifosh, P., Lovett-Barron, M., Turi, G. F., Reardon, T. R. & Losonczy, A. Septo-hippocampal GABAergic signaling across multiple modalities in awake mice. *Nat. Neurosci.* **16,** 1182–4 (2013).

62. Daberkow, D. P. *et al.* Amphetamine paradoxically augments exocytotic dopamine release and phasic dopamine signals. *J. Neurosci.* **33,** 452–63 (2013).

63. Fenno, L., Yizhar, O. & Deisseroth, K. The development and application of optogenetics. *Annu. Rev. Neurosci.* **34,** 389–412 (2011).

64. Urban, D. J. & Roth, B. L. DREADDs (Designer Receptors Exclusively Activated by Designer Drugs): Chemogenetic Tools with Therapeutic Utility. (2015). at <http://www.annualreviews.org/doi/abs/10.1146/annurev-pharmtox-010814-124803>

65. Luo, J., Busillo, J. M. & Benovic, J. L. M3 muscarinic acetylcholine receptor-mediated signaling is regulated by distinct mechanisms. *Mol. Pharmacol.* **74,** 338–47 (2008).

66. Alexander, G. M. *et al.* Remote control of neuronal activity in transgenic mice expressing evolved G protein-coupled receptors. *Neuron* **63,** 27–39 (2009).

67. Zhang, F., Wang, L.-P., Boyden, E. S. & Deisseroth, K. Channelrhodopsin-2 and optical control of excitable cells. *Nat. Methods* **3,** 785–92 (2006).

68. Britt, J. P., McDevitt, R. A. & Bonci, A. Use of channelrhodopsin for activation of CNS neurons. *Curr. Protoc. Neurosci.* **Chapter 2,** Unit2.16 (2012).

69. Adelsberger, H., Grienberger, C., Stroh, A. & Konnerth, A. In vivo calcium recordings and channelrhodopsin-2 activation through an optical fiber. *Cold Spring Harb. Protoc.* **2014,** pdb.prot084145 (2014).

Chapter 5: Experimental

5.1 Experimental A (Chapter 2)

5.1.1 General Acute Murine Brain Slice Preparation and Imaging Parameters

This section includes a general description of the acute murine brain slice preparation that is applicable to all acute brain slice experiments unless otherwise noted. All wild-type animals used for slice striatal experiments were 2–4 month old male C57BL/6 mice obtained from the Jackson Laboratory (Bar Harbor, ME). All animal protocols were approved by the IACUC of Columbia University. For striatal slice preparation, mice were decapitated and acute 300μm thick coronal slices were cut on a vibratome at 4°C artificial cerebrospinal fluid (ACSF) containing (in mM): 125 NaCl, 2.5 KCl, 26 $NaHCO_3$, 0.3 KH_2PO_4, 2.4 $CaCl_2$, 1.3 $MgSO_4$, 0.8 NaH_2PO_4, 10 glucose (pH 7.2–7.4, 292–296 mOsm/L). After cutting, acute slices were allowed to recover for 1h before use at room temperature in oxygenated (95% O_2, 5% CO_2) ACSF.

Slices were then transferred to an imaging chamber (QE-1, Warner Instruments, Hamden, CT), held in place with a platinum wire and nylon custom-made holder[1], and superfused (1–2 mL/min) with oxygenated ACSF. After appropriate loading conditions described in each section, fluorescent structures were visualized at >20μm depth in the slice using a Prairie Ultima Multiphoton Microscopy System (Prairie Technologies, Middleton, WI) with a titanium-sapphire MaiTai laser (Spectra-Physics) equipped with a 60 × 0.9 NA water immersion objective. Images were captured in 16-bit 512×512 pixel resolution with a dwell time of 10 μs/pixel using Prairie View software. Sections with modified imaging parameters will further describe any deviations from this protocol.

5.1.2 Using FFN102 to study DA Release Depression with Cocaine and Methylphenidate (2.2.1)

For data collection and analysis parameters from constant potential amperometry (CPA) experiments, refer to the corresponding author, Dr. Nicola Mercuri (University of Rome) and the methods section of our published paper[2].

For FFN experiments, the DA-selective and pH-sensitive FFN102 was used. FFN102 was incubated with the acute slice for 30min at 10µM. After a 5min washing period, FFN102 was imaged with two-photon laser excitation set to a wavelength of 760nm (near the protonated excitation maximum), and emitted light of wavelengths between 440-500nm were collected. FFN102 puncta in a 37x37µm field of view (FOV) in the dorsal striatum were imaged (512x512 pixels) for 10min of more washing, and 10min following application of 30µM cocaine (or 30µM methylphenidate) that was added to the perfusion ACSF. Each time point also includes the images from 5 z-stacks (1µm each step) to account for any shifts in the z-plane, resulting in a final imaging rate of 12sec per image. Tonic electrical stimulation of 6000 pulses (200µs x 200µA) at 10Hz was applied using a local bipolar stainless-steel electrode controlled by a Master-8 pulse generator. For all local stimulation experiments, the AMPA inhibitor, NBQX (10µM), and the NMDA inhibitor, AP-5 (50µM), were included in the perfusion ACSF. This was repeated in 2-3 slices per animal for 5 different animals for the 30µM cocaine condition and 3 different animals for the 30µM methylphenidate condition.

To analyze the rate of washing, the stack of images in the z of t dimension were registered using the 3-D colocalization registration macro included with the FIJI version of ImageJ. Next, the Multiple Thresholds plug-in (created by Damon Poburko, Simon Fraser University, Burnaby, BC, Canada) was used for fluorescent puncta identification at each time

point. Upon visual inspection, objects that did not conform to defined properties (appropriate size, rounded shape, and well delimited boundaries) were discarded, as well as puncta that moved significantly out of the object mask during the time frame. After puncta selection, the average fluorescence of the puncta were collected for each time point and the rate of change pre-cocaine treatment was compared to the rate post-treatment. The rate post-cocaine treatment was also compared to the rate from untreated acute slices. For measuring the magnitude of the FFN flash, the total fluorescence of the each trace was normalized with an exponential fit generated from the images pre-treatment. The maximum fluorescence relative to initial fluorescence was then compared between each condition.

5.1.3 Using FFN102 to Study DA Release under Phasic Firing Conditions (2.2.2)

Acute slices were incubated with FFN102 at 10μM for 30min. The slices were then allowed to wash for 10min prior to imaging. Compared to protocol described in 5.1.1, imaging parameters were modified for a faster imaging rate. A small 5x5μm region of interest for only 1 z-plane was scanned, but at the same resolution used in 5.1.1, resulting in an imaging rate of 10Hz. For electrical stimulation, the same setup described in 5.1.2 was used, except the stimulation sequence was set for 5 pulses at 20Hz. The fluorescence from the whole FOV was collected and then compared over time. Changes in fluorescence from the whole FOV pre-stimulation were fit with an exponential and used to normalized fluorescence over the whole trace. This condition was compared to conditions in which no electrical stimulus was applied or 200μM $CdCl_2$ was included in the perfusing ACSF. For the VMAT2-hypomorph experiments, mice of this genotype were sacrificed and used in parallel with wild-type mice from the same litter. To compare to FFN200, the optimized FFN200 loading conditions were used instead of FFN102. This included a 30min incubation with FFN200 (10μM), followed by a 45min wash

period[3]. All other steps were identical. This was repeated for 2-3 slices per animal for 3 different animals for each condition. FFN102 was repeated more as it was used as a positive control in 1 slice from each animal.

5.1.4 Using FFN102 to Study DA Release from Single Pulses and Paired Pulses (2.2.3/2.2.4)

For this set of experiments, the protocol in 5.1.3 was modified to only deliver 1 electrical pulse, and also acquire images at a faster rate. An increase in imaging rate was obtained by switching to a spiral scanning protocol of a 2x2µm region of interest at the same dwell time and resolution. This resulted in an imaging rate of 67Hz. Again, the total fluorescence change over the whole FOV was compared to the initial fluorescence from the whole FOV.

This experiment was then repeated using a pair of individual pulses separated at different temporal intervals. To compare with cyclic voltammetry (CV) measured DA release, half the slices from each brain were used for CV, and half for FFN imaging. In both conditions FFN102 was loaded, and the stimulation sequence was the same. The stimulation sequence was described as follows: a pair of pulses spaced 5sec, 5min wait, pair spaced 10sec, 5min wait, pair spaced 30sec, 5min wait, pair spaced 45sec, 5min wait, and then finally a pair spaced 60sec. After each slice the order of spacing was reversed and then repeated (60, 45, 30, 10, and then 5). The ratio between the fluorescence maximum after each pulse was then compared to the ratio of DA release as measured by CV. This was repeated in 2-3 slices per animal for 2 different animals.

5.1.5 Using FFN to Study Single Pulse Release Kinetics (2.2.5)

A similar protocol as described in 5.1.4 was repeated, but using a lower resolution image, as determined by the Nyquist sampling calculation for two-photon images taken at 760nm (10.48 zoom, at 128x128µm FOV). From this FOV, a smaller 20x20pixel region of interest surrounding 1 puncta was selected and used for imaging. For these experiments, longer dwell times (30µs)

were used. This resulted in an improvement of the imaging rate to 100ms per frame, but still comparable signal to noise ratio. For these experiments, 1μM of FFN102 was also included in the perfusion ACSF to refill lost vesicular stores during each 5min wait period. Additionally, instead of delivering just 1 pulse, individual electrical pulses (EPs) were delivered 10 times and spaced 2sec apart. This was repeated ~10 times per slice before moving to the next one. This also was repeated without any stimulation as a negative control. This sequence was collected in 2-3 slices per animal, from 6 different animals.

For data analysis a MATLAB script was created, that automated the following described steps. The fluorescence trace from the whole FOV was divided into 10 smaller traces of 150 time points (1.5sec) surrounding each individual pulse. The 50 time points prior to stimulation of each trace were used to generate an exponential best fit that was used to normalize the rest of the individual trace. After normalizing, a moving group of 5 time points were run through a t-test to determine the probability that this group was above 0. This t-test was conducted on the moving group of points for the whole trace, and the p-values for each test were collected. Sections of the p-value set that were below 0.05 for 3 or more groups of points in a row were considered significant increases in fluorescence. This was repeated for each of the 10 EPs, within a set and then for every set.

The periods of increase for each pulse (all EP1s, all EP2s, etc.) were then averaged together to see when relative to the stimulation each EP was resulting in an increase. This data is plotted in Chapter 2 **Figure 9** and **10**. These plots compare each of the EPs to one another, such as the change in release probability between EP1 and EP2. To compare the different release sites imaged in each set with one another. For this, we analyzed the data by setting a temporal window post stimulation and then determined whether or not a significant increase occurred within that

time frame. This was repeated for each EP of the 10 EPs for each imaging set, to determine how many times an increase was observed in that FOV (out of 10 possible). This data is plotted in Chapter 2 **Figure 12** and **13**.

5.1.6 Using FFNs to Measure Changes in Vesicular Loading (2.3.3)

For all experiments performed in fly brain and details about murine viral injections, contact the corresponding author of our paper in preparation, Dr. Zachary Freyberg (Columbia University).

For experiments in acute murine brain slice, FFN loading was prepared as described in 5.1.2. For using FFN102 to measure intracellular pH changes, a second laser was also used (Coherent Ultra II) for interlaced scanning. The maximum change in fluorescence ratio of FFN102 at pH 5 and 8 using two-photon imaging was observed when imaging at 680nm (protonated form, and laser wavelength minimum) and 740nm (deprotonated). However, when either of the lasers were tuned to the minimum of 680nm, there were periods where the laser stopped pulsing and all black imaged were collected. Therefore, all the data included in 2.3.3 used laser wavelengths of 740nm and 690nm, which gave much more reliable results. Using interlaced scanning, fluorescence from FFN102 at both wavelengths was alternatingly collected in one channel (440-500nm). Imaging was performed on a z-stack of 5 1µm z-planes, with a FOV of 12x12µm (80x80 pixels) for each plane. The dwell time for these experiments was increased slightly (20µs) to compensate for the extra noise introduced when looking at ratios, resulting in an image collected every 1.7sec.

After loading with FFN102, the slice was washed for 10min prior to imaging. Then imaging was started, and 10mM KCl in ACSF (prepared by isotonic replacement of NaCl), was perfused over the slice after ~1min. The exact time that it takes the solution to reach the slice

through the perfusion tubing was measured previously using a fluorophore in the same setup. The change in fluorescence of the whole FOV generated from each laser was then measured and used to generate a ratio between the two excitation conditions. This ratio was fitted with an exponential best fit, which was used to normalize the whole trace. Each trace was then temporally aligned to when exocytosis started to occur (drastic basification shift), and the average magnitude collected from the slices of a particular animal were averaged and used to normalize the traces between each animal. The alkalization peak was set to 100%, and the acidification dips are all relative to that increase. This was repeated in 1-2 slices per animal for 6 different WT animals with and without KCl. This was next repeated in 3 different animals for each injection condition.

5.2 Experimental B (Chapter 3)

5.2.1 Photophysical and Cell Culture Characterization

For data collection and analysis parameters from photophysical characterization and cell culture experiments with APP+, refer to the methods section of our published paper[4] or the graduate thesis of Dr. Richard J. Karpowicz[5].

5.2.2 Imaging Catecholamine Neuronal Cell Bodies with APP+ in Acute Brain Slices (3.2.3)

All acute slices were prepared as described in 5.1.1, except that midbrain coronal slices were collected from TH-GFP mice 20 – 25 days old due to a reported downregulation of NET on the surface of noradrenergic cell bodies in the LC after 30 days postnatal[6,7]. Dopaminergic cell bodies in the midbrain, from both the substantia nigra and ventral tegmental areas, and noradrenergic cell bodies from the locus coeruleus were identified by GFP fluorescence. Slices that included the appropriate brain regions were incubated using 500nM APP+ for 30min. The midbrain slice was then washed with ACSF for 10min prior to imaging. In order to minimize crosstalk between fluorophores, APP+ was detected using an excitation of 800nm and an

emission range of 435–485nm, and GFP was detected using an excitation of 950nm and an emission range of 500–550nm. To ensure that no shift in the z-plane occurs while the laser switches between wavelengths, a second APP+ image was collected at the end and compared to the first. Cell body images were captured in a larger 112 × 112μm FOV at 1024 × 1024 pixel resolution and a dwell time of 10μs.

For quantification of colocalization in coronal midbrain slices, cells were considered positive for either fluorophore if their mean fluorescence intensity was above 2 times the SD of the mean background fluorescence intensity, which was determined in an area devoid of fluorescent puncta/cells. The number of cells was manually counted in images from at least three different positions per slice, 2-3 slices per animal, from 3 different animals.

5.2.3 Imaging APP+ and TH-GFP or FFN102 Labeled Dopaminergic Axonal Processes in the Dorsal Striatum of Acute Brain Slices (3.2.4)

All acute slices were prepared as described in 5.1.1. For experiments in the dorsal striatum, 100nM of APP+ was perfused over this area for 15min, followed by a 10min wash. Colocalization experiments in striatal slices of TH-GFP animals were imaged with the same acquisition protocol as midbrain experiments described above (5.2.2), in order to minimize signal crosstalk between fluorophores. To ensure that no shift in the z-plane occurs while tuning the laser between wavelengths, a second APP+ image was collected after GFP acquisition and compared to the first. Control experiments showed a lack of GFP signal using APP+ acquisition parameters, however, unlike in cell bodies, approximately 10% of APP+ puncta signal were apparent in the 500–550nm channel when using GFP acquisition parameters (Chapter 3 **Figure 10**). To further assess whether APP+ signal was localized to dopaminergic neurons, we also

measured colocalization of APP+ with the previously established dopaminergic marker FFN102, which has an excitation/emission spectrum that is more readily separated from APP+.

For colocalization with FFN102, striatal slices were pre-incubated with 10μM FFN102 for 30min and then added to the imaging chamber where 100nM APP+ was perfused over the slices for 15min. After a 5min wash, APP+ was imaged with an excitation of 810nm and an emission of 570–640nm. FFN102 was imaged with an excitation of 740nm and an emission of 430–500nm. To ensure that no shift in *z* occurs during laser tuning between wavelengths, a second APP+ image was collected at the end and compared to the first. We confirmed a lack of signal in the APP+ and FFN102 channels by their alternative fluorophore using control slices incubated in either only APP+ or FFN102.

Quantification of colocalization of fluorophores was determined using Volocity image analysis software version 4.4 (Improvision, PerkinElmer). Fluorescent puncta were identified by defining a threshold of intensity as well as size and shape parameters (see Volocity user guide for a more detailed description of the object identification tasks). After an automatic selection of the objects by the program, a manual inspection was performed, where each object was visually inspected to confirm its validity. Selected objects that did not conform to a certain number of properties (appropriate size, rounded shape, and well-delimited boundaries) were discarded.

We then determined object colocalization between APP+ and either FFN102 or GFP channels using Volocity's "Measure Object Colocalization" task that calculates a colocalization coefficient for each individual object, which indicates the fraction of the signal above threshold in one channel that exists as colocalized with a second channel. Colocalization coefficients ranging from 0 (none of the signal above threshold in that channel exists as colocalized with the other channel) to 1 (all of the signal above threshold in that channel exists as colocalized with the

other channel) for each of the selected objects were then obtained. A colocalization coefficient of 0.5 or higher was considered to be indicative of colocalization. Results are expressed as percentage of APP+ objects that colocalize with FFN102 or GFP ± SD, and were calculated from 2-3 slices per animal, 3 different animals (~150 puncta per slice).

5.2.4 Inhibition of APP+ Loading in the Striatum with Nomifensine (3.2.4)

DAT-dependent loading of APP+ in the dorsal striatum was determined through inhibition of DAT through a 15min pre-incubation of acute slices with 2µM nomifensine. Following this pre-incubation, nomifensine was then also added to the perfusion ACSF that contained APP+ (100nM) used for loading. After 15min of APP+ loading, the perfusion ACSF was switched to ASCF without APP+, but still with nomifensine. Images were collected in the typical 512x512 pixels and 37x37µm FOV with a dwell time of 10µs, and excitation/emission parameters as described in 5.2.2. The resulting staining was then quantified using the same puncta picking protocol described in 5.2.3 using Volocity software and compared to repeated conditions without nomifensine. This was repeated for 2-3 slices per animal for 3 different animals per condition. The final changes of puncta number were then compared using an unpaired two-tailed *t* test to determine statistical significance.

5.2.5 APP+ Destaining with KCl in Acute Brain Slice (3.2.5)

For experiments with KCl induced depolarization, APP+ was loaded as described in 5.2.3. There was significant slice distortion when 40mM KCl was used, which made tracking the same objects over time difficult. For these experiments, 50µm *z*-stacks comprising 10 images, each image taken at 5µm intervals, were collected every 1 min. The start of the *z*-stack would begin above the surface of the slice and continue down past the 20µm depth required to avoid damage. From this data, it was possible to determine which *z*-plane contained the surface of the

slice, and then the slice that was ~25μm from the surface was used for quantification. Only slices from the same approximate depth were compared over time. Images collected were 512x512 pixels and 37x37μm FOV with a dwell time of 10μs. Image collection started 5min before treatment, and then 40mM KCl in ACSF (prepared by isotonic replacement of NaCl) was perfused over the slice and imaged for another 10min.

Volocity was used to identify puncta from slices at each time point during incubation with and without KCl. For KCl experiments, mean intensity values of selected objects at each time point were normalized to the time point just before KCl stimulation and then plotted as a function of time. The final changes of puncta fluorescence and puncta number at each time point were then compared to an untreated control using an unpaired two-tailed *t* test to determine statistical significance. Data presented as averages ± SD from 2-3 slices per animal, from 3 different animals.

5.2.6 APP+ Destaining with Electrical Stimulation in Acute Brain Slice (3.2.5)

For electrical destaining experiments in the dorsal striatum, the same stimulation setup described in 5.1.2 was used (local 10Hz stimulation of 3600 pulses). For imaging parameters, to compensate for shifts in the z-plane during the time course, z-stacks were acquired. To reduce photobleaching and more readily facilitate the tracking of puncta throughout the experiment, 10μm *z*-stacks comprising 10 images separated by 1μm were collected every 1 min over a total of 9 min (3 min with no stimulation to monitor baseline, followed by 6 min of electrical stimulation). Images collected were 512x512 pixels and 37x37μm FOV with a dwell time of 10μs.

For electrical destaining experiments, ImageJ was used for analysis, as Volocity cannot correct for shifts in the z-plane. Images were registered using the 3-D colocalization registration

macro included with the FIJI version of ImageJ. The Multiple Thresholds plug-in (created by Damon Poburko, Simon Fraser University, Burnaby, BC, Canada) was then used for fluorescent puncta identification at each time point. Upon visual inspection, objects that did not conform to defined properties (appropriate size, rounded shape, and well delimited boundaries) were discarded, as well as puncta that moved significantly out of the object mask during the time frame analyzed. The mean intensity and number of puncta at each time point were then normalized to the time point before stimulation and plotted as a function of time. The final changes of puncta fluorescence and puncta number after stimulation were then compared using an unpaired two-tailed *t* test for statistical significance. Data presented as averages ± SD from 2-3 slices per animal, from 3 different animals.

5.2.7 APP+ Toxicity Does not Affect FFN102 Loading for Acute Experiments in Dopaminergic Neurons (3.2.5)

To determine whether APP+ was acutely toxic (~1-2hours) to loaded neurons, the APP+ dopaminergic cell body loading experiments were repeated as described in 5.2.2. Following loading of APP+ for 45min, 10µM FFN102 was then added to the perfusion ACSF and loaded in the same dopaminergic cell bodies over 30min. Imaging of both APP+ and FFN102 was performed as described in 5.2.3 and the relative FFN102 was qualitatively compared to FFN102 dopaminergic cell body loading without APP+, as published[8]. This was repeated in 2-3 slices per animal for 2 different animals.

5.3 Experimental C (Chapter 4)

5.3.1 hNET-HEK Cells (4.2.2)

For hNET experiments, HEK293 cells stably transfected with hNET were maintained in Dulbecco's Minimal Essential Medium (DMEM) with GlutaMAX (Invitrogen) supplemented with 10% (v/v) fetal bovine serum (FBS, Atlantis Biologicals), 500µg/mL G418 (Calbiochem) to

maintain the transgene, 100μg/mL Penicillin, and 100 U/mL Streptomycin (Invitrogen). HEK293 cells to serve as a negative control were maintained in the same culture medium without G418, and otherwise treated identically. All cells were routinely cultured in 10cm polystyrene culture plates (Falcon), were subcultured before reaching confluence (every 3-4 days), and were maintained in a humidified atmosphere at 37 ˚C containing 5% CO_2. On the day of experiments, the growth medium was replaced by experimental medium (DMEM minus phenol red with 4mM L-glutamine (Invitrogen), 1% (v/v) FBS (Atlanta Biologicals), 100 U/ml penicillin (Invitrogen) and 100μg/ml streptomycin (Invitrogen)) with and without inhibitors as described below.

5.3.2 Fluorometric Assay for Evaluation of hNET Substrate Activity in Cell Culture (4.2.2)

Stably hNET-transfected HEK cells were seeded at a density of 0.08-0.09 x 10^6 cells/well in white solid-bottom 96-well plates and allowed to proliferate in growth medium for ~2 days at 37ºC to reach confluence. On the day of the experiment, the complete growth medium was aspirated, wells were washed with 200μL PBS, and treated with 100μL experimental medium with DMSO (vehicle, 0.02% v/v) or nomifensine (2μM). The cells were incubated for 60min at 37°C, and experimental FFNs (100μL/well of 10μM solution in experimental medium with DMSO (vehicle) or nomifensine 2μM) were added for a final concentration of 5μM FFN concentration in wells. Cells were then incubated for 30min at 37ºC. The experiment was terminated by two rapid PBS washes (200μL/well) followed by addition of fresh PBS buffer (120μL/well). The fluorescence uptake in cells was immediately recorded using a BioTek H1MF plate reader (3x3 area scan, bottom read mode) with excitation and emission wavelengths set at 370nm and 460nm respectively. Substrate activity was determined using signal to basal ratio (S/B): mean fluorescence uptake (with DMSO vehicle) divided by that in the presence of

nomifensine. Data presented as normalized uptake ± SD from three independent experiments (eight separate measurements per condition per experiment).

For cell culture imaging, hNET-HEK cells or their respective controls, HEK293, were plated onto poly-D-lysine (conc. = 0.1mg/mL) coated clear bottom six-well plates at a density of 0.15-0.20 x 10^6 cells per well and grown at 37°C in 5% CO2. Following ~4 days of growth, the cells had reached 80-90% confluence. The culture medium was removed by aspiration, and the cells were washed with PBS (Invitrogen, 1.0mL/well). To investigate the inhibitory effects of nomifensine and cocaine on experimental FFN uptake, cells were incubated in 0.9mL of experimental media containing the inhibitor (2μM) or DMSO vehicle as a control at 37°C in 5% CO2 for 1h. The FFN uptake was initiated by adding 0.1mL of experimental media containing probe (200μM, with a final probe concentration of 20μM in the uptake assay) with and without nomifensine (2μM) or cocaine (1μM). Following incubation at 37° C in 5% CO2 for 30 min, the media was removed by aspiration and the cells were washed with PBS (1mL/well) and maintained in fresh experimental media (1mL/well). Fluorescence images (at least 3 images/well in duplicate wells) were acquired with a Leica FW 4000 imaging system (Leica Microsysytems) equipped with a Chroma custom filter cube (ex = 350±25nm, em =460±25nm; Chroma Technology Corporation) and a Leica DFC-360FX camera. Fluorescence and bright field images were acquired with exposure time set at 600ms and 37ms respectively. All images were adjusted using the same contrast and brightness level using ImageJ software.

5.3.2 Fluorescence Microscopy Imaging of Probes in VMAT-HEK cells (4.2.3)

VMAT-HEK (described here[9]) and TetR-HEK cells were plated at a density of 0.15-0.20 x 10^6 cells per well on poly-D-lysine coated 6-well optical plates and grown at 37° C in 5% CO2. Following ~4 days of growth, the cells had reached 80-90% confluence. The culture medium was

removed by aspiration, the cells were washed with PBS (1.0 mL/well), and the wells were pretreated with experimental medium with or without the VMAT2 inhibitors reserpine (1μM) or dihydrotetrabenazine (dTBZ, 2μM) for approximately 60min. To initiate uptake, solutions of experimental probe with or without inhibitor were added to the appropriate wells for a final concentration of 20μM probe with or without reserpine (1μM) or dTBZ (2μM). Cells were incubated at 37˚C for 2h, at which point the probe solutions were removed by aspiration and wells were gently washed with PBS (2mL). Wells were maintained in fresh experimental medium and were imaged as described above (5.3.2).

As described in 5.1.2, the Multiple Thresholds ImageJ plug-in (created by Damon Poburko, Simon Fraser University, Burnaby, BC, Canada) was used for quantification of fluorescent puncta in images of VMAT2-HEK cells obtained from fluorescence microscopy. Puncta were identified as objects conforming to defined parameters: appropriate size, rounded shape, and well delimited boundaries. The mean intensity and number of these puncta structures per image were collected and compared to those collected in inhibited conditions (reserpine or dTBZ) or TetR-HEK cells from four independent experiments (six images per condition per experiment).

5.3.3 Imaging Noradrenergic Neuronal Cell Bodies with FFN270 in Acute Brain Slice (4.2.4)

All acute slices were prepared as described in 5.1.1, and specifically for the locus coeruleus, as described in 5.2.2. Acute murine brain slices from TH-GFP mice containing the noradrenergic cell bodies of the locus coeruleus, as identified by GFP signal, were incubated with 10μM FFN270 for 30min. After a 10min washing period, FFN270 was imaged with two-photon laser excitation set to a wavelength of 760nm (near the protonated excitation maximum), and emitted light between 440-500nm was collected. GFP was imaged with an excitation

wavelength of 920nm and emitted light between 570-640nm was collected. Images were of a 112x112µm FOV (1024x1024 pixels) taken with a 10µs dwell time.

For quantification of colocalization in coronal midbrain slices, cells were considered positive for either fluorophore if their mean fluorescence intensity was above 2 times the SD of the mean background fluorescence intensity, which was determined in an area devoid of fluorescent puncta/cells. The number of cells was manually counted in images from at least three different positions per slice, 2-3 slices per animal, from 3 different animals.

5.3.4 Imaging Noradrenergic Projections in Layer 1 of the Barrel Cortex in Acute Brain Slice (4.2.4)

All acute slices were prepared as described in 5.1.1. For these experiments, acute coronal slices containing the barrel cortex were used. FFN270 was loaded into noradrenergic axonal projection through a 30min incubation at 10µM. Slices were then washed for 10min prior to imaging. FFN270 was imaged using an excitation wavelength of 760nm and emission collection of 440-500nm. Due to the sparse nature of these projections, 112x112µm images at 512x512 pixels (10µs dwell time) of 20 z-planes separated 1µm apart were acquired and then later z-projected in ImageJ.

To determine if NET was required for loading in the barrel cortex, FFN270 loading was repeated in the presence of nomifensine (2µM) or reboxetine (500nM). For each inhibitor condition, slices were pre-incubated with the inhibitor for 15min, followed by a co-incubation with FFN270 and inhibitor. After FFN270 loading, the inhibitor was also included in the perfusing ACSF during the wash step. This was repeated for 2-3 slices per animal for 3 different animals per condition.

Quantification of fluorescent puncta in cortical slices with and without inhibitors was preformed using Volocity image software version 4.4 (Improvision, PerkinElmer). By defining a threshold of intensity as well as size and shape parameters (see Volocity user guide for a more detailed description of the object identification tasks) puncta objects were automatically selected. After an automatic selection of the objects by the program, a manual inspection was performed, where each object was visually inspected to confirm its validity. Selected objects that did not conform to a certain number of properties (appropriate size, rounded shape, and well-delimited boundaries) were discarded.

For colocalization experiments, this process was repeated in TH-GFP mice. All FFN270 loading and imaging conditions, as described above (except the excitation wavelength was lowered to 740nm to deter crosstalk between the fluorophores), remained the same. GFP images were acquired with an excitation wavelength of 920nm and emission collection of 570-640nm. For quantification, Volocity software was again used. After puncta selection described above, the colocation feature was used, as described in 5.2.3, to determine colocalization of FFN270 puncta to GFP.

5.3.5 Release of FFN270 from Noradrenergic Release Sites with KCl and Electrical Stimulation in Acute Brain Slice (4.2.5)

All acute slices were prepared as described in 5.1.1. For depolarization with KCl experiments, images were collected as described in 5.3.4. Due to the physical deformations of the slice caused by 40mM KCl treatment, no time course was collected, only pre- and 5min post-KCl treatment images were collected. After the washing period, ACSF with 40mM KCl (prepared by isotonic replacement of NaCl) was perfused over the slice for 5min. The FFN270

labeling of noradrenergic axonal puncta before and after treatment was then compared to the fluorescent labeling in blood vessels or non-axonal puncta.

For electrical destaining experiments, FFN270 was loaded and imaged as described in 5.3.4, except only 5 z-planes spaced 1μm apart were collected to improve imaging rate (image every 15s). Electrical stimulation was performed as described in 5.1.2 (10Hz local stimulation for 3600 pulses). FFN270 puncta were imaged for 3min prior to stimulation and for 5min after stimulation started. The set of images was then analyzed using a MATLAB macro that registered and identified destaining puncta. Registration in the z-dimension was performed by choosing a group of z-planes that correlated well with each other based on a two-dimensional cross-correlation in frequency. X/Y registration was performed using a subpixel fast Fourier transform algorithm. After final registration each image was thresholded using a multiple thresholding methods that incrementally forms ROIs over puncta. These ROIs were then slightly enlarged based on the interpunctal distance using a seeded watershed transform to account for any puncta movement not corrected by registration. Any ROIs present throughout the pre-stimulation baseline had there fluorescence measured throughout the whole time course. The background-subtracted intensity for each ROI was normalized to the time point prior to stimulation and corrected for the baseline rundown using an exponential best fit. Puncta were then classified as destaining based on their weightings in the first principal component, using k-means clustering in order to minimize the total variance within each cluster. TO identify outliers, a Z-score was calculated for each intensity value after stimulation relative to the mean and standard deviation of the baseline values. The puncta post-stimulation needed to have a Z-score below -2 standard deviations of the mean baseline. Destaining puncta were identified that met both principal component and outlier tests. This MATLAB macro will be described in more detail in the

submitted paper of our laboratory[3]. Destaining puncta were identified from 2-3 slices per animal for 3 different animals. This experiment and analysis was repeated in 200mM $CdCl_2$ condition to block calcium channels, and the number of identified destaining puncta was compared to conditions without cadmium ions.

5.3.6 Optimization of in vivo *FFN270 loading condition in Layer 1 of the Barrel Cortex (4.2.6)*

For *in vivo* experiments, mice were anesthetized with isoflurane prior to surgery. The head was shaved and disinfected with alternating alcohol and betadine swabs. The skull was exposed and 2mm diameter circle of bone, centered over the barrel cortex (from bregma: AP: -1.5-2.5mm, ML: 1.0-2.0mm), was removed with a high speed drill. We applied gel foam soaked in sterile cortex buffer to stop any bleeding. For initial "bath loading" the dura was removed and 50µM FFN270 was directly applied in a small drop to the open brain tissue. For injection loading, a glass pipette on a Nanoject II (Drummond Scientific) was used to inject 100µl of FFN at each 100µm and 50µm measured from the surface. Injections were delivered in 10µl boluses spaced by 30 seconds. A headpost was affixed to the skull with cyanoacrylate and small plastic ring was glued around the window to hold ACSF during imaging. The mouse was anesthetized with ketamine and xylazine for imaging. Images were collected at 512x512 pixels (10µs dwell time) over a 112x112µm FOV. Due to the increased movement observed *in vivo*, 30 z-planes spaced 1µm apart were imaged over the time course. After registering using the 3-D colocalization registration macro included with the FIJI version of ImageJ, this usually resulted in about 15-20 z-planes that remained consistent over the whole time course. These registered images were then z-projected and used for analysis.

5.3.7 Release of FFN270 in vivo *with Amphetamine (4.2.7)*

FFN270 was loaded into the barrel cortex of anesthetized mice through injection as described in 5.3.6. 30min post FFN270 loading injection, the mouse was help in place under the microscope and imaged as described in 5.3.6. Stacks of images were collected every 5min starting at 30min post-loading. After 15min of imaging, amphetamine was I.P. injected into the mouse at 1mg/kg or 10mg/kg. The time point right before and 5min after amphetamine injection were registered using the 3-D colocalization registration macro included with the FIJI version of ImageJ. Next, the Multiple Thresholds plug-in (created by Damon Poburko, Simon Fraser University, Burnaby, BC, Canada) was used for fluorescent puncta identification at each time point. The percent change in the number of puncta after amphetamine injections were compared to control mice that only received an I.P. injection of PBS. This was repeated for 3 different animals for each AMPH condition and 6 control animals.

5.3.8 DREADDs and Optogenetics in vivo *setup and preliminary evaluation (4.2.8)*

For the preliminary experiment with DREADDs, the noradrenergic specific DREADDs virus (AAV9 PRSx8-hM3DQ DREADD, gift from Gary Aston-Jones, Rutgers University) was injected into the locus coeruleus (from bregma: AP: -9.0-10.0mm, ML: 1.5mm, DV: 7.5mm) at least two weeks prior to imaging. After waiting for two weeks for adequate viral protein expression, FFN270 was injected-loaded in the barrel cortex as described in 5.3.6. 30min post-FFN270 injection, imaging as described in 5.3.7 was conducted every 5min. After 15min of imaging, clozapine-N-oxide was injected at 10mg/kg. Each time point was registered as described in 5.3.7 and the average intensity of identified puncta were compared throughout the time course. Further analysis is required to rigorously understand FFN270 changes in this system. The data presented is only from one animal. Optogenetics experiments have also started, but not ready for data collection. For these experiments, mice were injected in the locus

coeruleus as described above, except with AAV9-CAG-ChR2-mCherry virus (UPenn Viral Core).

5.4 References

1. Wong, M. Y., Sulzer, D. & Bamford, N. S. Imaging presynaptic exocytosis in corticostriatal slices. *Methods Mol. Biol.* **793,** 363–76 (2011).

2. Federici, M. *et al.* Paradoxical abatement of striatal dopaminergic transmission by cocaine and methylphenidate. *J. Biol. Chem.* **289,** 264–74 (2014).

3. Pereira, D. B. Imaging fluorescent false neurotransmitter release and Ca2+ at individual striatal dopaminergic boutons reveals a low density of active release sites. *Submitted*

4. Karpowicz, R. J., Dunn, M., Sulzer, D. & Sames, D. APP+, a fluorescent analogue of the neurotoxin MPP+, is a marker of catecholamine neurons in brain tissue, but not a fluorescent false neurotransmitter. *ACS Chem. Neurosci.* **4,** 858–69 (2013).

5. Karpowicz, R. J. Advanced Fluorescent False Neurotransmitters for the study of Monoamine Transporter Activity and Synaptic Transmission. *Columbia Univ. Ph.D Thesis* (2014).

6. Sanders, J. D., Happe, H. K., Bylund, D. B. & Murrin, L. C. Development of the norepinephrine transporter in the rat CNS. *Neuroscience* **130,** 107–17 (2005).

7. Murrin, L. C., Sanders, J. D. & Bylund, D. B. Comparison of the maturation of the adrenergic and serotonergic neurotransmitter systems in the brain: implications for differential drug effects on juveniles and adults. *Biochem. Pharmacol.* **73,** 1225–36 (2007).

8. Rodriguez, P. C. *et al.* Fluorescent dopamine tracer resolves individual dopaminergic synapses and their activity in the brain. *Proc. Natl. Acad. Sci. U. S. A.* **110,** 870–5 (2013).

9. Adam, Y., Edwards, R. H. & Schuldiner, S. Expression and function of the rat vesicular monoamine transporter 2. *Am. J. Physiol. Cell Physiol.* **294,** C1004–11 (2008).